Quantum Nonequilibrium Dynamics: Transport, Entanglement, and Thermalization

Hyungwon Kim

A Dissertation
Presented to the Faculty
of Princeton University
in Candidacy for the Degree
of Doctor of Philosophy

Recommended for Acceptance
by the Department of
Physics
Adviser: Professor David A. Huse

September 2014

Abstract

We study three aspects of quantum nonequilibrium dynamics; (1) transport of conserved quantities, (2) entanglement spreading, and (3) construction of local operators which slowly relax to thermal equilibrium. Motivated by recent progresses in ultracold atom experiments, we first analyze transport phenomena of a population imbalanced two-component fermi gas with arbitrary strength of inter-species interaction in three dimension. Using the Boltzmann kinetic equation at dilute regime, we obtain the transport coefficients of linear responses to gradients of temperature and chemical potential imbalance. We identify the magneto-caloric effects, and determine how these effects depend on interaction strength and population imbalance. Then, we propose an experimental protocol to observe these effects in an experiment with ultracold atoms. Next, we study entanglement spreading in a one-dimensional quantum Ising chain with longitudinal and transverse fields, which is diffusive and nonintegrable. Fully diagonalizing the Hamiltonian matrix, we explicitly show that the entanglement spreading is ballistic, thus faster than diffusive transport of conserved quantities. We provide a local spreading picture of entanglement entropy in terms of logarithmic negativity. Then, we discuss a role of energy conservation in entanglement spreading through analyzing a Floquet system. Lastly, we construct local operators that relax slowly to equilibrium with the same one-dimensional Hamiltonian. By showing that the Hamiltonian satisfies the eigenstate thermalization hypothesis, we first conclude that this model relaxes local operators to thermal equilibrium. Then, we systematically construct local operators that relax slower than conventional diffusive modes.

Acknowledgements

First of all, I would like to thank my advisor, Professor David Huse. David is one of the most brilliant physicists I have ever interacted with. He is always available for students, which should not be taken for granted from established professors, coming up with interesting problems, and giving me the right guidance. Personally, I think his most incredible ability is being able to understand the essence of what others try to say no matter how vague they make the arguments. This certainly helped me to transform my clumsy work to something meaningful. Also, he gave me many opportunities to attend various conferences, including international ones, to meet people outside Princeton, which were great privileges. Among them, the most extraordinary event was to spend three months in the Max-Planck-Institute for Quantum Optics in Germany to collaborate with physicists in the theory group there. Chapter 4 of this dissertation is the result of the visit. I thank David for every single aspect during my graduate work.

I would also like to thank Professor Ignacio Cirac and Dr. Mari Carmen Bañuls at Max-Planck-Institute. Ignacio kindly hosted me in his group at MPQ and introduced me very interesting problems. He always gave penetrating comments and suggestions to bring the work to the next level. Mari Carmen was essentially my advisor in Germany: she patiently taught me numerical techniques, gave me physical insights, and answered to my uneducated questions. I would love to visit MPQ again whenever available. I had a great time.

I also owe a lot to many Professors at Princeton, Andrei Bernevig, Shivaji Sondhi, Herman Verlinde, and Peter Meyers. Without Andrei's series of courses, I would not be able to understand another main-stream topic in condensed matter physics. Shivaji kindly brought me in a project in his group, which turned out to be an interesting one. Also I thank Shivaji for critical reading of the dissertation. I took all quantum-related courses from Herman, PHY 305 and PHY 510. He tried bringing the subject

to student's level. This was great help to me, who always struggled to understand quantum. During my experimental project, I enjoyed working in Peter's lab, where I made many friends in the department.

Speaking of life at Jadwin, sanity is not easy to keep without friends. My first thank should go to Yeje Park, my Korean comrade, who helped me adjusting myself to the department in the beginning of the journey. Also, I thank Akshay, Aris, Chaney, and Vedika for dining out at random restaurants and interesting discussions about physics and life. I especially thank Charles Mathy, who has been giving me academic and non-academic advices, and Arijeet Pal, who shared his tips to survive in academia. It was also valuable experience to interact with junior students, Bo Zhao and Liangsheng Zhang. All players in the softball team, the Big Bangers, deserve my acknowledgement. After all, my life at Jadwin cannot be pursued without resting at home. I thank my four-year long roommate, Jason Brodsky and first year roommate, Ben Landrum.

I should mention friends in Max-Planck-Institute. Juan Bermejo Vega and Xiaotong Ni made my stay in Germany delightful in all aspects.

A graduate life at Princeton is not all about research. Many friends outside physics made me a socially acceptable being, I believe. Special thanks to Junehyuk Jung - I will miss the trips to Florida, Hawaii, Alaska, and Canada. I owe a lot to John Kim, who always kept me interested in social science. I thank Taewook Oh, who essentially made all numerical works possible. I enjoyed discussing physics across the country with Younghyun Kim in Santa Barbara. Finally, I thank Shelly Lim for emotional support and Stuart Carter and Haillie Lee for long-standing friendship.

Last but not least, my family deserves an acknowledgement longer than this dissertation. My brothers, none of them are in academia, have always supported me for pursuing theoretical physics. I thank my parents for believing in me for all stages of my life. Without their encouragement, this dissertation would not be born.

To my family.

Contents

Abstract iii

Acknowledgements iv

List of Tables x

List of Figures xi

1 Introduction **1**

1.1 Physical Systems 2

1.1.1 Ultracold Atoms 2

1.1.2 One-dimensional Quantum Spin Chain 8

1.2 Methods 10

1.2.1 Boltzmann Equation 10

1.2.2 Exact Diagonalization 14

1.3 Physical Objects of Study 15

1.3.1 Transport of Conserved Quantities 15

1.3.2 Entanglement 17

1.4 Thesis Outline 18

2 Transport in Ultracold Atomic Gases: Boltzmann Equation **20**

2.1 Introduction 20

2.2 Transport Matrix and Qualitative Estimates of Transport Coefficients 22

2.2.1 Transport 23

2.2.2 Qualitative Estimates of Transport Coefficients 26
2.3 Spin and Heat Transport of a Two Component Fermi Gas - Quantitative Results 32
2.3.1 Linearized Boltzmann equation and its scaling 33
2.3.2 Approximate Solution 35
2.3.3 Estimate of the Spin Seebeck Effect 41
2.3.4 Perturbation of Exactly Solvable Model of the Boltzmann Equation 49
2.4 Structure of Transport Coefficients 52
2.4.1 Kubo Formula 52
2.4.2 Manifestation of the Onsager Relation 55
2.5 Conclusion 57

3 Entanglement Dynamics of 1D Nonintegrable Quantum Spin Chain: Exact Diagonalization 59
3.1 Introduction 60
3.2 The Model 61
3.2.1 Nonintegrability - Level Spacing Statistics 62
3.3 Entanglement Spreading 66
3.3.1 Ballistic Spreading of Entanglement 66
3.3.2 Real Space Picture of Entanglement Spreading 69
3.3.3 Roles of Energy Conservation in Entanglement Spreading . . . 75
3.4 Diffusive Energy Transport 77
3.5 Conclusion 80

4 Thermalization and Construction of Slowly Relaxing Operators in a Nonintegrable Quantum System 82
4.1 Introduction 83

4.2 Eigenstate Thermalization Hypothesis 85
4.2.1 ETH parameter 88
4.2.2 Results 90
4.3 Slowest Relaxing Local Operators - Construction 95
4.3.1 Objective 96
4.3.2 Method 99
4.4 Slowest Relaxing Local Operators - Results 104
4.4.1 Smallest Value of Commutator in the Frobenius Norm 104
4.4.2 The Operator Norm and the Distance from Thermal State . . 108
4.4.3 Real Time Relaxation 110
4.5 Outlook 113

A Scaling Form of Transport Coefficients of Ultracold Atoms 115
A.1 κ' and S'_s 115
A.2 D_s and P'_s 119

B Hamiltonian Parameter Choice 122

C Efficient algorithm to find slowest relaxing operators 127

Bibliography 131

List of Tables

List of Figures

1.1 Feschbach Resonance 4

1.2 BCS-BEC Crossover 6

1.3 Phase Diagram of Two-component Unitary Fermi Gas 7

2.1 Illustration of spin Seebeck effect 30

2.2 Seebeck Effect vs. Interaction Strength 39

2.3 Signature of Seebeck Effect at Unitarity 44

2.4 Signature of Seebeck Effect away from Unitarity 45

2.5 Time Evolution of Polarization 49

2.6 Extreme Density Deviation 50

3.1 Ratio Distribution of Level Spacing 66

3.2 Ballistic Spreading of Entanglement 68

3.3 Scaled Form of Spreading of Entanglement 68

3.4 Tripartite System 70

3.5 negativity 74

3.6 Negativity Onset Time 74

3.7 Floquet vs. Hamiltonian 77

3.8 Energy Diffusion 78

3.9 Entanglement Spreading and Energy Diffusion Comparison 80

4.1 Density of State 88

4.2 Expectation Values 91
4.3 Distribution of Expectation Values 92
4.4 Outliers of the Eigenstate Thermalization Hypothesis 93
4.5 Minimum of commutator with Hamiltonian in translation invariant system 104
4.6 M-scaling of diffusive operator 106
4.7 Minimum of commutator with Hamiltonian in a system with one open boundary 107
4.8 The Frobenius norm and the operator norm 109
4.9 Distance between initial expectation value and thermal expectation value 111
4.10 Real time relaxation of operators at early stage 112

B.1 Level Spacing Statistics of Parameter Choice 123
B.2 Density of States 124
B.3 Comparison between entanglement spreading and energy diffusion in another parameter choice 125
B.4 Finite size scaling of energy diffusion of another parameter choice . . 126

Chapter 1

Introduction

The Universe has never been static but has kept expanding to the best of our knowledge at the time. Arguably four most important equations in physics are Newton equation, Maxwell equations, Einstein field equation, and Scrödinger equation. All of these equations include the time variable and describe dynamics. Therefore, understanding dynamics is one of the most fundamental problems in physics.

On the other hand, the equilibrium statistical mechanics has achieved enormous success in explaining various phenomena in the physical world although the absolutely perfect equilibrium has never happened in anywhere. Therefore, it is important to understand to what extent and under what circumstances we may rely on the machinery of equilibrium statistical mechanics.

We believe that all underlying mechanisms of physical processes are quantum mechanical. For a closed system, the quantum dynamics is unitary and the unitary dynamics in principle preserves *all* information about the initial condition. However, the equilibrium statistical mechanics is very insensitive to details of the initial state. Therefore, we have another problem to resolve: does an isolated quantum system equilibrate?

In this thesis, we attempt to provide a partial answer to above questions, although we only cover a very tiny portion of the enormous object. We pick two popular physical systems, three-dimensional ultracold gases and one-dimensional quantum spin chains. Using analytical and numerical techniques, we study the process of equilibration in detail.

1.1 Physical Systems

We study two physical systems; three-dimensional ultracold atomic gases and one-dimensional quantum spin chain. Three-dimensional ultracold atoms have already been realized in various experiments and are ideal tools to study macroscopic quantum nonequilibrium dynamics as we explain below. Most of their nonequilibrium dynamics can be well-understood by the standard Boltzmann equation. One-dimensional quantum spin chains are widely-used model systems to study quantum dynamics. In spite of their simple real-space structure, their quantum dynamics can show complex behaviors. Although not as perfect as three-dimensional cold gases in continuum space, one-dimensional quantum spin chains are also realized in experiments [63, 64].

We emphasize that we consider *isolated* quantum systems throughout this thesis. Once we prepare the system in a certain initial condition, all dynamics is governed by Hamiltonian of the system itself without any influence from external heat bath that we may have used when initializing the system. To a very good approximation, the ultracold atoms have realized this isolated quantum dynamics.

1.1.1 Ultracold Atoms

A typical temperature of ultracold atoms is $T \leq 1\mu$K and therefore, a typical time scale of dynamics of strongly interacting atoms is $\tau \geq 10\mu$s. This is substantially longer than a usual time scale in condensed matter physics. Slow process makes

it easier to directly observe dynamics and out-of-equilibrium physics (while it is a drawback to equilibrium phenomena). Cold atom systems are usually dilute, with a typical density of order $10^{11} \sim 10^{14}$ cm^{-3}, which implies its length scale is about a few hundred nanometers. This is also larger than a typical length scale in many condensed matter systems. Longer length scale means its behavior is more easily detected in the lab. As a result, dimensional analyses already make ultracold atomic gases be favorable candidates for direct investigation of quantum dynamics.

One of beautiful features of cold atom systems is the universality. Since cold atoms are dilute and electrically neutral, their inter-particle interactions are mostly captured by a single s-wave scattering length, a. Therefore, a cold atom system can be successfully described by a small set of parameters; s-wave scattering length, their masses, densities, and temperature, without a notion of microscopic details of interaction. Consequently, it is possible to use a simple pseudopotential that still captures all important physics. One of the standard pseudopotentials to explain the physics dominated by s-wave scattering is the regularized (momentum independent) contact interaction. The first application of this pseudopotential was made to explain the interactions between neutrons at relatively low densities in which s-wave scattering gives dominant contribution to the interaction [41, 14]. The Fermi gas with only contact interactions is indeed realized to a very good approximation in recent experiments [57, 87].

Another nice property of cold atoms is the controllability of individual populations and ability to create distinguishable particles from indistinguishable ones. For example, it is possible to separate the two lowest hyperfine state of ^{6}Li by applying the method of RF spectroscopy. Then, one can treat the hyperfine state as an internal degree of freedom of a particle so Li atoms belong to different hyperfine states are distinguishable from one other. Polarization is the standard measure to quantify the relative population. As is conventional, we call the majority species

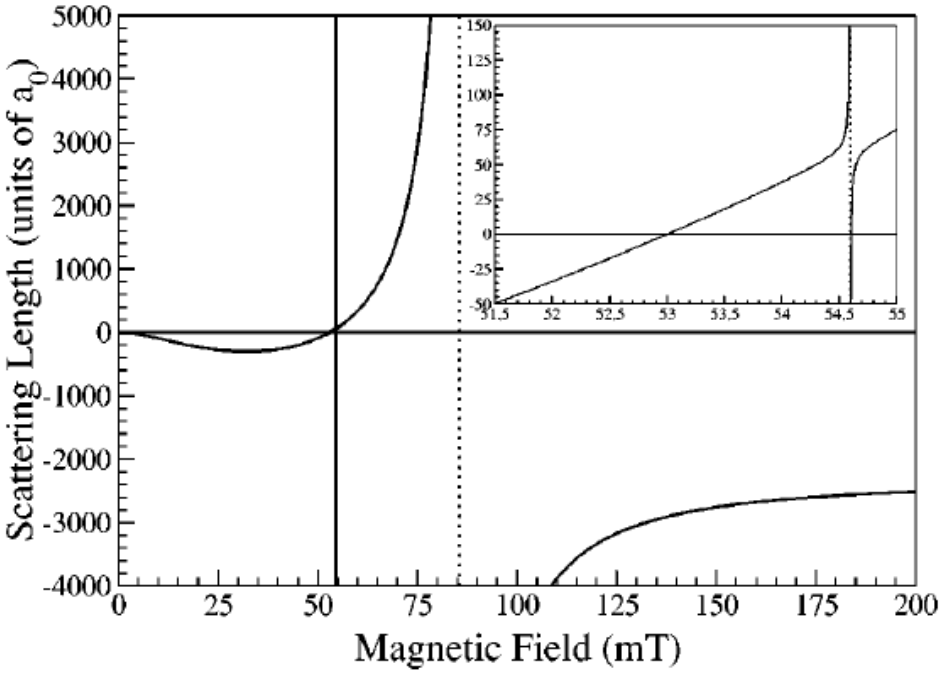

Figure 1.1: s-wave scattering length of unpolarized ^{6}Li at $T = 5\mu$K and $n = 3 \times 10^{13}$ cm^{-3} measured by O'hara *et al.* [90]. It shows both a narrow Feshbach resonance near $B = 550$ G and a broad Feshbach resonance near $B = 860G$ (At the moment, the precise location of the broad Feshbach resonance of ^{6}Li is known to be around 834G).

"up" $\uparrow$ and the minority (impurity) species "down" $\downarrow$. Then, the polarization p is $p = (n_\uparrow - n_\downarrow)/(n_\uparrow + n_\downarrow)$.

Perhaps the most important advantage of cold atoms is the tunability of interaction strength through a Feshbach resonance. A Feshbach resonance is defined as a value of magnetic field when the s-wave scattering length between two different hyperfine states diverges [38]. Empirically the s-wave scattering length can be written as

$$a(B) = a_{bg}\left(1 - \frac{\Delta B}{B - B_0}\right) , \tag{1.1}$$

where a_{bg} is the background scattering length which is far from the resonance. ΔB is the width of a Feshbach resonance. For a large ΔB, we call it a broad Feshbach resonance and for a small ΔB, we call it a narrow Feshbach resonance (^{6}Li is known

to have a narrow Feshbach resonance near $B_0 = 550$ G and 680 G [36, 90]). Most times, it is more convenient to use a wide Feshbach resonance when one explores thermodynamics or nonequilibrium phenomena at resonance. For instance, ^{6} Li indeed has a wide Feshbach resonance around $B_0 = 834$ G [11, 130]. Figure 1.1 shows a typical shape of s-wave scattering length a as a function of magnetic field. Indeed the scattering length can be tuned to any value by varying applied magnetic field, sweeping the Feshbach resonance from one side ($a < 0$) to another side ($a > 0$).

Note that the bare interaction is always attractive since inter-atomic van der Waals force is in general attractive unless two atoms get too close to each other where hard-core repulsion takes place. Only attractive interaction can possess both negative and positive scattering length (Figure 1.1). A positive scattering length is a signature of a molecular bound state and this state corresponds to Bose-Einstein Condensation (BEC) of pairs of Fermionic atoms [130]. For $a = 0$ this is the standard textbook noninteracting Fermi gas, while for weakly attractive a it is very close to the model used by Bardeen, Cooper and Schrieffer (BCS) to explain superconductivity. The limit of infinite a is the strongly-interacting unitary Fermi gas (unitarity limit). These regimes are illustrated in figure 1.2 [56].

One of the essential ingredients that come into the Boltzmann equation is the scattering cross section as we will see shortly. The universal scattering cross section in vacuum can be computed easily as a function of s-wave scattering length a:

$$\frac{d\sigma}{d\Omega} = \frac{a^2}{1 + \left(\frac{k_r a}{2}\right)^2} \ , \tag{1.2}$$

where $d\sigma/d\Omega$ is the standard differential cross section and k_r is the relative momentum of two scattering particles.

A mass imbalanced system ($m_\uparrow \neq m_\downarrow$) also has a lot of interesting physics, and in actuality, a ^{6}Li - ^{40}K mixture is known to have a Feshbach resonance in an accessible

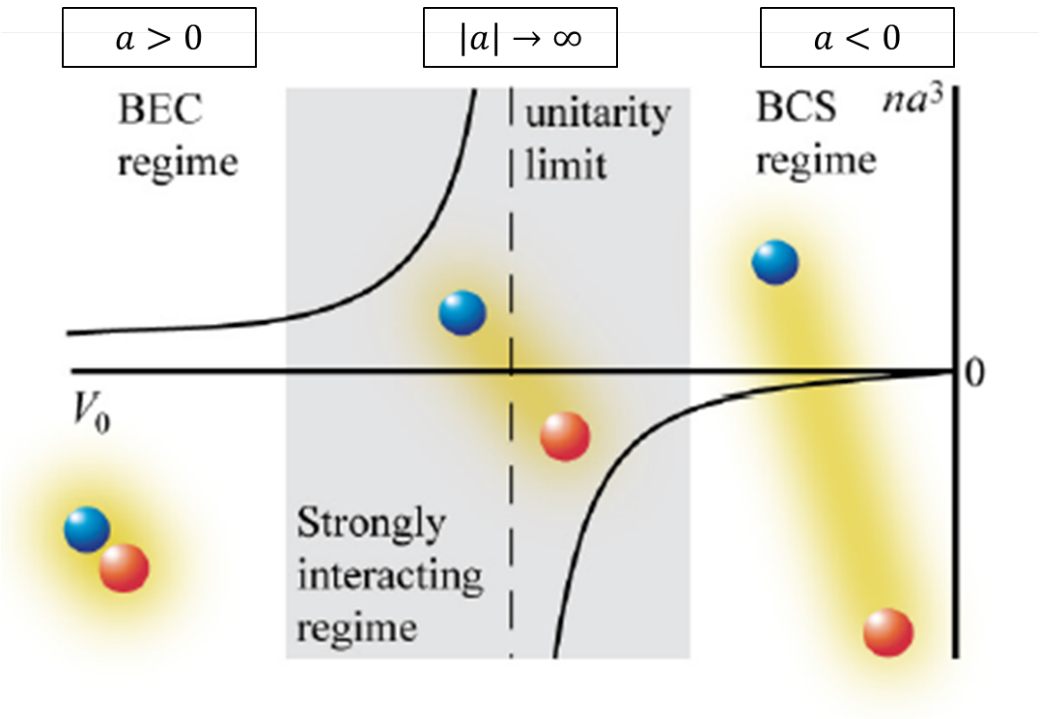

Figure 1.2: BCS-BEC Crossover. In BEC regime ($a > 0$), two atoms form a BEC molecule in real space. In BCS regime ($a < 0$), two atoms form a BCS pair in momentum space. These two regimes are smoothly connected by a single parameter, interaction strength a, via the Feshbach resonance. Figure from [56]

range of magnetic field in the lab [127]. However, in this thesis, we are mostly concerned with (bare) mass balanced case.

The total number density $n = n_\uparrow + n_\downarrow$, together with m and $\hbar$ set the characteristic length, time and energy scales. The scaled dimensionless properties of this universal Fermi gas then depend on only three dimensionless parameters, which can be chosen to be $1/(k_F a)$, T/T_F and the polarization $p = (n_\uparrow - n_\downarrow)/n$. We use a convention that the Fermi wavenumber and temperature k_F and T_F are defined by the total density, so that at high polarization $T_{F\downarrow} \ll T_F \approx T_{F\uparrow}$ and $k_{F\downarrow} \ll k_F \approx k_{F\uparrow}$. This universal Fermi gas has a variety of regimes of behavior : The polarization p can be low or zero so $n_\downarrow \cong n_\uparrow$ or it can be near one so $n_\downarrow \ll n_\uparrow$. The temperature can be higher, $T > T_{F\uparrow}$, or lower, $T < T_{F\downarrow}$, than both Fermi temperatures or, for $p > 0$ it can be in between them, $T_{F\downarrow} < T < T_{F\uparrow}$. The scattering can be near unitarity

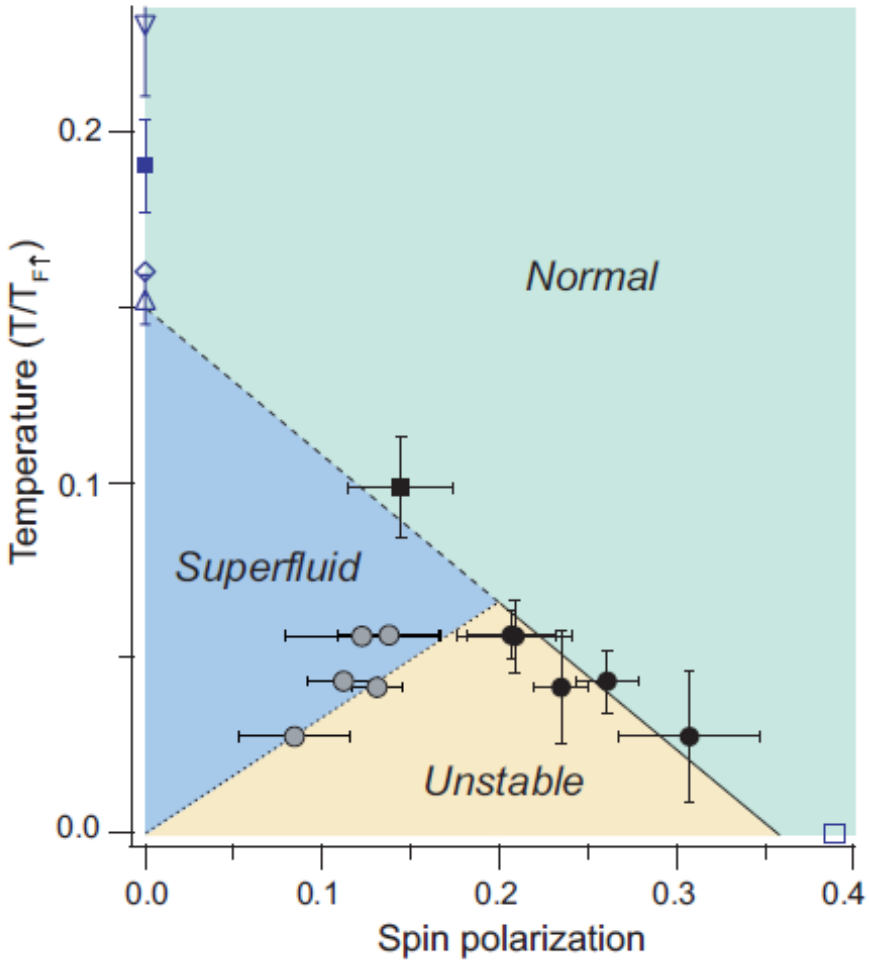

Figure 1.3: Phase diagram of two-component (two hyperfine state) ^{6}Li at unitarity as a function of temperature and polarization obtained by MIT group [112]. Superfluid pairing exists up to Chandrasekhar-Clogston limit [27, 32] of polarization. Phase separation and phase boundary are in a good agreement with theory and experiment (for detail of the diagram, see Ref[112]).

so $|k_F a|$ is of order one or more, or it can be far from unitarity so $|k_F a| \ll 1$. At high T it also matters whether $|a|$ is larger or smaller than the thermal de Broglie wavelength $\lambda \equiv \sqrt{2\pi\hbar^2/mT} \sim T^{-1/2}$. Lastly, in the unitarity limit, we eliminate one parameter, $1/(k_F a)$, so that we only have two parameters, T/T_F and p. The phase diagram of two-component Fermi gases with only two parameters are extensively investigated both experimentally [94, 129, 113, 95, 112, 111, 86] and theoretically [29, 74, 18, 21, 33, 51, 101, 81]. Fig.1.3 shows a phase diagram of two-component ^{6}Li gas at unitarity obtained by MIT group [112] as a function of polarization and temperature.

Although the universal Fermi gas can be described by a small number of parameters, it is in general very challenging to study transport properties analytically. It is mainly due to the fact that there are intrinsically no small parameters. [1] However, there are a two regimes we can find small parameters: (1) low temperature and high polarization, where T/T_F and $T_{F\downarrow}/T_{F\uparrow}$ are small and (2) low densities (classical regime), where $n_\uparrow\lambda^3$ and $n_\downarrow\lambda^3$ are small. In the following section, we will closely study the regime (2). Details of analysis of regime (1) can be found in Ref. [60].

1.1.2 One-dimensional Quantum Spin Chain

Theoretical investigation of dynamics in a three-dimensional system is very limited to certain classes of problems which require many steps of approximations. One-dimensional systems can be complimentary, since there are a few models that allow exact analytical solutions or efficient numerical analysis without too many premises.

[1] Conventional treatment of interacting gases relies on the smallness of inter-particle scattering length ($na^3 \ll 1$), which serves as a small expansion parameter. However, in ultracold atoms, this is no longer holds since the scattering length is another tuning parameter.

We will focus on the one-dimensional quantum spin chain of spin-1/2. The model is quantum Ising chain with transverse (g) and longitudinal (h) fields:

$$H = \sum_i \left(g\sigma_i^x + h\sigma_i^z + J\sigma_i^z\sigma_{i+1}^z \right) \ , \tag{1.3}$$

where σ's are Pauli operators. Since we have a freedom to scale all parameters by a constant factor, we always set $J = 1$ [2]. When either of fields g or h is zero, this model is integrable. When $g = 0$, this model reduces to just a trivial one-dimensional Ising chain and when $h = 0$, we can map this model to free Fermions via Jordan-Wigner transformation [107] and thus integrable. In the presence of both nonzero g and h, this model is nonintegrable and the exact solution is unknown so that we need to apply numerical methods.

Since we will study fast growth of entanglement entropy, we will use the exact diagonalization method. This method is greatly restricted by the dimension of Hilbert space, which grows exponentially with the system size. Therefore, the parameters should carefully be chosen to see "generic" properties. Otherwise specified, we use $h = (\sqrt{5}+1)/4 = 0.8090...$ and $g = (\sqrt{5}+5)/8 = 0.9045...$ [3]. We avoid using simple a few digit numbers to minimize chances of accidental degeneracies that may arise from finite-size effects. At this set of parameters, the system is gapped [4], although we do not use this property in this thesis. Appendix B gives more rationales of this parameter choice. The boundary condition will depend on the problem: we use open boundary condition for entanglement spreading and energy transport and periodic boundary condition for testing the eigenstate thermalization hypothesis.

[2] When $J = 0$, each spin is independent so there is no nontrivial dynamics

[3] These golden-ratio "descendent" parameters turn out to be "golden-parameters".

[4] Gappedness can be inferred from the facts that (1) ground state energy can be easily computed using the method of iMPS (infinite Matrix Product State), and (2) there is no divergence in entanglement entropy of ground state.

Lastly, we emphasize that this model is not just a nice theoretical tool. To a good approximation, this quantum spin chain is found in real materials [121] and also realized in ultracold atomic system.

1.2 Methods

There are a number of theoretical methods to address nonequilibrium problems; Boltzmann kinetic equation, Linblad master equation, time-dependent Density Matrix Renormalization Group (t-DMRG), and exact diagonalization to name a few. Each method has its own applicable realms so that we should choose appropriate method(s) in accordance with the nature of problem. The Linblad master equation formalism is suitable to study dissipative and driven open systems. t-DMRG is widely used to study dynamics of one-dimensional system, where entanglement growth rate is slower than exponential. In this thesis, we extensively use the Boltzmann equation and the exact diagonalization method. The Boltzmann equation is a top-down approach that we assume the existence of a coarse-grained distribution function which is a smooth function of time and phase space and the equation governs the time evolution of the distribution function. The exact diagonalization method is a bottom-up approach that we only use the first principle of quantum mechanics and numerically study exact quantum dynamics.

In Chapter 4, we develop a new numerical approach, which is very close to the exact diagonalization. Since it is not (yet) a standard method, we postpone its introduction to Chapter 4.

1.2.1 Boltzmann Equation

One of the standard methods to address nonequilibrium phenomena is kinetic theory founded by Clausius, Maxwell, Boltzmann and others in the late nineteenth century.

Especially, Ludwig Boltzmann developed an important tool to study the dynamics of a gas, namely the Boltzmann transport equation [10], and his method is widely used to this day.

The Boltzmann equation was originally designed to describe nonequilibrium phenomena of dilute gases in a sense that the typical distance between two molecules or atoms is much longer than the range of interaction. Therefore, when we work in the regime where Boltzmann equation is valid, we may consider the interaction between particles are essentially instantaneous and the paths of particles can only be (discontinuously) altered by instantaneous scattering process, which is captured in the collision integral of the Botlzmann equation. In the presence of external field, the "free-motion" (without scattering) of particles is modified from a straight line to a curved one but the influence of external field is still continuous in phase space so it is distinguishable from that of scattering process. In a dense liquid, however, the effects of external field and inter-particle collision may not be clearly distinguished since inter-particle separation is comparable to the range of interaction. This is the regime where the Boltzmann approach breaks down. Another reason why Boltzmann equation breaks down is that it only considers the conservation of kinetic energy whereas what is really conserved is the total energy. Thus, the Boltzmann equation is applicable only when the potential energy, or the interaction energy is very small compared to the kinetic energy [55]. There are, of course, many interesting physical systems in dense (or degenerate) regimes where we want to understand nonequilibrium transport properties. This is when the concept of quasiparticles developed by Landau becomes useful. Quasiparticle picture enables us to transform strongly interacting particles to weakly interacting quasiparticles for which the Boltzmann approach is applicable [115] (e.g. Landau Fermi Liquid theory)).

The central entity in the Boltzmann's formalism is the particle density $f(\mathbf{r}, \mathbf{k}, t)$ ($\mathbf{r}$ is real-space coordinate and $\mathbf{k}$ is wave vector), which represents the number density of

particles in the $2d$-dimensional phase space $(\mathbf{r}, \mathbf{k})$ at time t. When there is no particle sink, the total number of particles, N,

$$N = \frac{1}{(2\pi)^d} \int d^d\mathbf{r} d^d\mathbf{k} f(\mathbf{r}, \mathbf{k}, t) \tag{1.4}$$

is time independent.

The Boltzmann equation is essentially the time-differential of the particle density:

$$\left(\frac{\partial}{\partial t} + \frac{\partial \mathbf{r}}{\partial t}\frac{\partial}{\partial \mathbf{r}} + \frac{\partial \mathbf{k}}{\partial t}\frac{\partial}{\partial \mathbf{k}} \right) f(\mathbf{r}, \mathbf{k}, t) = \left. \frac{\partial f(\mathbf{r}, \mathbf{k}, t)}{\partial t} \right|_{coll} . \tag{1.5}$$

The left hand side is the *streaming* term, where changes in f is *continuous* at all times while the right hand side is the *collision integral*, where changes are altered by *instantaneous* collision events. Therefore, the Boltzmann equation is an effective equation which governs the time-dependence of coarse-grained particle density. Once we identify $\partial \mathbf{r}/\partial t == \mathbf{v}$ (particle velocity) and $\partial \mathbf{k}/\partial t = \mathbf{F}_{ext}$ (external force in appropriate unit), then the Boltzmann equation is

$$\left(\frac{\partial}{\partial t} + \mathbf{v} \cdot \frac{\partial}{\partial \mathbf{r}} + \mathbf{F}_{ext} \cdot \frac{\partial}{\partial \mathbf{k}} \right) f(\mathbf{r}, \mathbf{k}, t) = \left. \frac{\partial f(\mathbf{r}, \mathbf{k}, t)}{\partial t} \right|_{coll} . \tag{1.6}$$

It is notoriously difficult to find a solution of the Boltzmann equation because of the collition integral. If the interaction is short-ranged and dominated by two-particle scattering, the collision integral is formally the following:

$$\begin{aligned} &\left. \frac{\partial f(\mathbf{r}, \mathbf{k}, t)}{\partial t} \right|_{coll} = \\ &\int \frac{d^d\mathbf{k}' d^d\mathbf{q}' d^d\mathbf{q}}{(2\pi)^{3d}} \Big[W(\mathbf{k}', \mathbf{q}' \to \mathbf{k}, \mathbf{q}) (f(\mathbf{r}, \mathbf{k}', t) f(\mathbf{r}, \mathbf{q}', t) (1 \pm f(\mathbf{r}, \mathbf{k}, t)) (1 \pm f(\mathbf{r}, \mathbf{q}, t))) \\ &\qquad - W(\mathbf{k}, \mathbf{q} \to \mathbf{k}', \mathbf{q}') (f(\mathbf{r}, \mathbf{k}, t) f(\mathbf{r}, \mathbf{q}, t) (1 \pm f(\mathbf{r}, \mathbf{k}', t)) (1 \pm f(\mathbf{r}, \mathbf{q}', t))) \Big]. \end{aligned} \tag{1.7}$$

Here, $W(\mathbf{k}, \mathbf{q} \to \mathbf{k}', \mathbf{q}')$ is the scattering amplitude that connects the scattering process of two incoming particles of momenta $\mathbf{k}, \mathbf{q}$ with two outgoing particles of momenta $\mathbf{k}', \mathbf{q}'$. In $(1 \pm f(\mathbf{r}, \mathbf{k}, t))$, $+$ $(-)$ corresponds to Bose enhancement (Pauli blocking) factor. We can just ignore this factor in the classical regime. If the Hamiltonian is time-reversal invariant, the scattering amplitude should be invariant under exchange of incoming and outgoing momenta. Therefore, $W(\mathbf{k}', \mathbf{q}' \to \mathbf{k}, \mathbf{q}) = W(\mathbf{k}, \mathbf{q} \to \mathbf{k}', \mathbf{q}')$. Once we recall the definition of the differential scattering cross section [5], we can express the scattering amplitude in terms of scattering cross section:

$$\frac{d^d\mathbf{q}' d^d\mathbf{k}'}{(2\pi)^{2d}} W(\mathbf{k}', \mathbf{q}' \to \mathbf{k}, \mathbf{q}) = v \frac{d\sigma}{d\Omega} d\Omega \ , \tag{1.8}$$

where $v = \frac{\hbar}{m}|\mathbf{k} - \mathbf{q}|$ is the relative speed of two incoming particles and $\frac{d\sigma}{d\Omega}$ is the differential scattering cross section.

Imposing the energy-momentum conservation in the right hand side, we obtain the final form of the collision integral:

$$\int \frac{d^d\mathbf{q}}{(2\pi)^d} d\Omega \frac{d\sigma}{d\Omega} v \Big[(f(\mathbf{r}, \mathbf{k}', t) f(\mathbf{r}, \mathbf{q}', t)(1 \pm f(\mathbf{r}, \mathbf{k}, t))(1 \pm f(\mathbf{r}, \mathbf{q}, t))) \\ - f(\mathbf{r}, \mathbf{k}, t) f(\mathbf{r}, \mathbf{q}, t)(1 \pm f(\mathbf{r}, \mathbf{k}', t))(1 \pm f(\mathbf{r}, \mathbf{q}', t)) \Big] \ . \tag{1.9}$$

Note that the equilibrium distribution (Fermi-Dirac, Bose-Einstein, or Maxwell-Boltzmann) makes the terms in the square bracket vanish. Therefore, the collision term does not affect the time evolution of the particle density at equilibrium, as expected.

A typical strategy to solve the Boltzmann equation is the following: (1) First, find a time-independent solution of the Boltzmann equation. In the presence of a driving force (nonequilibrium steady-state), an exact solution to the Boltzmann equation is

[5] Given the flux of incoming particles, the number density of outgoing particles at a differential solid angle $d\Omega$.

unknown for almost all forms of the scattering cross section. Thus, we need to find an approximate solution or solve it numerically. (2) Using the time-independent solution and the continuity equation, we can write a diffusion equation in terms of the particle density. (3) Solve the diffusion equation in accordance with the boundary conditions.

In chapter 2, we will solve the Boltzmann equation in the absence of external force.

1.2.2 Exact Diagonalization

Undoubtedly, the Boltzmann equation is one of the most widely accepted approaches to study transport phenomena. However, its applicability is limited to cases where lifetime of excited states is long enough and its solution is intrinsically not exact. Sometimes we want to compute properties of a quantum system exactly or almost exact. When exact analytic solution is unknown, we should resort to numerical method such as quantum Monte Carlo, Density Matrix Renormalization Group (DMRG), Tensor Network, or Krlyov Expansion. In this thesis, we extensively use probably the most primitive yet very powerful method, the exact diagonalization.

The method of exact diagonalization is simply to write the Hamiltonian in a matrix form and numerically diagonalize the Hamiltonian matrix. Once we know the exact eigenvalues and eigenstates, we can compute any quantity of interest exactly up to machine precision. Since the size of matrix grows exponentially with the system size, this method can only explore relatively small system size. There are two major factors that limit the accessible system size; memory and computation time. The memory grows as the square of the dimension of Hilbert space and the time to diagonalize scales with cubic power of the dimension. Therefore, whenever available, we need to maximally utilize the discrete symmetry of the Hamiltonian to make the Hamiltonian in block-diagonal form. For example, our spin Hamiltonian 1.3 with open boundary condition has a inversion symmetry with respect to the center so that we can write

the Hamiltonian in a parity basis (even and odd under inversion) and diagonalize each parity sector separately. In case of translation invariance, a lattice momentum is a good quantum number and thus we can diagonalize individual momentum sector. This procedure saves the required computational resource by a few factors, which can be significant in exact diagonalization. At current computation power, the maximum system size that we can diagonalize in a reasonable time [6] is 16 spins in open boundary condition and 19 spins in periodic boundary condition.

1.3 Physical Objects of Study

Dynamics itself is not a physical quantity that we can measure or calculate. We need "physical" objects to compute. Here we explain two widely studied objects in quantum dynamics: local conserved quantity and entanglement entropy.

1.3.1 Transport of Conserved Quantities

When a hermitian operator commutes with the Hamiltonian, the corresponding object is conserved. If such an operator is a sum of *local* operators, then this local density can be transported from one side to another and measured [7]. The local conservation laws define conserved currents via the continuity equations. A typical system has three conservation laws; particle number, total energy, and total momentum. Therefore, in d-dimensional system with N species, there are $d+N+1$ continuity equations for

[6] within 24 hours of computation time using a 3.2GHz CPU and 20 GB of RAM

[7] When an operator cannot be written as a sum of local terms (global or discrete symmetry), there is no transport. For example, a Hamiltonian can commute with a parity operator but transport of parity is meaningless.

particle current $\mathbf{J}_s$, energy current $\mathbf{J}_e$, and momentum current tensor Π_{ij}:

$$\frac{\partial n_s}{\partial t} + \nabla \cdot \mathbf{J}_s = 0 \tag{1.10}$$

$$\frac{\partial \epsilon}{\partial t} + \nabla \cdot \mathbf{J}_e = 0 \tag{1.11}$$

$$\frac{\partial g_i}{\partial t} + \nabla_j \Pi_{ij} = 0 \ , \tag{1.12}$$

where n_s is particle density of species s, ϵ is energy density, and g_i is i'th component of momentum density.

In the absence of external applied force, these currents are driven by generalized forces leading to entropy production. Inhomogeneous chemical potential (non-uniform particle density) induces particle current, inhomogeneous temperature (non-uniform energy density) generates heat current (energy current), and inhomogeneous velocity profile (non-uniform momentum density) drives momentum current. These dissipative currents increase entropy and bring the system back to thermal equilibrium. When inhomogeneity of a potential (chemical potential, temperature, etc) is not strong so that the system is close to equilibrium, there is a linear relation between the current and the gradient of potential, which is called the generalized Fick's law (linear response). The proportionality constant is the transport coefficient (diffusivities, in case of dissipative transport). The transport coefficient is what experiments often measure and most theories compute.

Using Boltzamnn equation, we will compute the transport coefficients of a ultracold atomic gas. Also, using the exact diagonalization method, we will explicitly demonstrate the diffusive transport of energy density in a nonintegrable quantum system, Eq. 1.3.

1.3.2 Entanglement

Entanglement is one of the unique features of quantum mechanics that does not exist in classical physics. Originally quantum entanglement was viewed with some scepticism about local realism of quantum mechanics [39, 109], but recently the study of entanglement has become a central part of many-body quantum physics and quantum information science.

One way to quantify entanglement is the entanglement "entropy". In case of a pure state $|\psi\rangle$, the bi-partite entanglement entropy is defined by the following: Divide the entire space into two regions [8], A and B, then trace out one region A (or B). The remaining part can be written as a probability operator (a.k.a. density matrix) ρ_B (or ρ_A), and the entanglement entropy is the von Neumann entropy of the remaining probability operator.

$$\rho_B = Tr_A|\psi\rangle\langle\psi| \tag{1.13}$$

$$S_B = -\rho_B \log \rho_B = S_A \ . \tag{1.14}$$

Note that the entanglement entropy does not depend on whether we trace out the region A or B. For a spin-1/2 spin chain, usually we measure the entanglement entropy in bits (logarithm of base 2) so that maximum entanglement entropy between two spins is one.

Apparently, entanglement entropy is neither a conserved quantity nor a local obeservable [9]. Thus, it cannot be "transported" like energy or particle densities. This implies that the dynamics of entanglement can fundamentally be different from diffusive transport of local conserved observables. Previous works [70, 13] have demonstrated the existence of an upper bound to the rate of production of quantum "information". Thus, entanglement can only "spread", possibly faster than transport

[8] Division need not be in real space.

[9] There are two non-local operations: tracing out and computing entropy

of conserved quantities. As we will see later, entanglement spreading is faster than local energy transport while there still exists a notion of "locality" in entanglement spreading.

1.4 Thesis Outline

In this thesis, we study three aspects of nonequilibrium quantum dynamics. In chapter 2, we study the diffusive transport of ultracold cold atomic fermi gases. Especially, we consider a two-component fermi gas with population imbalance and a tunable inter-species interaction strength. Using Boltzmann equation, we first estimate the heat and spin conductivities and show that there is nontrivial transport, magneto-caloric effects, due to population imbalance and variable interaction strength. These nontrivial phenomena are the spin Seebeck effect, which is the spin current induced by an inhomogeneous temperature profile, and the spin Peltier effect, which is the heat current generated by spin voltage. We propose an experimental protocol to observe such phenomena.

In chapter 3, we study entanglement spreading in a diffusive nonintegrable quantum spin chain in one spatial dimension. Obtaining entire spectrum of eigenvalues and their eigenstates from full diagonalization of the Hamiltonian matrix, we show that entanglement spreading is ballistic while energy transport is diffusive. Although entanglement entropy is not a local quantity, we give a numerical evidence that local picture of entanglement spreading is indeed possible. In addition, we study the role of energy conservation in entanglement spreading and show that the later stage of entanglement spreading is indeed slowed down by the conservation law, even though entanglement is not a conserved quantity.

Finally, chapter 4 deals with more fundamental questions: how an isolated nonequilibrium quantum system approaches thermal equilibrium. First we review

and test one of the most widely accepted mechanisms of thermalization of isolated quantum system, the eigenstate thermalization hypothesis (ETH). Validating ETH, we next consider the time scale of thermalization. We explicitly construct a local operator which relaxes slowly, even slower than conventional diffusion suggests. We then discuss remaining open questions.

Chapter 2

Transport in Ultracold Atomic Gases: Boltzmann Equation

Kinetic theory of gases are mostly developed by three historic giants; Rudolf Clausius, James Clark Maxwell, and Lugwig Eduard Boltzmann. Since more than a century ago, namely the "Boltzmann Equation" has been one of the standard methods to analyze transport properties of interacting many particle systems. Relatively recently, around two decades ago, a new type of quantum system - ultracold atoms - is realized. Remarkable progresses in the field of ultracold atoms have opened a new window to study dynamics of strongly interacting quantum systems.

In this chapter, we investigate what we can learn from combining these two tools. The results of this chapter are published in the paper[59].

We set Boltzmann's constant $k_B = 1$ but explicitly keep Planck's constant $\hbar$.

2.1 Introduction

The transport properties of condensed matter systems are often measured by driving currents externally and measuring the resulting voltages or temperature differences. In cold atomic gas clouds, on the other hand, transport is more often measured by set-

ting up transient out-of-equilibrium initial conditions and measuring the subsequent relaxation towards equilibrium [116, 117, 96, 120, 122, 69]. In the approximation that the cloud is isolated and has an infinite lifetime (no loss of atoms or exchange of energy with any degrees of freedom outside of the gas cloud), the conserved currents of interest include the energy current and currents of each of the atomic species present. In the absence of optical lattices or random potentials that violate momentum conservation, one can also ask about the transport of momentum (viscosity).

In this chapter we consider the diffusive transport of heat and of atoms. We mostly focus on the case of a two-species Fermi gas with only inter-species contact interactions, but start with a somewhat more general discussion here. The system may, in addition to diffusive transport, also have underdamped or propagating sound or other "collective" modes. A gas cloud in a smooth trap will have such sound modes, with the longest-wavelength sound modes being the often-discussed collective modes of the cloud's oscillations within the trap. Here we consider a gas cloud in a smooth trap, with the cloud at global *mechanical* equilibrium, so that any pressure gradients in the cloud are sufficiently balanced by trapping forces that no underdamped sound or collective modes are excited. We also assume that the cloud is everywhere near *local* thermodynamic equilibrium, so the local temperature $T(\mathbf{r})$ and local chemical potentials $\mu_i(\mathbf{r})$ can be defined. However, the cloud may still have gradients in the local temperature and in the local chemical potentials of the various species of atoms. If the equilibrium equation of state of the system is known (for the unitary Fermi gas, see [66, 86]) then measurements of the local densities of each species allows these gradients of T and the μ_i's to be measured. Thus, for example, the local densities can be used as local thermometers to allow a measurement of the thermal diffusivity by an approach similar to that used in [116, 117] to measure the spin diffusivity (but with an initial temperature gradient instead of a composition gradient).

The transport currents that we examine in this chapter are those that arise in linear response to these gradients. In a trap, convection currents may also appear in linear response, as temperature and/or composition gradients may produce density inhomogeneities, and the "heavier" regions of the gas cloud will sink towards the bottom of the trap while the "lighter" regions rise. These convection currents are damped by the viscosity. Convection will be strongest in wide clouds and should be much weaker in high-aspect-ratio clouds with the gradients in T and the μ_i's oriented along the long axis of the cloud. For simplicity we restrict ourselves in a gas trapped in a spatially uniform potential, so such convection currents do not appear in linear response. Then mechanical equilibrium is indeed a sufficient condition to have a convectionless gas [115].

The structure of this chapter is the following: We first summarize the transport properties of a two-component ultracold Fermi gas. Using heuristic arguments, we qualitatively estimates the scaling of transport coefficients. Then, we thoroughly study the transport of this ultracold Fermi gas in dilute regime by finding quantitative solution of the Boltzmann equation. Our analysis reveals various transport coefficients in terms of interaction strength, densities, and temperature. By the end of the chapter, we have both qualitative and quantitative understandings of transport of spin and heat.

2.2 Transport Matrix and Qualitative Estimates of Transport Coefficients

Although finding quantitative solutions of dynamical problem of an interacting system is very challenging, we can find a fair amount of information by simply applying qualitative physical arguments.

2.2.1 Transport

The conservation laws of this Fermi gas are: total energy (E), total momentum ($\mathbf{\Pi}$), and the total number of each of the species ($N_\uparrow$ and $N_\downarrow$). The viscosity measures the transport of momentum, which we mostly do not consider here. Thus we consider primarily the transport of atoms and of heat. If there is a nonuniform pressure in the system that is not balanced by a trapping potential, the gas will accelerate and this will produce free motion or propagating sound waves. Here we consider the diffusive spin and heat transport in a gas with no trapping potential and spatially uniform pressure P, so it is at mechanical equilibrium. The gas is near *local* thermodynamic equilibrium, but with possible weak gradients in the local temperature and/or the spin polarization. A smooth trap potential may be added via the local density approximation (LDA).

In general, an inhomogeneity of the Fermi gas consists of gradients in the local temperature and of the local densities of the two atomic species. Mechanical equilibrium imposes a constraint on these gradients and thus there are only two independent linear combinations of the three gradients. One way of describing the diffusive dynamics is in terms of the atomic densities n_i and the currents $\mathbf{j}_i$ of each species $i =\uparrow,\downarrow$, leaving the temperature and the heat current implicit, since they are dictated by the equilibrium equation of state, e.g., $T(P, n_\uparrow, n_\downarrow)$ (temperature as a function of pressure P and densities $n_\uparrow$, $n_\downarrow$). This description of the transport has the virtue that it is in terms of what appears to be the most accessible local observables in experiment, namely the local densities of each species. Since the system in the absence of a trapping potential is Galilean-invariant, we have a certain amount of flexibility in what inertial frame we use to specify the currents. For most of this work, we consider the frame where the center of mass of the whole cloud is at rest and let the gas have long-wavelength temperature, density and/or composition modulations, but always with a spatially uniform pressure. The diffusive currents are related to the density

gradients as

$$\begin{pmatrix} \mathbf{j}_\uparrow \\ \mathbf{j}_\downarrow \end{pmatrix} = - \begin{pmatrix} \mathfrak{D}_{\uparrow\uparrow} & \mathfrak{D}_{\uparrow\downarrow} \\ \mathfrak{D}_{\downarrow\uparrow} & \mathfrak{D}_{\downarrow\downarrow} \end{pmatrix} \begin{pmatrix} \nabla n_\uparrow \\ \nabla n_\downarrow \end{pmatrix} \ . \tag{2.1}$$

The diffusion matrix in (1) has two eigenmodes. At zero polarization, the symmetry between $\uparrow$ and $\downarrow$ implies $\mathfrak{D}_{\uparrow\uparrow} = \mathfrak{D}_{\downarrow\downarrow}$ and $\mathfrak{D}_{\uparrow\downarrow} = \mathfrak{D}_{\downarrow\uparrow}$. Therefore one eigenmode is odd under exchanging species, $\frac{1}{\sqrt{2}}(1,-1)$; the current in this odd mode carries only spin and no net density or energy. The other eigenmode is the even mode, $\frac{1}{\sqrt{2}}(1,1)$; the current in this even mode carries both net density and energy, but no spin. Away from zero polarization, when $n_\uparrow \neq n_\downarrow$, we no longer have this symmetry between species. The diffusive eigenmodes are then no longer purely spin or purely not spin, instead they are mixtures, thus producing the spin Seebeck and Peltier effects. The eigenmode where the currents of the two species are in opposite directions we will call the "spin" mode with diffusivity $\mathfrak{D}_s$, while the other mode where they are parallel we will call the "thermal" (or heat) mode with diffusivity $\mathfrak{D}_T$.

Another standard representation of the transport matrix in terms of the heat current $\mathbf{j}_{heat}$ and spin current $\mathbf{j}_{spin}$ is the following:

$$\begin{pmatrix} \mathbf{j}_{heat} \\ \mathbf{j}_{spin} \end{pmatrix} = - \begin{pmatrix} \kappa & P_s \\ S_s & \sigma_s \end{pmatrix} \begin{pmatrix} \nabla T \\ \nabla(\mu_\uparrow - \mu_\downarrow) \end{pmatrix} \ , \tag{2.2}$$

where κ is the thermal conductivity and σ_s is the spin conductivity. S_s and P_s are the spin Seebeck and Peltier coefficients, respectively, and they are related by the Onsager relation, $P_s = TS_s$. This matrix explicitly shows the direct responses (diagonal elements) and magnetocaloric effects (off-diagonal elements), and the Kubo formula is explicit, as we discuss below.

The currents in (2) must be defined properly so that they are the transport currents, namely the currents of heat and spin relative to the average local motion of the gas. Let the local current density of atoms be $\mathbf{j}_n = \mathbf{j}_\uparrow + \mathbf{j}_\downarrow$. These atoms carry the

average heat, sT, where s is the average entropy per particle, and the average spin polarization p. Therefore the local heat and spin transport currents are

$$\mathbf{j}_{heat} = \mathbf{j}_\epsilon - \mu_\uparrow \mathbf{j}_\uparrow - \mu_\downarrow \mathbf{j}_\downarrow - sT\mathbf{j}_n \tag{2.3}$$

$$\mathbf{j}_{spin} = \frac{1}{2}\left(\mathbf{j}_\uparrow - \mathbf{j}_\downarrow - \frac{(n_\uparrow - n_\downarrow)}{n}\mathbf{j}_n\right) = \frac{n_\downarrow}{n}\mathbf{j}_\uparrow - \frac{n_\uparrow}{n}\mathbf{j}_\downarrow \ , \tag{2.4}$$

where $\mathbf{j}_\epsilon$ is the local energy current. Since the above currents measure only the transport relative to the average motion of the gas, they are *reference frame independent*. For more details of definitions of currents, see e.g. Ref [26].

If the full equation of state of the system is known, then measurements of the pressure and the local densities can be converted to local temperatures and chemical potentials. But the local density n and polarization p are directly observable without requiring knowledge of the equation of state, so yet another convenient form of the transport equations is

$$\begin{pmatrix} \mathbf{j}_{heat} \\ \mathbf{j}_{spin} \end{pmatrix} = - \begin{pmatrix} \kappa' & P_s' \\ S_s' & D_s \end{pmatrix} \begin{pmatrix} \nabla T \\ n\nabla p \end{pmatrix} \ . \tag{2.5}$$

At $p = 0$, we have $\kappa' = \kappa$ and $D_s = \mathfrak{D}_s$, but when $p \neq 0$ these quantities in general differ due to the mixing between spin and heat transport. It is possible that S_s' is the most directly accessible version of the spin Seebeck coefficient: if one can set up an initial condition at mechanical equilibrium and local thermodynamic equilibrium with a temperature gradient but no polarization gradient and then measure the resulting spin current, this is a measurement of S_s' and does not require knowledge of the equation of state.

Note that the three representations, Eq. (2.1), Eq. (2.2) and Eq. (2.5) are related by the equation of state, the mechanical equilibrium condition, and definitions of spin and heat currents. Hence, they are *equivalent*.

2.2.2 Qualitative Estimates of Transport Coefficients

Before embarking detailed calculation, we first present rough "power-counting" estimates of four transport coefficients; thermal diffusivity, spin diffusivity, and two magnetocaloric effects. Most of past work in the context of ultracold atoms have focused on the spin diffusivity.

Let's first estimate spin and thermal diffusivities, D_s and D_T. At the level of power-counting the differences between the various possible definitions of these diffusivities are small and are ignored here. Previous work [116, 15] on the unpolarized gas ($p = 0$) shows that D_s for $T > T_F$ is the larger of $\frac{\hbar}{m}(\frac{T}{T_F})^{3/2}$ and $\frac{\hbar}{mk_F^2a^2}\sqrt{\frac{T}{T_F}}$. In the recent experiment, which was performed at unitarity [116], this high-T behavior is observed, with significant deviations apparently beginning between $T = 2T_F$ and T_F as T_F is approached from above. Staying in this high-T regime, as we move to high polarization (p near 1) at a given n and T, the scattering time of species i is roughly $\tau_i \sim \frac{1}{n_j\sigma v_r}$ where $i \neq j$ and $v_r = |\mathbf{v}_\uparrow - \mathbf{v}_\downarrow|$ and σ is the $s-$wave scattering cross section (see Eq. (2.12)) evaluated at a typical value of momentum. Thus, the scattering time of the down atoms $\tau_\downarrow$ decreases by only a factor of two due to the increase of the density $n_\uparrow$ of the up atoms that they scatter from. The up atom scattering time $\tau_\uparrow$, on the other hand, increases by a factor of $n_\uparrow/n_\downarrow$ as the down atoms that they scatter from become dilute. At high polarization, the spin current consists of the down atoms moving with respect to the up atoms at typical speed $v_\downarrow \sim \sqrt{T/m}$, so $D_s \sim v_\downarrow^2\tau_\downarrow$ is not strongly polarization dependent for $T > T_{F\downarrow}$; the experimental results [116, 117] are consistent with this. The heat, on the other hand, is mostly carried by the up atoms at high polarization, resulting in $D_T \sim D_s n_\uparrow/n_\downarrow$, a relation between the two diffusivities that appears to remain true at high polarization for all T away from the superfluid phases. At $p = 0$ and high T the two diffusivities are comparable, but D_T remains larger than D_s because a single s-wave scattering event completely randomizes the total spin current carried by the two atoms, while

the component of the heat current carried by their center of mass is preserved. Thus it appears that the heat mode always diffuses faster than the spin mode.

Moving towards lower T, let's next pause at $T = T_{F\uparrow}$, noting that here $v_\uparrow \sim v_\downarrow \sim \sqrt{T/m}$, and $\tau_\downarrow$ is the larger of $\frac{\hbar}{T}$ and $\frac{\hbar}{Tk_F^2a^2}$. For the polarized gas $\tau_\uparrow \sim \tau_\downarrow n_\uparrow/n_\downarrow$.

We next (still just power-counting) look at the polarized gas in the intermediate temperature regime $T_{F\downarrow} < T < T_{F\uparrow}$ where the majority atoms are degenerate ($v_\uparrow \sim \sqrt{T_{F\uparrow}/m}$), while the minority atoms are not ($v_\downarrow \sim \sqrt{T/m}$). Some changes from the high-T regime are: only up atoms with energy within $\sim T$ of $T_{F\uparrow}$ are involved in the scattering and all but a fraction $T/T_{F\uparrow}$ of the final states of the scattering are Pauli-blocked due to the degeneracy of the up atoms. This increases $\tau_\downarrow$ by a factor of $(T_{F\uparrow}/T)^2$, and $\tau_\uparrow$ by a factor of $T_{F\uparrow}/T$, compared to their values at $T = T_{F\uparrow}$. Thus, $\tau_\downarrow$ is the larger of $\frac{\hbar}{T_{F\uparrow}}\left(\frac{T_{F\uparrow}}{T}\right)^2$ and $\frac{\hbar}{T_{F\uparrow}k_{F\uparrow}^2a^2}\left(\frac{T_{F\uparrow}}{T}\right)^2$. As a result, $D_s \sim v_\downarrow^2\tau_\downarrow$ is the larger of $\frac{\hbar T_{F\uparrow}}{mT}$ and $\frac{\hbar T_{F\uparrow}}{mTk_{F\uparrow}^2a^2}$, while D_T is again larger than D_s by a factor $n_\uparrow/n_\downarrow$. This estimate of D_s is consistent with a previous quantitative calculation [17, 60]. Note that the temperature dependence of D_s crosses over from a decreasing function of T at low T to an increasing function at high T. The recent measurements [117] of the spin drag in a polarized unitary gas show this crossover occurring at roughly $T = 0.4T_{F\uparrow}$. On the BEC side of the Feshbach resonance, the minority atoms bind in to bosonic Feshbach molecules at low enough T. But as long as these molecules remain nondegenerate and thus not superfluid, the above estimates of the diffusivities should hold.

For $T < T_{F\downarrow}$, the minority atoms become degenerate. This leads to superfluidity on the BEC side of the Feshbach resonance as well as at low polarization near unitarity. But there are regimes on the BCS side of the resonance as well as near unitarity at high polarization where the minority atoms (near unitarity strongly "dressed" as polarons) form a degenerate Fermi gas. Here the important change from the intermediate temperature regime at the level of "power-counting" is that only minority atoms with energy within $\sim T$ of $T_{F\downarrow}$ are involved in the scattering and they have momentum

$k_{F\downarrow}$ instead of a thermal momentum. This increases the diffusivities by a factor of $T_{F\downarrow}/T$, so the spin diffusivity in these degenerate Fermi liquid regimes is the larger of $\frac{\hbar T_{F\uparrow}T_{F\downarrow}}{mT^2}$ and $\frac{\hbar T_{F\uparrow}T_{F\downarrow}}{mT^2 k_{F\uparrow}^2 a^2}$. We expect that D_T is still greater than D_s by a factor of $n_\uparrow/n_\downarrow$ but this question should be examined more carefully within Fermi liquid theory.

At low temperature, the polarized Fermi liquid may become a p-wave superfluid, with pairing within one species mediated by the attraction to the other species [20]. Or it may have a Fulde-Ferrell-Larkin-Ovchinnikov (FFLO) phase with Cooper pairs of nonzero total momentum [110, 19, 68]. In the superfluid phases, the thermal diffusivity should diverge to infinity, as heat is carried ballistically by second sound modes. The spin diffusivity presumably remains finite in the superfluid phases, although, as we discuss below, the spin Seebeck effect appears to generally be divergent in a polarized superfluid.

More challenging to estimate than these spin and thermal diffusivities are the effects that mix spin and heat transport, namely the spin Seebeck and the spin Peltier effects. Here we present "simple" arguments for the signs of these effects in two regimes: (1) far away from unitarity for all temperature ranges, and (2) at unitarity in the classical regime. Here we always consider a spin-polarized gas, since these "magnetocaloric" effects vanish by symmetry in the case of an unpolarized gas where the two species also have equal mass.

(1) Well away from unitarity ($|k_F a| \ll min\{1, \sqrt{T_F/T}\}$), the scattering cross section is essentially a^2 and independent of momentum for all temperatures, since the interaction is weak and the atoms are not thermally excited to $\lambda < |a|$. Generally, the scattering rate is proportional to the *cross section* $\times$ *relative speed*. Thus, in this (low energy) regime, the scattering rate is $\sim a^2|\mathbf{v}_\uparrow - \mathbf{v}_\downarrow|$. This implies minority atoms will scatter more frequently with the majority atoms of higher energy than majority atoms of lower energy since higher-energy majority atoms have higher relative speed. Consequently, the direction of the minority current is along the flow of higher-energy

("hot") majority atoms and thus parallel to the heat current. For a uniformly spin-polarized gas with a temperature gradient, where the spin Seebeck effect occurs, the primary current is the heat current transporting "hot" majority atoms from the hot region to the cold region and transporting "cold" majority atoms from the cold region to the hot region. The fact that the minority current is aligned with that of the "hot" majority atoms means the direction of the net spin current (spin Seebeck current) is opposite from that of the heat current. Thus, the initially cold region becomes less polarized due to minority atoms transported by the spin Seebeck current.

For a polarized gas with a polarization gradient but zero temperature gradient, where the spin Peltier effect occurs, the primary current is the spin current which transports minority atoms from the less-polarized region to the more-polarized region. Since again these minority atoms scatter more often with "hot" majority atoms, the resulting heat current is towards the more-polarized region, resulting in a spin Peltier (heat) current whose direction is opposite to the primary spin current. In summary, for a gas far from unitarity, the primary currents and the magnetocaloric currents are in opposite directions. In other words, the off-diagonal elements in Eq. (2.5) are negative while the diagonal elements are positive.

(2) At high temperatures ($T \gg T_{F\uparrow}$) and near unitarity ($|k_F a| \gg k_F\lambda > 1$), the s-wave scattering cross section is $1/(k_r/2)^2$ and thus is momentum-dependent, where $k_r = |\mathbf{k}_\uparrow - \mathbf{k}_\downarrow|$ is the relative momentum. Therefore, the scattering rate is roughly $\sim \frac{1}{k_r^2} \times v_r \sim \frac{1}{k_r}$. As a result, now minority atoms scatter more often with "cold" majority atoms. Since this is exactly the opposite from the case of far away from unitarity, the spin Seebeck and spin Peltier currents are reversed relative to the above discussion in (1). Therefore, at high temperature and unitarity, the primary currents and the magnetocaloric currents are in the same directions, giving S_s' in Eq. (2.5) positive sign. As we will see in the next section, the spin Peltier coefficient P_s' in Eq. (2.5) is negative for low polarization and becomes positive for high polarization.

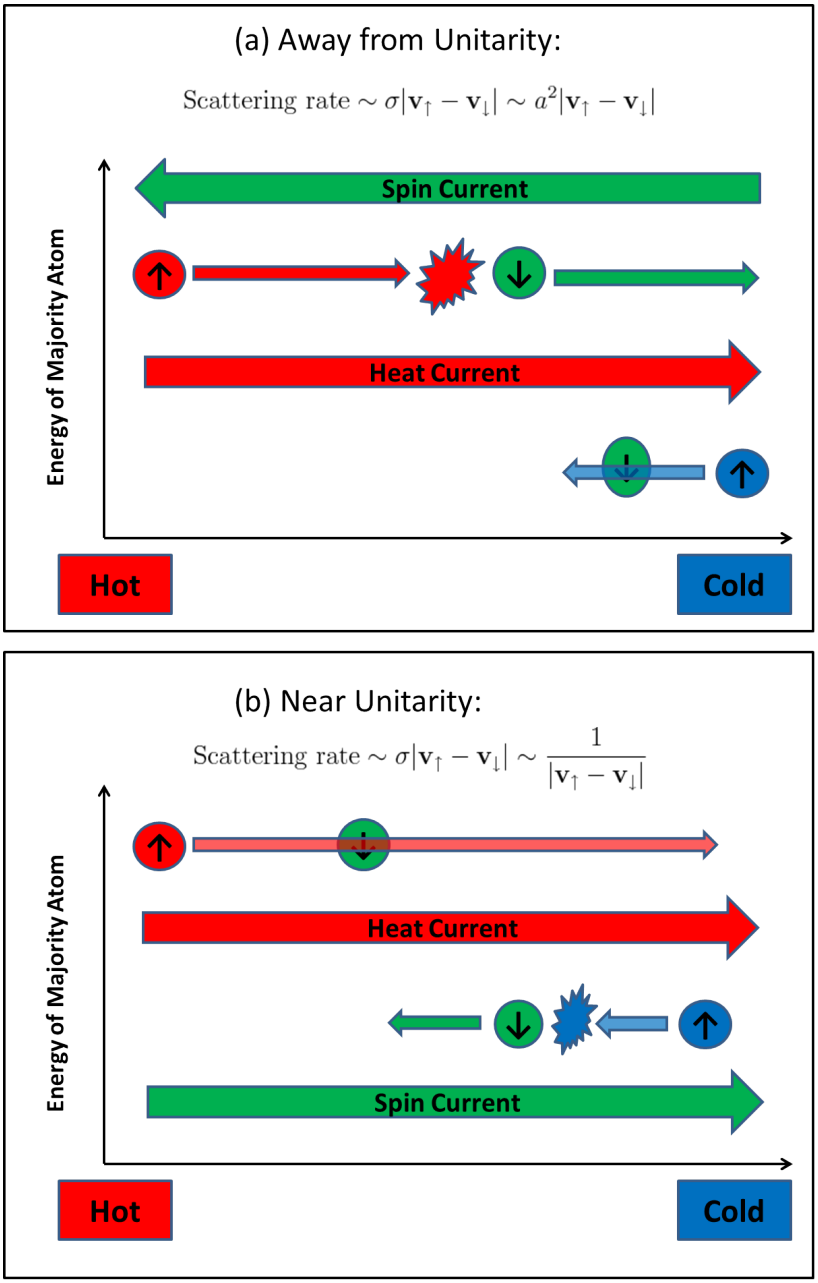

Figure 2.1: Illustration of the spin Seebeck effect. (a) Far away from unitarity, the scattering rate is proportional to the relative speed. Thus, "hot" majority ($\uparrow$) atoms (top) collide more often with minority ($\downarrow$) atoms than do "cold" majority atoms (bottom), giving the spin Seebeck current and the heat current opposite directions. (b) At unitarity, the scattering rate is inversely proportional to the relative speed. Therefore, the direction of the spin Seebeck current is reversed relative to (a).

This sign change in P_s' comes from the definition of currents and choice of driving forces and this will be clarified in the section 2.3 where we discuss the Kubo approach. Directions of the spin Seebeck effect in both limiting regimes are illustrated in figure 2.1.

At low temperatures and unitarity, it is not straightforward to apply the above argument to predict the direction of spin Seebeck and/or spin Peltier currents since the many body effects may significantly modify the scattering cross section [16, 30], which begins to depend on the center of mass momentum as well as the relative momentum. There is, however, a different line of argument that indicates that the sign of the spin Seebeck effect near unitarity remains the same as the temperature is lowered. Consider low enough temperatures and polarization less than the Chandrasekhar-Clogston limit [32, 27], in the superfluid phase [129, 113]. When there is a temperature gradient in the system, heat flows "ballistically" from the hot region to the cold region by flow of the normal fluid with respect to the superfluid (in the usual two-fluid description of the superfluid phase). In the reference frame where the total particle density current vanishes (center of mass frame), the superfluid flows in the opposite direction to counterbalance the mass current of the normal fluid. Since the s-wave superfluid consists of equal numbers of majority and minority atoms, both the spin current and the heat current are carried only by the normal fluid. As a result, the spin Seebeck current and the heat current are in the same directions at low temperature in and, presumably, near the superfluid phase. Therefore, we expect the sign of the spin Seebeck effect to remain the same for all temperatures at unitarity. Both the thermal conductivity and the spin Seebeck coefficient will diverge at the transition to the superfluid phase.

As another approach to these questions, there is an interesting artificial interaction, namely the Maxwellian interaction where the scattering cross section is proportional to $1/v_r$ and the Boltzmann equation can be solved exactly in the high

temperature limit. Since the scattering rate does not depend on relative velocity ($(1/v_r) \times v_r$ = constant), there are no spin Seebeck or spin Peltier currents in this case. Then, if we perturb the scattering cross section around the Maxwellian case, putting in an additional relative-velocity dependence to the scattering rate "by hand", we can perturbatively calculate the spin Seebeck and spin Peltier currents and manipulate the direction of these currents by changing the sign of the perturbation. This allows us to explicitly show how the magnetocaloric currents are generated from a relative-velocity-dependent cross section. This will be discussed in the following section in detail.

2.3 Spin and Heat Transport of a Two Component Fermi Gas - Quantitative Results

Quite generally, a temperature gradient drives a heat current and a gradient of chemical potential difference drives a composition ("spin") current, consisting of opposing currents of the two (or more) atomic species. We call these "direct" responses to a temperature gradient and a gradient of chemical potential difference "primary currents". In addition to these "primary currents", there are the magnetocaloric currents, namely spin Seebeck currents (spin currents induced by a temperature gradient) and spin Peltier currents (heat currents induced by gradients of chemical potential difference). These magnetocaloric effects have been one of the central research topics in the field of spintronics [128]. The spin Seebeck effect [62, 123] and the spin Peltier effect [42] have already been observed in condensed matter systems, while they are yet to be detected in cold atomic clouds. In this section we discuss the origin and the physics of these effects in a cold atomic Fermi gas, and estimate how large these effects can be in realistic experiments.

Note that Ref. [23] discusses a rather different situation that they are also calling the "spin Seebeck effect": they consider an unpolarized gas with the two species at different temperatures (thus *not* in *local* equilibrium) and a gradient in this temperature difference. Also, Ref. [49] studies a different system, a "two terminal geometry", considering transport through a narrow constriction between two reservoirs held at different temperatures and chemical potentials. For this constriction, they discuss "off-diagonal" elements in the transport matrix which they call effective Seebeck and Peltier effects.

In the following subsection, these qualitative descriptions are justified by approximate solutions of the Boltzmann transport equation in the classical regime. We then compute experimentally verifiable signals of the spin Seebeck effect. These results are tested against an exactly solvable model, namely atoms with a "Maxwellian" scattering cross section.

The various effects discussed in this section are probably most accessible experimentally for the unitary Fermi gas at temperatures of order the Fermi temperature, where the diffusivities are at their smallest, so the diffusive relaxation towards equilibrium is slowest and most easily studied.

2.3.1 Linearized Boltzmann equation and its scaling

Now we are ready to quantitatively confirm the previous qualitative argument by extensive usage of the Boltzmann equation.

In the limit of high temperature $T \gg T_F$, the gas is effectively classical, and its dynamics obey the Boltzmann equation. In the absence of external forces but with gradients in local temperature and local densities, the steady-state Boltzmann

equation for species i ($i =\uparrow$ or $\downarrow$) is the following ($i \neq j$):

$$\frac{\hbar}{m}\mathbf{k}_i \cdot \nabla f_i = \int \frac{d^3\mathbf{k}_j}{(2\pi)^3} d\sigma \frac{\hbar|\mathbf{k}_\uparrow - \mathbf{k}_\downarrow|}{m}(f(\mathbf{k}'_\uparrow)f(\mathbf{k}'_\downarrow) - f(\mathbf{k}_\uparrow)f(\mathbf{k}_\downarrow)), \tag{2.6}$$

where $f(\mathbf{k}_i)$ is the momentum distribution of species i, and the velocity is $\mathbf{v}_i = \hbar\mathbf{k}_i/m$. $\mathbf{k}'_\uparrow$ and $\mathbf{k}'_\downarrow$ are momenta after collision and satisfy the energy momentum conservation. Working near equilibrium, we linearize the Boltzmann equation by introducing a small deviation ψ_i:

$$f_i = f_i^0(1 + \psi_i), \tag{2.7}$$

where f_i^0 is the equilibrium distribution. In this high temperature regime, the equilibrium distribution is the Boltzmann distribution, $f_i^0(k) = n_i\lambda^3 \exp(-E(k)/T)$ and $E(k) = \frac{\hbar^2k^2}{2m}$ where $\lambda = \sqrt{2\pi\hbar^2/(mT)}$ is the thermal de Broglie wavelength. Since the most relevant length scale in the classical regime is the thermal de Broglie wavelength λ, it is convenient to scale the wave vector $\mathbf{k}$ with λ; $\mathbf{k} = \mathbf{q}/\lambda$. Then, $E(q)/T = \frac{q^2}{4\pi}$.

Let's impose the mechanical equilibrium condition. In this classical limit, it is enough to use the ideal gas pressure at equilibrium; $P = nT = (n_\uparrow + n_\downarrow)T$. From the spatially uniform pressure condition we can relate the density gradients and the temperature gradient via

$$\frac{\nabla n}{n} = -\frac{\nabla T}{T}, \tag{2.8}$$

to linear order in the gradients. This relation enables us to express the currents in terms of any two linearly-independent "driving" terms such as $(\nabla n_\uparrow, \nabla n_\downarrow)$, $(\nabla T, n\nabla p)$, $(\nabla T, \nabla(\mu_\uparrow - \mu_\downarrow))$ or any other convenient combinations. It is convenient to work with $(\nabla n_\uparrow, \nabla n_\downarrow)$ in intermediate stages of the calculation and then transform it to the desired combination of driving forces using the equilibrium equation of

state. Then the λ scaled linearized Boltzmann equations we need to solve become

$$\frac{1}{n_i}\nabla n_i \cdot \mathbf{q}_i - \frac{1}{n}\left(\frac{q_i^2}{4\pi} - \frac{3}{2}\right)\nabla n \cdot \mathbf{q}_i = n_j \int \frac{d^3\mathbf{q}_j}{(2\pi)^3} d\sigma e^{-q_j^2/4\pi}(\psi'_\uparrow + \psi'_\downarrow - \psi_\uparrow - \psi_\downarrow)|\mathbf{q}_\uparrow - \mathbf{q}_\downarrow| \ , \tag{2.9}$$

with $i \neq j$. ψ'_i takes $\mathbf{q}'_i$ as an argument.

We follow the standard definitions of the particle and energy currents of each species [1],

$$\mathbf{j}_i = \int \frac{d^3\mathbf{k}_i}{(2\pi)^3} f_i \mathbf{v}_i = n_i \int \frac{d^3\mathbf{q}_i}{(2\pi)^3} e^{-q_i^2/4\pi}\psi_i \frac{\hbar}{m}\frac{\mathbf{q}_i}{\lambda} \tag{2.10}$$

$$\mathbf{j}_{\epsilon i} = \int \frac{d^3\mathbf{k}_i}{(2\pi)^3} f_i \mathbf{v}_i E_i = n_i \frac{T}{4\pi} \int \frac{d^3\mathbf{q}_i}{(2\pi)^3} e^{-q_i^2/4\pi}\psi_i \frac{\hbar}{m}\frac{q_i^2\mathbf{q}_i}{\lambda} \ . \tag{2.11}$$

Because of Galilean invariance, we need to specify an inertial frame. Except when specified otherwise, we work in the frame where the local particle current is zero: $\mathbf{j}_n = \mathbf{j}_\uparrow + \mathbf{j}_\downarrow = \mathbf{0}$.

2.3.2 Approximate Solution

The s-wave scattering cross section that captures most physics of a short-range interaction is

$$\frac{d\sigma}{d\Omega} = \frac{a^2}{1 + \left(\frac{k_r a}{2}\right)^2} = \lambda^2 \frac{(a/\lambda)^2}{1 + \left(\frac{q_r a}{2\lambda}\right)^2} \ , \tag{2.12}$$

where we scaled the scattering length a with λ. An exact solution of the Boltzmann equation for such a cross section is not known and thus we need to resort to approximation methods. One of the standard ways to find an approximate solution of a linearized Boltzmann equation is the moment expansion method (for example, see [31]). Considering all symmetries and assuming the true solution is analytic near

[1] In the limit of high temperature, a gas is still dilute enough so that kinetic energy gives the dominant contribution to the total energy. This is a necessary condition to use the Boltzmann approach.

small $\mathbf{q}$, we take the following ansatz for ψ_i ($i =\uparrow,\downarrow$):

$$\psi_i = -\lambda \sum_{j=\uparrow,\downarrow} \sum_{\ell=0}^{L} C_{\ell ij} q_i^{2\ell} \frac{\nabla n_j \cdot \mathbf{q}_i}{n_j} \ . \tag{2.13}$$

We only consider the case where $\nabla n_\uparrow$ and $\nabla n_\downarrow$ are both parallel to the z axis. We need to determine the dimensionless coefficients $\{C_{\ell ij}\}$.

The procedure to obtain an approximate solution of the Boltzmann equation is the following: First, insert the above ansatz into the right hand side of Eq. (2.9). Then multiply both sides of Eq. (2.9) by $q_i^{2\ell} q_{iz} \frac{1}{(2\pi)^3} \exp[-q_i^2/4\pi]$ ($\ell = 0, 1, 2, ...L$) and integrate out all momenta. Matching coefficients of density gradients gives $4(L+1)$ linear equations for the $\{C_{\ell ij}\}$, all of which, however, are not linearly independent due to Galilean invariance. We need to fix the reference frame to uniquely determine a solution. Once we choose an appropriate reference frame (usually $\mathbf{j}_\uparrow + \mathbf{j}_\downarrow = 0$), we have $4(L+1)$ linearly independent equations for the $\{C_{\ell ij}\}$. Determining the $\{C_{\ell ij}\}$, we have an approximate solution to the Boltzmann equation, *i.e.* an approximate momentum distribution from which we can calculate all currents of interest. Here we present results of two limiting cases, far away from unitarity ($\frac{d\sigma}{d\Omega} = a^2$) and at unitarity ($\frac{d\sigma}{d\Omega} = \frac{4}{k_r^2}$), which allow an analytic solution (of this approximation) without special functions. These correspond to the two limits $\lambda/|a| \gg 1$ and $\lambda/|a| \ll 1$, respectively. For a general scattering length a, it is still possible to find a closed form expression in terms of exponential integrals and incomplete Gamma functions whose arguments depend on $\lambda/|a|$.

Obtaining $C_{\ell ij}$ from a straightforward calculation in the $\mathbf{j}_\uparrow + \mathbf{j}_\downarrow = 0$ frame, we can express the heat current and spin current in terms of $\nabla n_\uparrow$ and $\nabla n_\downarrow$. Here we choose to express final results in the format of Eq. (2.5) since we want to study the spin Seebeck coefficient S_s' in detail, which could be the most directly accessible signature of the spin Seebeck effect in experiments. Therefore, we transform these two gradients to

∇T and $n\nabla p$, using the equilibrium equation of state and the mechanical equilibrium condition. The transformation matrix is

$$\begin{pmatrix} \nabla n_\uparrow \\ \nabla n_\downarrow \end{pmatrix} = \begin{pmatrix} -\frac{T}{n} & -\frac{T}{n} \\ \frac{2n_\downarrow}{n} & -\frac{2n_\uparrow}{n} \end{pmatrix}^{-1} \begin{pmatrix} \nabla T \\ n\nabla p \end{pmatrix} . \tag{2.14}$$

Since the left hand side of Eq. (2.9) is a third-order polynomial in q, the simplest ansatz is with $L = 1$. In principle, we can go up to any order in L we want, but an $L \geq 2$ ansatz complicates the computation, while the simplest ansatz already exhibits nontrivial results. Furthermore, we find that the change in S'_s on moving from the $L = 1$ to the $L = 2$ approximation is quite small: about a 1% change near unitarity and in the value of $\lambda/|a|$ at the zero crossing, growing to near 7% far from unitarity. Therefore, here we only present results of $L = 1$.

We present our results in the conventional format (without λ scaling): Near unitarity ($|a| \gg \lambda$),

$$\begin{pmatrix} \mathbf{j}_{heat} \\ \mathbf{j}_{spin} \end{pmatrix} = -\frac{45\pi^{3/2}}{608\sqrt{2}} \left(\frac{\hbar}{m}\left(\frac{T}{T_F}\right)^{3/2}\right) \begin{pmatrix} \kappa'_u & \frac{1}{2}\frac{(n_\uparrow - n_\downarrow)Tn}{n_\uparrow n_\downarrow} - \frac{39}{10}T\ln\left(\frac{n_\uparrow}{n_\downarrow}\right) \\ \frac{(n_\uparrow - n_\downarrow)}{T} & \frac{39}{10} \end{pmatrix} \begin{pmatrix} \nabla T \\ n\nabla p \end{pmatrix} , \tag{2.15}$$

where κ'_u (proportional to the thermal conductivity at unitarity) is

$$\kappa'_u = \frac{5}{16}n\left(\frac{(73n_\uparrow^2 + 82n_\uparrow n_\downarrow + 73n_\downarrow^2)}{n_\uparrow n_\downarrow}\right) - (n_\uparrow - n_\downarrow)\ln\left(\frac{n_\uparrow}{n_\downarrow}\right) . \tag{2.16}$$

Far away from unitarity ($|a| \ll \lambda$),

$$\begin{pmatrix} \mathbf{j}_{heat} \\ \mathbf{j}_{spin} \end{pmatrix} = -\frac{15\pi^{3/2}}{224\sqrt{2}} \left(\frac{\hbar}{m(k_F a)^2} \sqrt{\frac{T}{T_F}} \right) \times \begin{pmatrix} \kappa_a' & -\frac{1}{2}\frac{(n_\uparrow - n_\downarrow)Tn}{n_\uparrow n_\downarrow} - \frac{43}{10} T \ln\left(\frac{n_\uparrow}{n_\downarrow}\right) \\ -\frac{(n_\uparrow - n_\downarrow)}{T} & \frac{43}{10} \end{pmatrix} \begin{pmatrix} \nabla T \\ n\nabla p \end{pmatrix}, \tag{2.17}$$

where κ_a' (proportional to the thermal conductivity far away from unitarity) is

$$\kappa_a' = \frac{5}{8} n \left(\frac{(29 n_\uparrow^2 + 26 n_\uparrow n_\downarrow + 29 n_\downarrow^2)}{n_\uparrow n_\downarrow} \right) + (n_\uparrow - n_\downarrow) \ln\left(\frac{n_\uparrow}{n_\downarrow}\right). \tag{2.18}$$

The above matrices clearly exhibit the existence of the spin Seebeck and spin Peltier effects (non-vanishing off diagonal terms) only for nonzero polarization. We will mostly focus now on the spin Seebeck coefficient S_s', which gives the spin current due to a temperature gradient in the absence of a spin polarization gradient.

As argued in the previous section, the spin Seebeck coefficient changes sign as a function of interaction strength. Near unitarity (Eq. 2.15), it is positive so the spin Seebeck current and the heat current are in the same direction. Far away from unitarity (Eq. 2.17), it is negative so the spin Seebeck current and the heat current are in the opposite direction.

Next let's consider the polarization dependence of the transport coefficients. The heat current and the temperature gradient are even under spin index exchange while the spin current and the polarization gradient are odd. Therefore, thermal conductivity and spin diffusivity are even functions of polarization while magnetocaloric effects are odd functions of polarization. The above matrices satisfy these polarization parity constraints and the form of the polarization dependence of the transport coefficients is the same in both limits of large and small $\lambda/|a|$. In fact, we can show that the polarization dependence (thus $n_\uparrow$ and $n_\downarrow$ dependence) of the transport coefficients

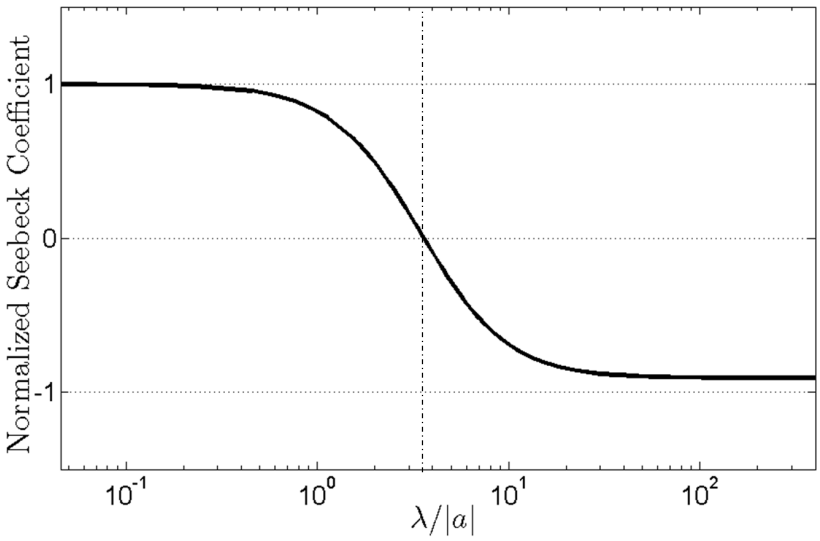

Figure 2.2: Normalized Seebeck coefficient S'_s as a function of $\lambda/|a|$ in the classical regime. The normalization is by a factor of $\frac{15}{608\sqrt{2}}\left(\frac{\hbar}{m}\frac{1}{T\lambda^3}\frac{1+4\pi(a/\lambda)^2}{(a/\lambda)^2}\right)\frac{(n_\uparrow-n_\downarrow)}{n}$. This choice of normalization, which is inversely proportional to a typical value of scattering cross section with scaled scattering length a/λ, gives finite values at both limits and gives the Seebeck coefficient 1 at unitarity (Eq. (2.15)). We can see that S'_s changes sign near $\lambda/|a| \simeq 3.62$. Since we factored out all explicit temperature and polarization dependence in the normalization choice and scaled the scattering length, this plot remains the same for all temperature and polarization ranges at this order of approximation ($L = 1$).

maintains this form for all values of $\lambda/|a|$ and to all orders of approximation. The proof is given in Appendix A. Here we study the Seebeck coefficient S'_s in detail, which is our prime interest.

Although it is conventional to scale the scattering length a with k_F (as we did in the above matrices), it is easier to see the structure of the Seebeck coefficient in terms of $\lambda/|a|$ in classical regime. Once we obtain an approximate solution of the Boltzmann equation with a general $\lambda/|a|$ and $L = 1$, we can explicitly show that

$$S'_s = \frac{\hbar}{m}\frac{n_\uparrow - n_\downarrow}{n\lambda^3}\frac{1}{T}h_1(\lambda/|a|) \ , \tag{2.19}$$

where $h_1(x)$ is a dimensionless function that contains $Ei(x)$, the exponential integral, and diverges as $\lambda/|a| \to \infty$ (see Eq. (2.17)). Since it contains no explicit temperature or polarization dependence, $h_1(x)$ is independent of polarization and temperature at this order of approximation ($L = 1$). Therefore, once we scale the scattering length by λ and factor out dimensionful parameters and polarization, the dependence of S_s' on the scattering length is determined by $h_1(x)$ and the value of $\lambda/|a|$ at which S_s' crosses zero is solely determined by the equation $h_1(x) = 0$, which is independent of temperature and polarization. In the $L = 1$ approximation, the zero-crossing value is $\lambda/|a| \simeq 3.62$. Figure 2.2 is a plot of the normalized S_s' as a function of $\lambda/|a|$. In the $L = 2$ approximation, we find that the scaling function $h_1(x)$ slightly changes to $h_2(x)$ and the zero-crossing point remains at $\lambda/|a| \simeq 3.62$. In Appendix A, we show that the structure of Eq. (2.19) (and other transport coefficients in a similar manner) remains to all orders of approximation. Therefore, we may conclude that in this classical regime the Seebeck coefficient is linearly proportional to the polarization p and inversely proportional to $T\lambda^3$, once we scale the scattering length by λ.

Note that Eqs. (2.15) and (2.17) do not explicitly satisfy the Onsager relation and the spin Peltier coefficient P_s' is still negative for low polarization even near unitarity. These come from the definition of diffusive currents and choice of representation and will be discussed in detail in the next section in terms of the Kubo formula. For now, we will focus on the spin Seebeck coefficient S_s' which appears to be the most promising candidate of the magnetocaloric effects to be detected in experiments.

From the Einstein relation, we obtain the thermal diffusivity D_T after dividing κ_u' and κ_a' by $C_P = 5n/2$, the heat capacity per volume at fixed pressure and polarization. These results confirm the "power-counting" estimates of diffusivities: In case of an unpolarized gas ($n_\uparrow = n_\downarrow$), D_s at unitarity is $\cong 1.1\frac{\hbar}{m}\left(\frac{T}{T_F}\right)^{3/2}$, which is consistent with previous work [116, 15]. Also, the thermal diffusivity does satisfy the inequality,

$D_T > D_s$ at zero polarization. Furthermore, for a highly polarized gas ($n_\uparrow \gg n_\downarrow$), $D_T \sim \frac{n^2}{n_\uparrow n_\downarrow} D_s \sim \frac{n_\uparrow}{n_\downarrow} D_s$, which is also as expected from the "power-counting" estimates.

2.3.3 Estimate of the Spin Seebeck Effect

The spin Seebeck effect seems to be more accessible to experiment than the spin Peltier effect, since the measurement of spin currents has already been done [116, 117] and seems more straightforward than measuring heat currents. Also, the spin mode diffuses slower than the heat mode, so the change in spin polarization produced by the spin Seebeck effect will relax slowly, enhancing its detectability. An initially fully equilibrated spin-polarized gas could be heated at one end, producing a temperature gradient, and then the resulting spin current could be measured if it is large enough.

Let's make quantitative estimates of signatures of the spin Seebeck effect that are relevant to such a proposed experiment. We will make our estimates for a gas in a uniform potential, but the results should be roughly correct for a gas cloud in a trap if one compares points at opposite ends of the cloud that are at the same potential so will have the same local densities and polarization at equilibrium. First, apply a small, long wavelength temperature inhomogeneity along the z axis. In mechanical equilibrium, nonuniform temperature implies nonuniform total density (by Eq. (2.8)), thus temperature modulation implies density modulation. This enables us to write the initial total density as

$$n(t = 0, z) = n_0 + \delta n_0 \cos wz, \tag{2.20}$$

where w ($= \pi/M$) is the wavenumber of the modulation, M is the length of the system over which the full temperature difference is applied, and δn_0 is the small deviation of total density from the mean value n_0 due to this temperature difference (at uniform pressure). Eq. (2.8) implies that if we initially locally heat $z = M$ relative to $z = 0$,

then this location initially has lower density because of thermal expansion. From the initial condition of uniform polarization, the density of each spin component at $t = 0$ is

$$n_i(t = 0, z) = n_{i0} + \delta n_{i0} \cos wz \tag{2.21}$$

$$\delta n_{i0} = \frac{n_{i0}}{n_0} \delta n_0. \tag{2.22}$$

where δn_0 is the maximum value of total density deviation from the average density.

In order to calculate the change of densities of each species, which is directly measurable in experiment and contains the signature of the spin Seebeck effect, we need the space-time dependence of the density of each species. We will use the diffusion matrix and the continuity equation to derive the space-time dependence of densities. Since the continuity equation for the particle number density is $\partial_t n_i + \nabla \cdot \mathbf{j}_i = 0$, it is practical to write diffusion equation in the format of Eq. (2.1). With this initial condition, a nonuniform particle current flows, but in this classical limit, there is no net energy current. Thus we work in the reference frame where the local energy current vanishes ($\mathbf{j}_{\epsilon\uparrow} + \mathbf{j}_{\epsilon\downarrow} = 0$). Thanks to Galilean invariance, this choice of a reference frame does not affect the physics.

Following a similar procedure as described before, but in this zero energy current frame, we can determine all coefficients $C_{\ell ij}$ ($\ell = 0, 1$) and express the particle current of each species in terms of $\nabla n_\uparrow$ and $\nabla n_\downarrow$. Then, we can write currents in the diffusion matrix format as in Eq. (2.1):

Near unitarity,

$$\begin{pmatrix} \mathbf{j}_\uparrow \\ \mathbf{j}_\downarrow \end{pmatrix} = -\frac{9\pi^{3/2}}{9728\sqrt{2}} \left(\frac{\hbar}{m} \left(\frac{T}{T_F} \right)^{3/2} \right) \begin{pmatrix} \frac{365n_\uparrow^2 + 354n_\uparrow n_\downarrow + 733n_\downarrow^2}{nn_\downarrow} & \frac{381n_\uparrow^2 + 42n_\uparrow n_\downarrow + 405n_\downarrow^2}{nn_\downarrow} \\ \frac{405n_\uparrow^2 + 42n_\uparrow n_\downarrow + 381n_\downarrow^2}{nn_\uparrow} & \frac{733n_\uparrow^2 + 354n_\uparrow n_\downarrow + 365n_\downarrow^2}{nn_\uparrow} \end{pmatrix} \begin{pmatrix} \nabla n_\uparrow \\ \nabla n_\downarrow \end{pmatrix}. \tag{2.23}$$

Far from unitarity,

$$\begin{pmatrix} \mathbf{j}_\uparrow \\ \mathbf{j}_\downarrow \end{pmatrix} = -\frac{3\pi^{3/2}}{896\sqrt{2}} \left(\frac{\hbar}{m(k_F a)^2} \sqrt{\frac{T}{T_F}} \right) \begin{pmatrix} \frac{145n_\uparrow^2+158n_\uparrow n_\downarrow+289n_\downarrow^2}{nn_\downarrow} & \frac{137n_\uparrow^2-14n_\uparrow n_\downarrow+125n_\downarrow^2}{nn_\downarrow} \\ \frac{125n_\uparrow^2-14n_\uparrow n_\downarrow+137n_\downarrow^2}{nn_\uparrow} & \frac{289n_\uparrow^2+158n_\uparrow n_\downarrow+145n_\downarrow^2}{nn_\uparrow} \end{pmatrix} \begin{pmatrix} \nabla n_\uparrow \\ \nabla n_\downarrow \end{pmatrix} . \tag{2.24}$$

These matrix equations contain two eigenmodes, one is the thermal mode with eigenvalue $\mathfrak{D}_T$ ($\mathbf{j}_\uparrow$ and $\mathbf{j}_\downarrow$ are in the same directions) and the other is the spin mode with eigenvalue $\mathfrak{D}_s$ ($\mathbf{j}_\uparrow$ and $\mathbf{j}_\downarrow$ are in opposite directions). As expected, $\mathfrak{D}_T > \mathfrak{D}_s$ for all polarizations in both of these limits. Applying continuity equations to the above diffusion matrix equations while keeping all differential operators linear (we restrict ourselves in a linear response theory), we obtain two-component heat equations in terms of densities and thus we can immediately write the time evolution of each species in terms of the eigenmodes:

$$\begin{pmatrix} n_\uparrow(t,z) \\ n_\downarrow(t,z) \end{pmatrix} = \begin{pmatrix} n_{\uparrow 0} \\ n_{\downarrow 0} \end{pmatrix} + \alpha e^{-\mathfrak{D}_s w^2 t} \delta n_{\downarrow 0} \begin{pmatrix} \gamma \\ 1 \end{pmatrix} \cos wz + \beta e^{-\mathfrak{D}_T w^2 t} \delta n_{\downarrow 0} \begin{pmatrix} \zeta \\ 1 \end{pmatrix} \cos wz. \tag{2.25}$$

$(\gamma,\ 1)$ and $(\zeta,\ 1)$ are the eigenvectors of the spin mode and the thermal mode, respectively. γ is negative while ζ is positive. α and β are determined by the initial condition,

$$\begin{pmatrix} \delta n_{\uparrow 0} \\ \delta n_{\downarrow 0} \end{pmatrix} = \alpha \delta n_{\downarrow 0} \begin{pmatrix} \gamma \\ 1 \end{pmatrix} + \beta \delta n_{\downarrow 0} \begin{pmatrix} \zeta \\ 1 \end{pmatrix} . \tag{2.26}$$

It is straightforward to derive γ, ζ, α, β, $\mathfrak{D}_s$ and $\mathfrak{D}_T$. For example,

$$\alpha = \frac{1}{\gamma - \zeta} \left(\frac{n_{0\uparrow}}{n_{0\downarrow}} - \zeta \right) \tag{2.27}$$

$$\beta = 1 - \alpha \ . \tag{2.28}$$

Explicit expressions for γ, ζ, $\mathfrak{D}_s$ and $\mathfrak{D}_T$ are fairly lengthy so they are omitted here.

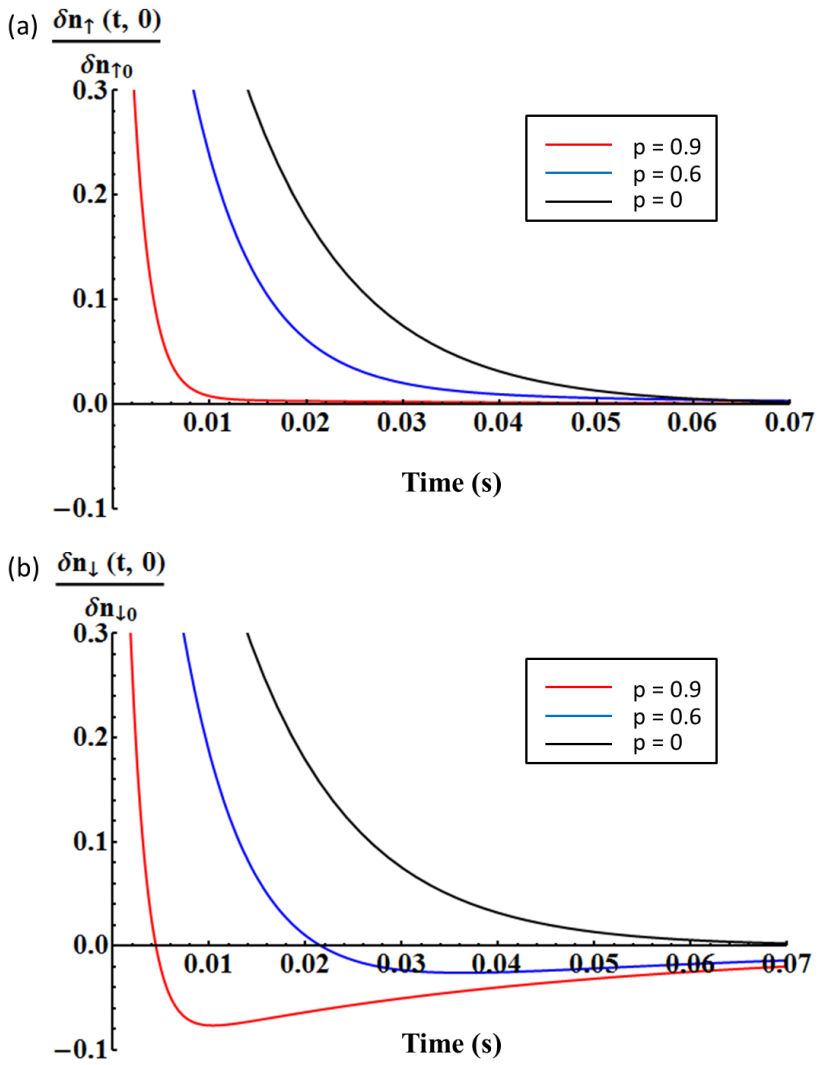

Figure 2.3: $\delta n_i(t,0)$ normalized by initial deviation δn_{i0} as a function of time near unitarity. (a) Majority density deviation relaxes monotonically for any polarization. (b) Minority density deviation shows nonmonotonic relaxation for $p > 0$ due to the spin Seebeck effect. Here we assume ^{6}Li atoms with $T/T_F = 4$ and the longitudinal length of the trap $L = 200\mu$m to set the time scale.

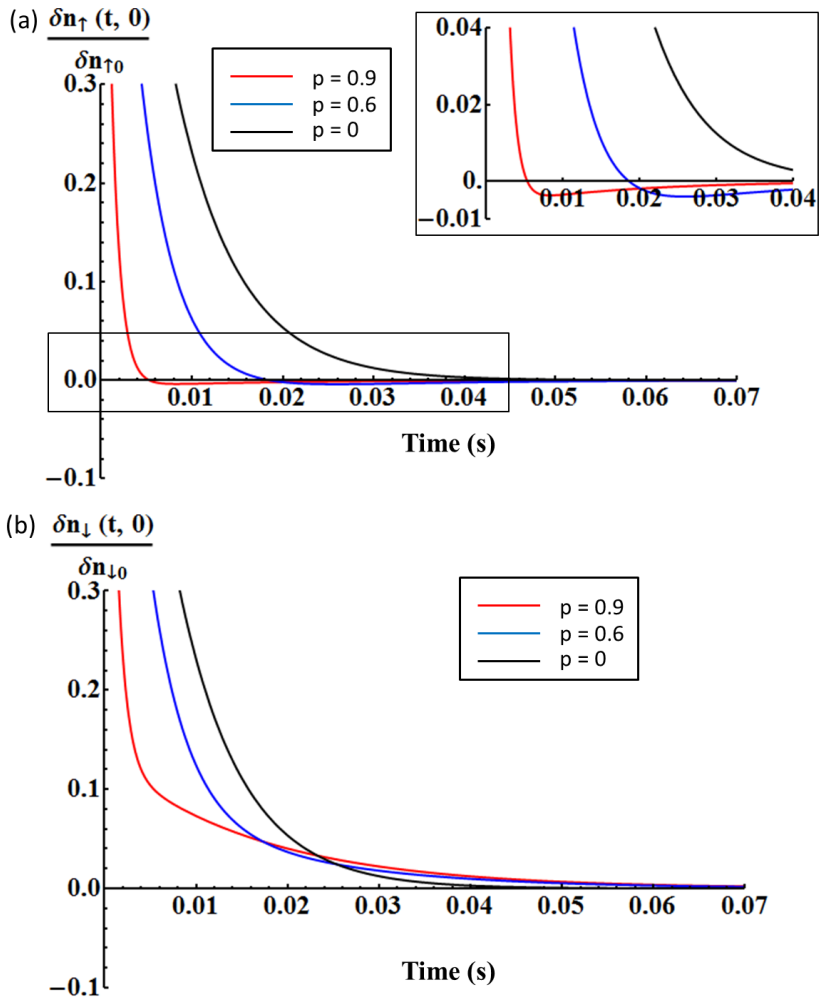

Figure 2.4: $\delta n_i(t,0)$ normalized by initial deviation δn_{i0} as a function of time far away from unitarity. (a) Majority density deviation relaxes nonmonotonically for $p > 0$ due to the spin Seebeck effect. Inset figure magnifies the nonmonotonic part of majority density deviations which are very weak compared to the minority density deviations at unitarity shown in Fig. 3. (b) Minority density deviation relaxes monotonically for any polarization. Here we assume ^{6}Li atoms with $T/T_F = 4$ and $\lambda/|a| = 4$ and the longitudinal length of the trap $L = 200\mu$m to set the time scale.

The spin Seebeck effect is most apparent when observing the densities at the edges of the system ($wz = 0$ or $wz = \pi$) so we choose to focus on the cold edge, $z = 0$. The uniform pressure condition implies that both majority and minority densities are initially higher than average at the cold side. Thus, initially $\delta n_\downarrow(t = 0, z = 0) > 0$. Even though the initial condition can be chosen to be the same for both unitarity and far away from unitarity, the time evolution of density of each species is qualitatively different for these two limiting cases.

Since $\mathfrak{D}_T > \mathfrak{D}_s > 0$ and $|\gamma|, |\zeta| \neq 1$, the density deviations of each species have different time evolution from one another. The density deviation of one species relaxes nonmonotonically while the density of the other species relaxes monotonically. This nonmonotonic relaxation of density deviation is a qualitative signature of the spin Seebeck effect. Near unitarity, we already know that the heat current and the spin current due to a temperature gradient are in the same direction. Therefore, the initially colder region ($z < \pi/2w$) becomes more polarized due to the spin Seebeck current. It turns out that the minority density deviation changes sign as it relaxes towards equilibrium. Far from unitarity, on the other hand, the initially cold region becomes less polarized, since the direction of the spin current is reversed, resulting in nonmonotonic relaxation of the majority density deviation. Figures 2.3 and 2.4 are plots of relaxation of the (normalized) density deviations of each species as a function of time for the two cases of near unitarity and of far away from unitarity.

Another consequence of the spin Seebeck effect is the change in polarization. From Eqs. (2.22) and (2.25), we can express the polarization as a function of time. Keeping

only linear term of δn_0, we obtain

$$\begin{aligned}\delta p(t,0) &= p(t,0) - p_0 \\ &= \frac{\delta n_0}{n_0}\left[\frac{n_{\downarrow 0}}{n_0}\left(\alpha(\gamma-1)e^{-\mathfrak{D}_s w^2 t} + \beta(\zeta-1)e^{-\mathfrak{D}_T w^2 t}\right)\right. \\ &\quad \left. - p_0\frac{n_{\downarrow 0}}{n_0}\left(\alpha(\gamma+1)e^{-\mathfrak{D}_s w^2 t} + \beta(\zeta+1)e^{-\mathfrak{D}_T w^2 t}\right)\right], \end{aligned} \tag{2.29}$$

As argued, the sign of the local polarization change depends on the direction of the spin Seebeck current. Figure 2.5 shows the (normalized) deviation of polarization from the average value as a function of time at $z = 0$. As expected, deviation is positive near unitarity and is negative far away from unitarity.

Perhaps one of the most easily accessible quantities in experiment is the density deviation of the species that shows nonmonotonic relaxation vs. time. A dimensionless measure of the extremum deviation is $\left|\frac{\delta n_i(t_{i,ext},0)}{\delta n_{i0}}\right|$, where $i =\uparrow$ away from unitarity and $i =\downarrow$ near unitarity and $t_{i,ext}$ is the time when density deviation of species i is its extremum of opposite sign from the initial condition. It is easy to derive formal expressions of $t_{i,ext}$ and a dimensionless measure, $\left|\frac{\delta n_i(t_{i,ext},0)}{\delta n_{i0}}\right|$.

Near unitarity,

$$t_{\downarrow,ext} = \frac{1}{(\mathfrak{D}_T - \mathfrak{D}_s)w^2}\ln\left|\frac{\mathfrak{D}_T\beta}{\mathfrak{D}_s\alpha}\right| \tag{2.30}$$

$$\left|\frac{\delta n_\downarrow(t_{\downarrow,ext},0)}{\delta n_{\downarrow 0}}\right| = \alpha\exp\left[-\frac{\mathfrak{D}_s}{\mathfrak{D}_T-\mathfrak{D}_s}\ln\left|\frac{\mathfrak{D}_T\beta}{\mathfrak{D}_s\alpha}\right|\right] + \beta\exp\left[-\frac{\mathfrak{D}_T}{\mathfrak{D}_T-\mathfrak{D}_s}\ln\left|\frac{\mathfrak{D}_T\beta}{\mathfrak{D}_s\alpha}\right|\right]. \tag{2.31}$$

Away from unitarity,

$$t_{\uparrow,ext} = \frac{1}{(\mathfrak{D}_T - \mathfrak{D}_s)w^2} \ln \left| \frac{\mathfrak{D}_T \beta\zeta}{\mathfrak{D}_s \alpha\gamma} \right| \tag{2.32}$$

$$\left| \frac{\delta n_\uparrow(t_{\uparrow,ext}, 0)}{\delta n_{\uparrow 0}} \right| = \frac{\alpha\gamma}{\alpha\gamma + \beta\zeta} \exp\left[-\frac{\mathfrak{D}_s}{\mathfrak{D}_T - \mathfrak{D}_s} \ln \left| \frac{\mathfrak{D}_T \beta\zeta}{\mathfrak{D}_s \alpha\gamma} \right| \right] + \frac{\beta\zeta}{\alpha\gamma + \beta\zeta} \exp\left[-\frac{\mathfrak{D}_T}{\mathfrak{D}_T - \mathfrak{D}_s} \ln \left| \frac{\mathfrak{D}_T \beta\zeta}{\mathfrak{D}_s \alpha\gamma} \right| \right] . \tag{2.33}$$

Figure 2.6 shows the dimensionless measure of the extremum density deviation as a function of polarization. Near unitarity (solid line), it is a monotonically increasing function of polarization for $p < 1$ (at $p = 1$, $n_\downarrow$ is zero so the deviation of $n_\downarrow$ is undefined). Around $p \approx 0.8$, the strength of the spin Seebeck effect by this measure is about 5 %. Far from unitarity (dashed line), this signal is much weaker. This is expected since the spin Seebeck effect is a consequence of interaction and does not exist in the non-interacting gas. Thus, the spin Seebeck effect should be strongest near unitarity. Note that in both limits, the spin Seebeck effect disappears when the gas is unpolarized, $p = 0$.

The spin Seebeck effect is a small effect. In the regimes where we have been able to estimate it and using the measures we have been able to devise, it is less than a 10% effect. However, it is worth emphasizing that these computations are done in the classical regime, so the spin Seebeck effect does not demand extremely low temperatures to detect it. We expect it to be most readily detected at temperatures of order T_F, where the diffusivities are minimized so the resulting time scales are longest. In addition, the procedure to detect it discussed in this section does not require knowledge of the system's equation of state. Importantly, we propose a type of experiment where the the spin Seebeck effect is a *qualitative effect*, namely a nonmonotonicity of the system's relaxation to global equilibrium.

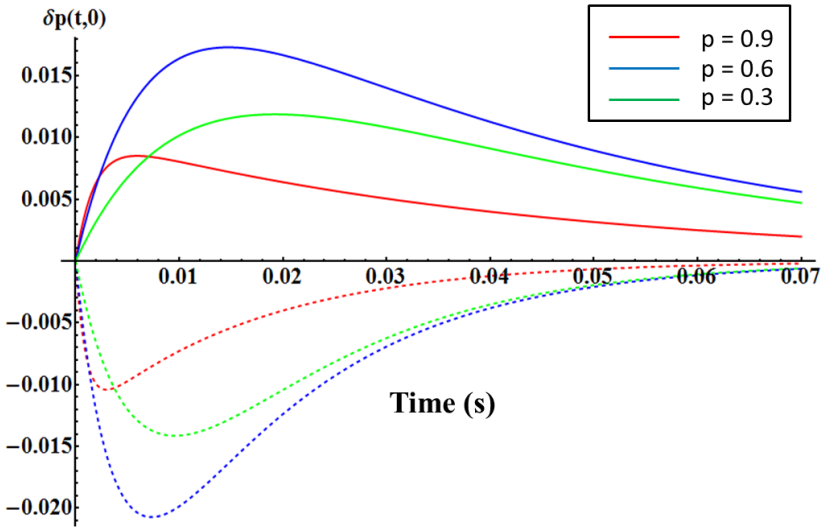

Figure 2.5: Normalized polarization deviation as a function of time for three global polarization values, p = 0.9 (lower curve), 0.6 (red), and 0.3 (blue). Near unitarity (green) the polarization deviation is positive while far away from unitarity (dashed lines) it is negative. We found that the polarization deviation is the largest near $p = 0.6$ in both limits. Same physical parameters as Figures 2.3 and 2.4 were used to fix the time scale. The polarization deviation $\delta p(t, 0)$ at the initially cold end of the cloud is normalized by the initial total density deviation, $\delta n_0/n_0$.

2.3.4 Perturbation of Exactly Solvable Model of the Boltzmann Equation

So far, our approach was based on an (uncontrolled) approximation method. Therefore, it is worthwhile to compare the main findings to a different approach, namely perturbing around the Maxwellian model, where the scattering cross section is inversely proportional of the relative speed [115]. The Maxwellian model corresponds to the central potential of the form $\sim 1/r^4$, where r is the inter particle distance. [2] Since this model has momentum *independent* scattering rate (product of scattering cross section and relative speed), we can solve the linearized Boltzmann equation exactly.

[2] Although Maxwell argued the existence of this potential in Nature, such a potential has not been found yet

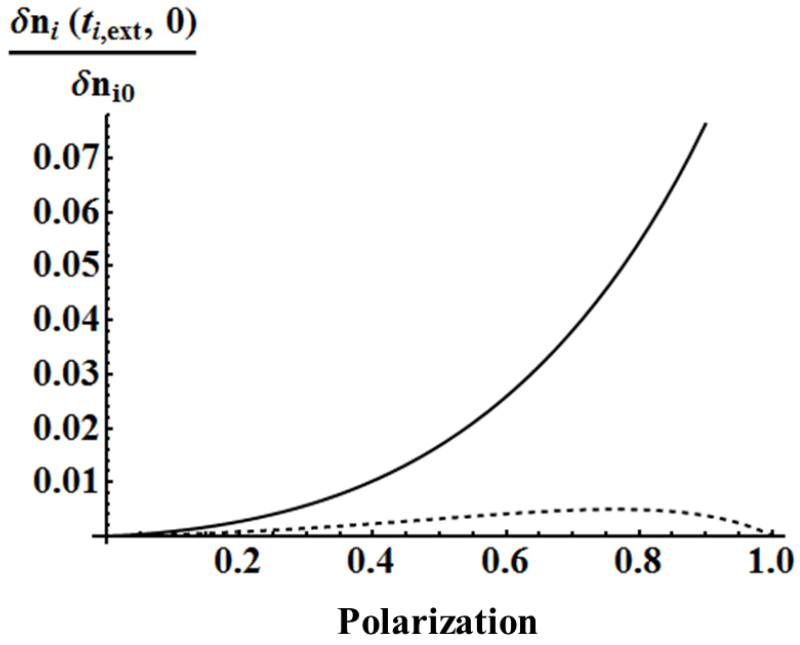

Figure 2.6: Extremum density deviation normalized by initial deviation, $\left|\frac{\delta n_i(t_{i,ext},0)}{\delta n_{i0}}\right|$ as a function of polarization. Near unitarity (solid line), $i =\downarrow$; far from unitarity (dashed line), $i =\uparrow$. $t_{i,ext}$ is the time when the density deviation of species i reaches its extremum. Far from unitarity (dashed line), the normalized extremum density deviation vanishes in the high polarization limit since there are no minority atoms to scatter from.

Let's recall the argument from which we determined directions of the magnetocaloric effects. Since the scattering rate is proportional to the product of the cross section and relative speed, the scattering rate is independent of momentum for the Maxwellian interaction. Therefore, we expect that $S_s' = 0$ for any polarization. It is straightforward to exactly solve the Boltzmann equation using the ansatz Eq. (2.13) with $L = 1$ to confirm this.

The next step is to perturb the Maxwellian scattering cross section to generate magnetocaloric currents. One simple way to perturb the cross section is to add a small term which depends linearly on relative momentum to the original cross section:

$$\frac{d\sigma}{d\Omega} = S_0 \left(\frac{1}{k_r} + \epsilon k_r\right), \tag{2.34}$$

where S_0 is a constant of the dimension of length and ϵ is a small expansion parameter. For a positive ϵ, the momentum dependence of the scattering rate is similar to the case away from unitarity, higher scattering rate for higher relative momentum. Thus we expect the resulting spin Seebeck current is in the opposite direction from the primary heat current. For a negative ϵ, the momentum dependence resembles the case near unitarity and therefore we expect the resulting spin Seebeck current is in the same direction as the primary heat current.

To find the solution of the Boltzmann equation up to linear order in ϵ, we need at least $L = 2$ in the ansatz of Eq. (2.13). After a straightforward calculation, we obtain the following results:

$$\begin{pmatrix} \mathbf{j}_{heat} \\ \mathbf{j}_{spin} \end{pmatrix} = -D_0 \begin{pmatrix} \kappa'_M & -\frac{\pi\epsilon(n_\uparrow - n_\downarrow)Tn}{2n_\uparrow n_\downarrow \lambda^2} - \frac{T}{10}\left(1 - \frac{20\pi\epsilon}{\lambda^2}\right)\ln\left(\frac{n_\uparrow}{n_\downarrow}\right) \\ -\frac{\pi\epsilon(n_\uparrow - n_\downarrow)}{\lambda^2 T} & \frac{1}{10}\left(1 - \frac{20\pi\epsilon}{\lambda^2}\right) \end{pmatrix} \begin{pmatrix} \nabla T \\ n\nabla p \end{pmatrix} , \tag{2.35}$$

where κ'_M (proportional to the thermal conductivity of the Maxwellian Model) is

$$\kappa'_M = \frac{1}{2}n\left(\frac{(n_\uparrow^2 + n_\uparrow n_\downarrow + n_\downarrow^2)}{n_\uparrow n_\downarrow} - \frac{3\pi\epsilon}{\lambda^2}\frac{(9n_\uparrow^2 + 10n_\uparrow n_\downarrow + 9n_\downarrow^2)}{n_\uparrow n_\downarrow}\right) + \frac{\pi\epsilon(n_\uparrow - n_\downarrow)}{\lambda^2}\ln\left(\frac{n_\uparrow}{n_\downarrow}\right) , \tag{2.36}$$

and D_0 is $\frac{5\hbar}{mS_0 n\lambda^2}$, with units of a diffusivity.

We immediately see that all off-diagonal elements vanish for zero polarization. When $\epsilon = 0$, we see that $S'_s = 0$ and thus we conclude that the spin Seebeck effect is a consequence of momentum dependence of the scattering rate. The sign of the spin Seebeck current at nonzero ϵ is as expected. For P'_s, we again see the logarithmic term which will be discussed in the following section. Perturbing the Maxwellian

scattering cross section re-confirms the sign argument for the spin Seebeck effect that we presented in the previous Section.

2.4 Structure of Transport Coefficients

Transport coefficients we have so far calculated are not completely independent. In fact, they possess inter-connected structures. In this section, we will examine the structure of transport matrix in detail.

2.4.1 Kubo Formula

The Kubo formula gives a formally exact expression for the transport coefficients in the linear response regime (see e.g. [82, 76]). For irreversible processes in the linear response regime, what the the Kubo formula gives are the transport coefficients for the dissipative forces and currents associated with the entropy production. At mechanical equilibrium for our two-species gas, the dissipative forces are ∇T and $\nabla(\mu_\uparrow - \mu_\downarrow)$ [26], thus what we obtain from the Kubo formula is the diffusion matrix in the form of Eq. (2.2), whose off-diagonal terms always satisfy the Onsager relation. Thus, the diffusion matrix in the form of Eq. (2.5), in which we summarized the results in the previous section, does not generally satisfy the Onsager relation, although it is possibly easier to observe experimentally. Shortly, we summarize the results in the form of Eq. (2.2) and explicitly show both our approximate solutions and the perturbative solution from the exactly solvable Maxwellian model indeed satisfy the Onsager relation.

Following Ref. [82] and from Eq. (2.2), the spin Seebeck coefficient S_s and Peltier coefficient P_s can be expressed via the Kubo formula as

$$TS_s = \frac{1}{3VT}\int_0^\infty dt\langle \mathbf{J}_{heat}(0)\cdot\mathbf{J}_{spin}(t)\rangle \tag{2.37}$$

$$= \frac{1}{3VT}\int_0^\infty dt\langle \mathbf{J}_{heat}(t)\cdot\mathbf{J}_{spin}(0)\rangle = P_s, \tag{2.38}$$

where V is the total volume of the system and the current $\mathbf{J}$ is the volume integral of local current density,

$$\mathbf{J}(t) = \int d^3\mathbf{x}\,\mathbf{j}(\mathbf{x},t). \tag{2.39}$$

The average is taken over the equilibrium distribution, which is just the Boltzmann distribution of each species in the high-temperature classical regime.

Since we assume Galilean invariance, the total momentum of the entire gas is conserved. Therefore, any physical quantity which is transported with the total particle current $\mathbf{J}_n$ remains finite for all time t and gives a divergent contribution in the Kubo formula, meaning that quantity moves "ballistically" rather than diffusively. Therefore, it is crucial to use the frame-independent definition of the local diffusive currents from Eq. (2.3) and Eq. (2.4). Let's write them again and slightly manipulate the heat current:

$$\mathbf{j}_{spin} = \frac{n_\downarrow}{n}\mathbf{j}_\uparrow - \frac{n_\uparrow}{n}\mathbf{j}_\downarrow \tag{2.40}$$

$$\mathbf{j}_{heat} = \mathbf{j}_\epsilon - \mu_\uparrow\mathbf{j}_\uparrow - \mu_\downarrow\mathbf{j}_\downarrow - sT\mathbf{j}_n = \mathbf{j}_\epsilon - \frac{5}{2}T\mathbf{j}_n - (\mu_\uparrow - \mu_\downarrow)\mathbf{j}_{spin}, \tag{2.41}$$

where $sT = \frac{5}{2}T - \frac{n_\uparrow}{n}\mu_\uparrow - \frac{n_\downarrow}{n}\mu_\downarrow$ and $\mathbf{j}_\epsilon = \mathbf{j}_{\epsilon\uparrow} + \mathbf{j}_{\epsilon\downarrow}$. Defining $\tilde{\mathbf{j}}_{heat} \equiv \mathbf{j}_\epsilon - (5T/2)\mathbf{j}_n$ [3], the Kubo formula gives us the following spin Seebeck coefficient:

$$TS_s = P_s = \frac{1}{3VT}\int_0^\infty dt[\langle \tilde{\mathbf{J}}_{heat}(0)\cdot\mathbf{J}_{spin}(t)\rangle - (\mu_\uparrow - \mu_\downarrow)\langle \mathbf{J}_{spin}(0)\cdot\mathbf{J}_{spin}(t)\rangle] \quad (2.42)$$

$$= \frac{1}{3VT}\int_0^\infty dt\left(\langle \tilde{\mathbf{J}}_{heat}(0)\cdot\mathbf{J}_{spin}(t)\rangle\right) - T\ln\left(\frac{n_\uparrow}{n_\downarrow}\right)\sigma_s, \quad (2.43)$$

where σ_s is the spin conductivity given in Eq. (2.2) and $\mu_\uparrow - \mu_\downarrow = T\ln(n_\uparrow/n_\downarrow)$. Therefore, in this representation, the spin Seebeck coefficient (and thus also the spin Peltier coefficient) always carries an additional term of the spin conductivity σ_s multiplied by $-\ln(n_\uparrow/n_\downarrow)$. This is the origin of that term in P_s' in Eqs. (2.15), (2.17), and (2.35). We can understand the reason why the spin Seebeck coefficient S_s' does not include such a term from the following observation: At mechanical equilibrium and high temperature, we have

$$\nabla(\mu_\uparrow - \mu_\downarrow) = \ln\left(\frac{n_\uparrow}{n_\downarrow}\right)\nabla T + T\frac{n^2}{2n_\uparrow n_\downarrow}\nabla p\ . \quad (2.44)$$

Therefore, that $\nabla p = 0$ implies $\nabla(\mu_\uparrow - \mu_\downarrow) = \ln(n_\uparrow/n_\downarrow)\nabla T$. The spin current now becomes

$$\mathbf{j}_{spin} = -\sigma_s\nabla(\mu_\uparrow - \mu_\downarrow) - S_s\nabla T \quad (2.45)$$

$$= -D_s n\nabla p - (\sigma_s\ln(n_\uparrow/n_\downarrow) + S_s)\nabla T = -D_s n\nabla p - S_s'\nabla T\ . \quad (2.46)$$

Thus the additional $\sim \ln(n_\uparrow/n_\downarrow)$ term from Eq. (2.44) exactly cancels the similar term from Eq. (2.43). Consequently, what we have computed for S_s' in the previous section is the first term in Eq. (2.43) to which the sign argument in section 2.2 should be applied.

[3] Since $5T/2$ is the thermal average enthalpy per particle in classical regime, $\tilde{\mathbf{j}}_{heat}$ is the local energy current relative to the local average motion of the gas.

We can extract more information from Eq. (2.41). In $\mathbf{j}_n = 0$ frame, the heat current is $\mathbf{j}_{heat} = \mathbf{j}_\epsilon - T\ln(n_\uparrow/n_\downarrow)\mathbf{j}_{spin}$. Thus, heat conductivity and spin Peltier coefficient always have contributions coming from spin current. Therefore, in the format of Eq. (2.5) we can write

$$\kappa' = \kappa'_1 - T\ln(n_\uparrow/n_\downarrow)S'_s \tag{2.47}$$

$$P'_s = P'_{s1} - T\ln(n_\uparrow/n_\downarrow)D_s \ , \tag{2.48}$$

where κ'_1 and P'_{s1} are first terms which do not originate from spin current. Results in the previous section clearly show this.

Lastly, we study the thermal conductivity, κ, in Eq. (2.2).

$$\kappa = \frac{1}{3VT^2}\int_0^\infty dt < \mathbf{J}_{heat}(t)\cdot\mathbf{J}_{heat}(0) > \tag{2.49}$$

$$= \frac{1}{3VT^2}\int_0^\infty dt < \tilde{\mathbf{J}}_{heat}(t)\cdot\tilde{\mathbf{J}}_{heat}(0) > -2T\ln\left(\frac{n_\uparrow}{n_\downarrow}\right)S'_s + T\left(\ln\left(\frac{n_\uparrow}{n_\downarrow}\right)\right)^2\sigma_s \ . \tag{2.50}$$

2.4.2 Manifestation of the Onsager Relation

For completeness, we present diffusion matrices of approximate solutions and the solution of the first order perturbation of the Maxwellian model in the form of Eq. (2.2) where the Onsager relation should be explicit. We simply transform the set of driving forces $(\nabla T, n\nabla p)$ to another set of driving forces $(\nabla T, \nabla(\mu_\uparrow - \mu_\downarrow))$ associated with the entropy production. Once we know the equation of state, this transformation is straightforward.

For approximate solutions we have the following:

At unitarity ($|a| \gg \lambda$),

$$\begin{pmatrix} \mathbf{j}_{heat} \\ \mathbf{j}_{spin} \end{pmatrix} = - D_u \begin{pmatrix} \kappa_u & (n_\uparrow - n_\downarrow) - \frac{39 n_\uparrow n_\downarrow}{5n} \ln\left(\frac{n_\uparrow}{n_\downarrow}\right) \\ \frac{(n_\uparrow - n_\downarrow)}{T} - \frac{39 n_\uparrow n_\downarrow}{5nT} \ln\left(\frac{n_\uparrow}{n_\downarrow}\right) & \frac{39 n_\uparrow n_\downarrow}{5nT} \end{pmatrix} \begin{pmatrix} \nabla T \\ \nabla(\mu_\uparrow - \mu_\downarrow) \end{pmatrix}, \tag{2.51}$$

where D_u and κ_u is

$$D_u = \frac{45\pi^{3/2}}{608\sqrt{2}} \left(\frac{\hbar}{m}\left(\frac{T}{T_F}\right)^{3/2}\right) \tag{2.52}$$

$$\kappa_u = \frac{5}{16} n \left(\frac{(73 n_\uparrow^2 + 82 n_\uparrow n_\downarrow + 73 n_\downarrow^2)}{n_\uparrow n_\downarrow}\right) - \ln\left(\frac{n_\uparrow}{n_\downarrow}\right)\left(\frac{10(n_\uparrow^2 - n_\downarrow^2) - 39 n_\uparrow n_\downarrow \ln(n_\uparrow/n_\downarrow)}{5n}\right). \tag{2.53}$$

Far away from unitarity ($|a| \ll \lambda$),

$$\begin{pmatrix} \mathbf{j}_{heat} \\ \mathbf{j}_{spin} \end{pmatrix} = - D_a \begin{pmatrix} \kappa_a & -(n_\uparrow - n_\downarrow) - \frac{43 n_\uparrow n_\downarrow}{5n} \ln\left(\frac{n_\uparrow}{n_\downarrow}\right) \\ -\frac{(n_\uparrow - n_\downarrow)}{T} - \frac{43 n_\uparrow n_\downarrow}{5nT} \ln\left(\frac{n_\uparrow}{n_\downarrow}\right) & \frac{43 n_\uparrow n_\downarrow}{5nT} \end{pmatrix} \begin{pmatrix} \nabla T \\ \nabla(\mu_\uparrow - \mu_\downarrow) \end{pmatrix}, \tag{2.54}$$

where D_a and κ_a is

$$D_a = \frac{15\pi^{3/2}}{224\sqrt{2}} \left(\frac{\hbar}{m(k_F a)^2}\sqrt{\frac{T}{T_F}}\right) \tag{2.55}$$

$$\kappa_a = \frac{5}{8} n \left(\frac{(29 n_\uparrow^2 + 26 n_\uparrow n_\downarrow + 29 n_\downarrow^2)}{n_\uparrow n_\downarrow}\right) + \ln\left(\frac{n_\uparrow}{n_\downarrow}\right)\left(\frac{10(n_\uparrow^2 - n_\downarrow^2) + 43 n_\uparrow n_\downarrow \ln(n_\uparrow/n_\downarrow)}{5n}\right). \tag{2.56}$$

For the first order perturbation of the Maxwellian model, we have the following:

$$\begin{pmatrix} \mathbf{j}_{heat} \\ \mathbf{j}_{spin} \end{pmatrix} = - D_0 \begin{pmatrix} \kappa_M & -\frac{\pi\epsilon(n_\uparrow - n_\downarrow)}{\lambda^2} - \frac{n_\uparrow n_\downarrow}{5n}\left(1 - \frac{20\pi\epsilon}{\lambda^2}\right)\ln\left(\frac{n_\uparrow}{n_\downarrow}\right) \\ -\frac{\pi\epsilon(n_\uparrow - n_\downarrow)}{\lambda^2 T} - \frac{n_\uparrow n_\downarrow}{5nT}\left(1 - \frac{20\pi\epsilon}{\lambda^2}\right)\ln\left(\frac{n_\uparrow}{n_\downarrow}\right) & \frac{n_\uparrow n_\downarrow}{5nT}\left(1 - \frac{20\pi\epsilon}{\lambda^2}\right) \end{pmatrix} \times \begin{pmatrix} \nabla T \\ \nabla(\mu_\uparrow - \mu_\downarrow) \end{pmatrix}, \tag{2.57}$$

where κ_M is

$$\begin{aligned} \kappa_M =& \frac{1}{2} n \left(\frac{(n_\uparrow^2 + n_\uparrow n_\downarrow + n_\downarrow^2)}{n_\uparrow n_\downarrow} - \frac{3\pi\epsilon}{\lambda^2} \frac{(9n_\uparrow^2 + 10 n_\uparrow n_\downarrow + 9 n_\downarrow^2)}{n_\uparrow n_\downarrow} \right) \\ &+ \frac{2\pi\epsilon \ln\left(\frac{n_\uparrow}{n_\downarrow}\right)}{n\lambda^2} \left((n_\uparrow^2 - n_\downarrow^2) + n_\uparrow n_\downarrow \left(\frac{\lambda^2}{10\pi\epsilon} - 2 \right) \ln\left(\frac{n_\uparrow}{n_\downarrow}\right) \right) \end{aligned} \tag{2.58}$$

The above matrices clearly exhibit the Onsager relation. Also each off-diagonal element carries a term proportional to $-\sigma_s \ln(n_\uparrow/n_\downarrow)$ as mentioned in Eq. (2.43). Lastly, the structure of thermal conductivity (Eq. (2.50)) is evident.

2.5 Conclusion

We have studied diffusive spin and heat transport in a two-species atomic Fermi gas with short-range interaction at general polarization, temperature and scattering length in dilute regime, where classical Boltzmann treatment is justified. Using "power-counting", we first estimated the spin and thermal diffusivities in all regimes. We suggested a method to measure the thermal diffusivity, which has not yet been experimentally measured.

Our main focus was on the magnetocaloric effects, namely the spin Seebeck and spin Peltier effects. Observing the connection between the interaction strength and the dependence of the scattering rate on the relative momentum of two atoms, we were able to develop a qualitative argument for the signs of magnetocaloric effects. Near unitarity, magnetocaloric currents are in the same direction as the "primary" spin and heat currents, while their directions are reversed as we move to far away from unitarity. We then quantitatively estimated diffusivities and magnetocaloric effects in the classical regime using approximate solutions of the Boltzmann kinetic equation, thereby confirming the "power-counting" estimates of diffusivities and the sign argument for the magnetocaloric effects. In Appendix A, we also prove the scaling of the transport coefficients is robust to all orders of approximation.

Remaining in the classical regime, we proposed an experimental procedure to detect the spin Seebeck effect as a qualitative effect: a nonmonotonic relaxation towards equilibrium. This method is nice in that it does not require knowledge of the equation of state of the gas. In order to confirm these results and obtain a better understanding of the origin of these magnetocaloric effects, we also performed a controlled perturbation to the exactly solvable Maxwellian model. This approach agrees well with the approximate solutions of the Boltzmann equation.

Chapter 3

Entanglement Dynamics of 1D Nonintegrable Quantum Spin Chain: Exact Diagonalization

As Einstein, Podolosky, and Rosen originally suggested as a skepticism to local realism of quantum mechanics (EPR paradox)[39], entanglement has been one of central concepts in quantum physics. It can be non-local in any space, which is impossible in classical physics, and is not a conserved quantity. Consequently, entanglement has very different dynamical aspects compared to conventional transport of local conserved quantities. Applying the method of exact diagonalization to a non-integrable model quantum system, we study how entanglement dynamics is different from diffusive transport of conserved energy. Most results of this chapter (ballistic spreading of entanglement and diffusive transport of energy) are published in the paper[61].

We set the Planck constant $\hbar$ and the Boltzmann constant k_B to unity.

3.1 Introduction

One natural question about entanglement is its quantum dynamics under unitary time evolution. If one starts an isolated quantum system in a nonentangled initial product pure state, how does the entanglement grow with time? Entanglement is not a conserved quantity like energy, that is transported. Instead it is more like an infection or epidemic [91] that multiplies and spreads. An initial state that is a product state has the information about the initial state of each local degree of freedom (spins in our model) initially localized on that degree of freedom. Under the system's unitary time evolution, quantum information about each spin's initial state can spread with time to other spins, due to the spin-spin interactions. This can make those spins that share this information entangled.

In real physical systems, information and entanglement can spread as fast as the speed of light (or sound). For a lattice spin model, which lacks propagating light or sound, an upper limit on the speed of any information spread is given by the Lieb-Robinson bound, which is set by the spin-spin interactions [70] (for recent reviews, see Refs. [83, 65]). For integrable one-dimensional models the entanglement does indeed spread ballistically [24, 43, 50], which is to be expected since such systems have ballistically propagating quasiparticles that can serve as carriers of the information. For various localized models, on the other hand, the entanglement has been shown to spread much more slowly, only logarithmically with time [43, 28, 40, 4, 126, 78, 52, 22, 85]. In the present chapter, we consider an intermediate case, a quantum Ising spin chain that is neither integrable nor localized, whose energy transport is diffusive.

Here we investigate the spread of entanglement in a diffusive nonintegrable system, at high temperature where there are no ballistically propagating quasiparticles and the only conserved quantity is the energy which moves diffusively (In integrable models, on the other hand, correlations of local observables can spread both diffusively and ballistically [114, 67]). Diagonalizing the entire Hamiltonian matrix, we

numerically study the time evolution of the entanglement and the diffusive dynamics of energy transport for highly-excited thermal states of the system [1]. We show that the entanglement spreads ballistically, while the energy moves only diffusively, and thus slowly. We also investigate the role of energy conservation in entanglement spreading by deliberately removing the conservation law and show that the energy conservation is indeed important in the late stage of entanglement spreading. Finally, we provide an insight about local and real space picture of entanglement spreading.

Although we choose a specific model Hamiltonian to study the quantum dynamics, this result should be valid generally for nonlocalized and nonintegrable systems that do not have ballistically propagating quasiparticles or long-wavelength propagating modes such as light or acoustic sound.

3.2 The Model

As a simple nonintegrable model Hamiltonian, we choose a spin-1/2 Ising chain with both transverse and longitudinal fields. The model is translationally invariant, except at the ends of the chain, which we leave open. Leaving the ends open allows the longest distance within the chain to be its full length, so we can study energy transport over that distance, and the spread of bipartite entanglement from the center of the chain to its ends. If we had used periodic boundary conditions instead, the longest distances that we could study would be cut in half. Given the limited lengths that one can study with exact diagonalization, this factor of two is quite important [2]. Our Hamiltonian is

$$H = \sum_{i=1}^{L} g\sigma_i^x + \sum_{i=2}^{L-1} h\sigma_i^z + (h-J)(\sigma_1^z + \sigma_L^z) + \sum_{i=1}^{L-1} J\sigma_i^z\sigma_{i+1}^z \ . \tag{3.1}$$

[1] Although conventional, here "thermal" should not be taken literally. Rather, it means high energy density

[2] Periodic boundary condition is useful for studying other problems, such as testing the eigenstate thermalization hypothesis (ETH).

σ_i^x and σ_i^z are the Pauli matrices of the spin at site i. As mentioned in the Introduction Chapter, we chose the longitudinal field $h = (\sqrt{5}+1)/4 = 0.8090\ldots$ and the transverse field $g = (\sqrt{5}+5)/8 = 0.9045\ldots$ and set the interaction $J = 1$ to see both fast entanglement spread and slow energy diffusion and none of the terms singly dominates the energy spectrum; all results reported here are for these values. Our qualitative results and conclusions do not depend on these parameter choices as long as g, h and J are all of similar magnitude to each other to keep the system robustly nonintegrable. Note that the magnitude of the energy "cost" to flip a spin in the bulk, from the applied longitudinal field and its interactions with its neighbors, is $2h$ or $4J \pm 2h$. To keep the end sites similar in this respect to the bulk, we reduce the strength of the longitudinal field on the end spins by J. This is to avoid having some slow low-energy modes near the ends that introduced small additional finite-size effects when we applied the same magnitude of longitudinal field also to the end spins.

This Hamiltonian has one symmetry, namely inverting the chain about its center. We always work with even L, so the center of the chain is on the bond between sites $L/2$ and $(L/2)+1$. This symmetry allows us to separate the system's state space into sectors that are even and odd under this parity symmetry, and diagonalize within each sector separately. Any mixed parity state can be obtained from a linear combination of even and odd parity states.

3.2.1 Nonintegrability - Level Spacing Statistics

Unlike classical systems, there is no simple critera to determine whether a quantum model is integrable or not. In fact, even the definition of quantum integrability is somewhat ambiguous[3]. Nonetheless, one of the widely adapted criterion to test integrability is the statistics of the energy level spacings. For a quantum Hamiltonian whose classical counterpart is integrable, Berry-Tabor conjecture says that the en-

[3]Private communication with Natan Andrei at New York City nonequilibrium conference in March 2013.

ergy level spacing follows Poissonian statistics [6]. For a quantum Hamiltonian whose classical counterpart is chaotic (nonintegrable), Bohigas, Giannoni, and Schmit conjectured that the energy level spacing follows one of the three classes of ensembles from random matrix theory (RMT)- Gaussian Orthogonal Ensemble (GOE), Gaussian Unitary Ensemble (GUE), and Gaussian Symplectic Ensemble (GSE) [9] [4]. We will show that the energy level spacing statistics of our time-reversal invariant Hamiltonian follows GOE statistics and conclude this model is nonintegrable.

The universality of RMT statistics of energy level spacing is only valid when the local density of states is set to unity [2]. Since each model do have different density of states, we have to bring the model to equal footing before comparing the energy level spacing with RMT statistics. There are two ways to achieve this goal; unfolding [99, 79] and looking at ratio of level spacings [89]. The heart of unfolding method is transforming true energy levels so that transformed levels have mean density of states equal to one. However, this unfolding method is not always possible especially large number of statistics is not easy to obtain [2]. Oganesyan and Huse introduced an alternative way to compare statistics of energy levels to that of RMT [89]: compare the statistics of *ratio* of energy level spacings instead of looking at energy level spacings. By taking ratio, the level statistics becomes independent of density of states. We will look at this ratio distribution to confirm our model follows GOE statistics thus nonintegrable.

Suppose we obtained energy levels of the many-body Hamiltonian in ascending order; $\{e_n\}$ $(e_{n-1} \leq e_n \leq e_{n+1})$. Then, the level spacing s_n and the ratio of level spacing r_n are,

$$s_n = e_{n+1} - e_n \tag{3.2}$$

$$r_n = \frac{s_{n+1}}{s_n} \ . \tag{3.3}$$

[4] One problem is that our spin system has no classical counterpart. We ignore this subtle issue.

Now we need a function to compare the distribution of r_n. The distribution of ratio $z = x/y$ of random variables x, y can be obtained by

$$P(z) = \int P_J(x,y)\delta\left(z - \frac{x}{y}\right) dxdy = \int_{-\infty}^{\infty} |y| P_J(zy, y) dy \ , \tag{3.4}$$

where $P_J(x, y)$ is the joint distribution of x and y. For Poissonian random variables, this is straightforward:

$$P(r) = \int_0^{\infty} |y| e^{-ry-y} dy = \frac{1}{(1+r)^2} \ . \tag{3.5}$$

Note that a Poissonian variable is always nonnegative.

For RMT variables, however, the exact form of distribution is fairly complicated. Therefore, Oganesyan and Huse originally generated many realizations of GOE to make a smooth curve of level ratio distribution that they compared with the data [89]. It was Atas *et. al.* that derived a closed form of approximate formula for the ratio distribution of RMT variables. Their derivation shares the same philosophy with the derivation of an approximate formula for the level spacing distribution of RMT variables originally suggested by Eugene Wigner, now called "Wigner's surmise"[79]. The Wigner's surmise is that the level spacing distribution of RMT variables can be approximated by the distribution of eigenvalue difference of 2×2 random matrix in the same symmetry class. The distribution of level spacing s is

$$P_W(s) = a_\beta s^\beta e^{-b_\beta s^2} \ , \tag{3.6}$$

with exactly known constants a_β and b_β ($\beta = 1, 2, 4$ correspond to GOE, GUE, and GSE, repectively). This formula is in excellent agreement with exact large-N expressions [37]. Applying the same principle, we can obtain an approximate formula of ratio distribution by studying eigenvalues of a 3×3 random matrix. The joint

probability distribution of eigenvalues of $N \times N$ random matrix is [79]

$$P_{\beta,N}(e_1, e_2, \ldots e_N) = C_{\beta,N} \prod_{1 \le i \le j \le N} |e_i - e_j|^\beta \prod_{i=1}^{N} e^{-\beta(e_i^2/2)} \ . \tag{3.7}$$

For a given N, we can determine the constant $C_{\beta,N}$ from normalization. Now we can derive an approximate form of ratio distribution by taking $N = 3$.

$$P_\beta(r) = \int_{-\infty}^{\infty} de_2 \int_{-\infty}^{e_2} de_1 \int_{e_2}^{\infty} de_3 P_{\beta,3}(e_1, e_2, e_3) \delta \left(r - \frac{e_3 - e_2}{e_2 - e_1} \right) \ . \tag{3.8}$$

Performing the integration, we obtain the following formula for GOE statistics ($\beta = 1$):

$$P_{GOE}(r) = \frac{8}{27} \frac{(r + r^2)}{(1 + r + r^2)^{5/2}} \ . \tag{3.9}$$

This functional form is first derived and tested against numerical analysis in Ref. [2]. We will compare our level ratio statistics in each parity sector to this formula.

There are 32896 energy levels in the even sector for $L = 16$, the largest system we have diagonalized. Figure 3.1 is the plot of ratio distributions of level spacing for parameter choices $(g, h) = ((\sqrt{5} + 5)/8, (\sqrt{5} + 1)/4)$ and $(g, h) = ((\sqrt{5} + 5)/8, 0)$. It is clear that the nonzero value of h makes the model drastically different from the integrable case ($h = 0$). The nonintegrable (integrable) case shows an excellent agreement with GOE statistics (Poissonian statistics). This is an evidence that our model with nonzero h is nonintegrable. Later, we will show that the energy transport in the system is diffusive, which is an explicit demonstration of nonintegrability of the model.

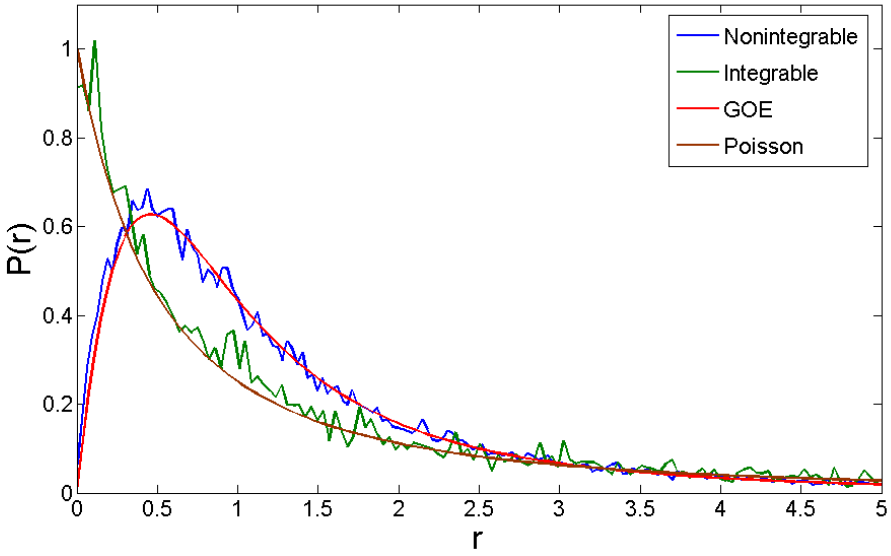

Figure 3.1: Ratio distribution of level spacing for two sets of parameter choices;$(g,h) = ((\sqrt{5}+5)/8, (\sqrt{5}+1)/4)$ and $(g,h) = ((\sqrt{5}+5)/8, 0)$. Nonzero h makes the model nonintegrable. r is the ratio of level spacings between two adjacent energy gaps. For $L = 16$, there are 32896 eigenvalues in even parity eigenstates, from which we obtain 32894 ratios. We clearly see that nonintegrable model closely follows Gaussian Orthogonal Ensemble (GOE) statistics by showing characteristic level repulsion (vanishing probability at $r = 0$), which is absent in the integrable case.

3.3 Entanglement Spreading

Given this model is nonintegrable, we compute the entanglement spreading. Spreading can be (1) ballistic as in the case of integrable system, (2) diffusive as transport of most local observables in a nonintegrable system, or (3) something else. We find the answer is (1).

3.3.1 Ballistic Spreading of Entanglement

We consider the time evolution of the bipartite entanglement across the central bond between the two halves of the chain. We quantify the entanglement entropy in bits using the von Neumann entropy $S(t) = -\mathrm{tr}\left[\rho_{\mathrm{A}}(\mathrm{t}) \log_2 \rho_{\mathrm{A}}(\mathrm{t})\right] = -\mathrm{tr}\left[\rho_{\mathrm{B}}(\mathrm{t}) \log_2 \rho_{\mathrm{B}}(\mathrm{t})\right]$ of the probability operators (as known as reduced density matrices) at time t of either

the left half (A) or the right half (B) of the chain. As initial states, we consider random product states (with thus zero initial entanglement), $|\psi(0)\rangle = |\mathbf{s}_1\rangle|\mathbf{s}_2\rangle...|\mathbf{s}_L\rangle$, where each spin at site i initially points in a random direction on its Bloch sphere,

$$|\mathbf{s}_i\rangle = \cos\left(\frac{\theta_i}{2}\right)|\uparrow_i\rangle + e^{i\phi_i}\sin\left(\frac{\theta_i}{2}\right)|\downarrow_i\rangle \ , \tag{3.10}$$

where $\theta_i \in [0, \pi)$ and $\phi_i \in [0, 2\pi)$. Such an initial state is in general neither even nor odd, and thus explores the entire Hilbert space of the pure states as it evolves with unitary Hamiltonian dynamics. This ensemble of initial states maximizes the thermodynamic entropy and thus corresponds to infinite temperature. For each time t, we generate 200 random initial product states, let them evolve to time t, compute $S(t)$ for each initial state, and then average. By doing so, the standard error at each time is uncorrelated. The results are shown in Figure 3.2. Ballistic linear growth of $S(t)$ at early time is clearly seen, and the growth rate before the saturation is independent of L. There is an even earlier time regime at $t \ll 1$ where the entanglement initially grows as $\sim t^2|\log t|$; this regime is just the initial development of some entanglement between the two spins immediately adjacent to the central bond for such behavior does not depend on the system size.

In the long time limit, the time evolved state, on average, should behave like a random pure state (a random linear combination of product states) [5]. In Ref. [93], it is shown that the average of the entanglement entropy of random pure states is

$$S^R = \log_2 m - \frac{m}{2n\ln 2} - \mathcal{O}\left(\frac{1}{mn}\right) \ . \tag{3.11}$$

where m and n are the dimension of the Hilbert space in each subsystem, with $m \leq n$. Since $m = n = 2^{L/2}$ in our case, $S^R \simeq \frac{L}{2}$ in the large L limit. This limiting value

[5] In fact, one can rigorously prove that the energy fluctuation in random product states are comparable to that in random pure states even though product states are a set of measure zero in the space of pure states.

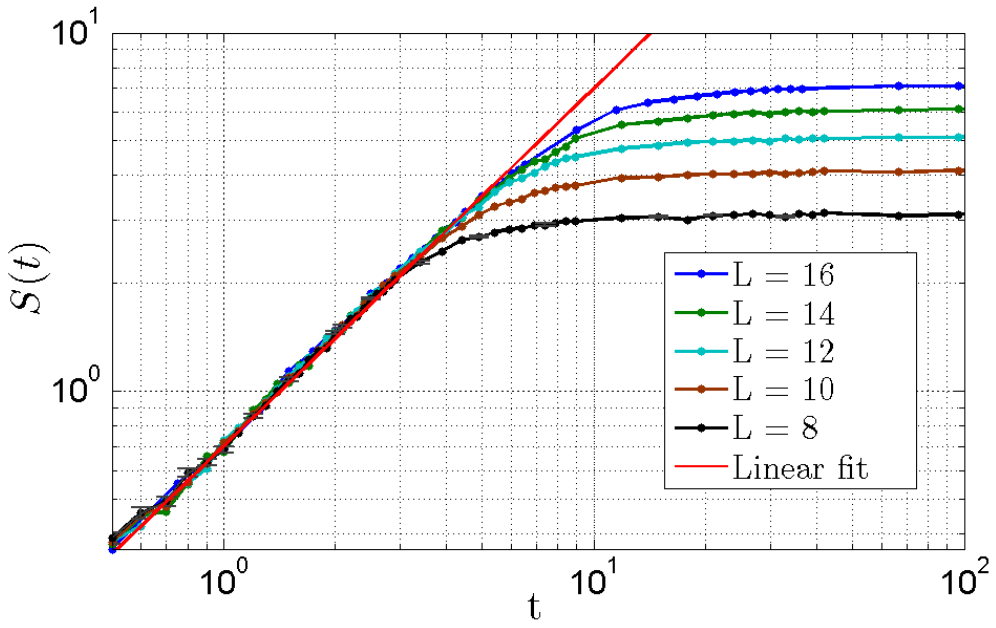

Figure 3.2: Spreading of entanglement entropy $S(t)$ for chains of length L. Initially the entanglement grows linearly with time for all cases, with the same speed $v \cong 0.70$. Then the entanglement saturates at long time. This saturation begins earlier for smaller L, as expected. The linear fit function is $f(t) = 0.70t$. Standard error is less than 0.04 for all points and thus the error bars are only visible at early times.

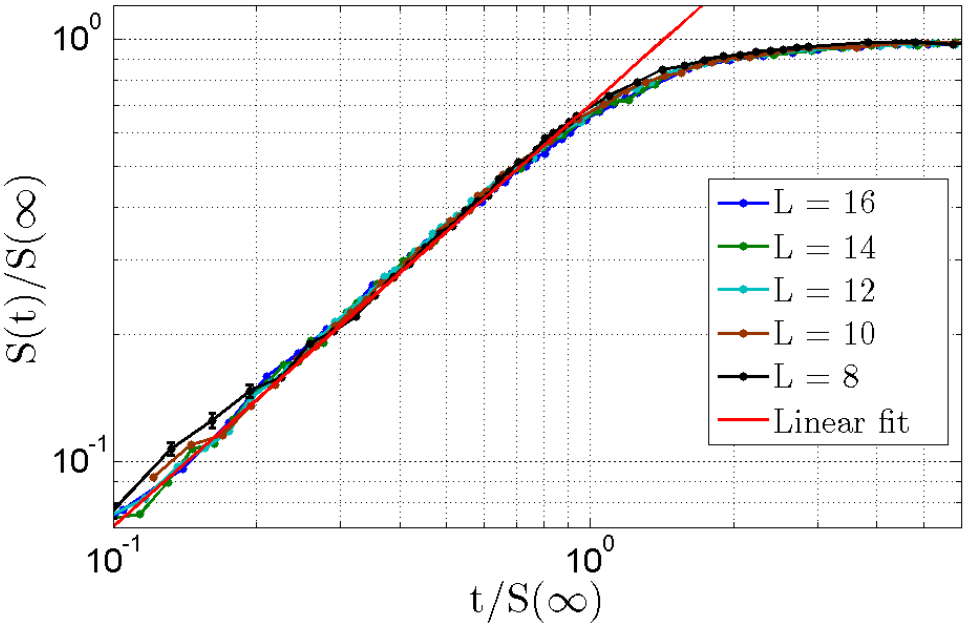

Figure 3.3: Entanglement entropy scaled by the infinite-time entropy for each L.

indicates that the entanglement spreads over the entire subsystem of length $L/2$. Therefore, before saturation begins, we can interpret $S(t)$ (in bits) as a measure of the distance over which entanglement has spread, and its growth rate thus as the speed of the ballistic entanglement spreading. This real-space picture of entanglement spreading is discussed later. It is clear from figure 3.2 that at long time ($t > 20 \sim 100$ depending on the system size) $S(t)$ saturates close to S^R. We found that the deviation of the saturation value from $L/2 - 1/(2\ln 2)$ (Eq. 3.11) is small (~ 0.19 for $L = 8$ and ~ 0.11 for $L = 16$) and expect this would be negligible in the thermodynamic limit.

This behavior suggests the finite-size and finite-time scaling form for the entanglement entropy:

$$S(t) \approx S_L(\infty) F(t/S_L(\infty)) \ , \tag{3.12}$$

where $S_L(\infty)$ is the infinite-time average value of the entanglement entropy [6] for chain length L, the scaling function $F(x) \sim vx$ for $x \to 0$ (v is the spreading rate), and $F(x) \to 1$ for $x \to \infty$. Figure 3.3 confirms that this scaling works well.

3.3.2 Real Space Picture of Entanglement Spreading

Entanglement entropy is by no means a local quantity and thus it is not easy to assign a local picture to spreading of entanglement [7]. On the other hand, the Lieb-Robinson bound states that the quantum information cannot spread arbitrarily fast by a short-range Hamiltonian [70] and Bravyi *et. al* has shown that the growth rate

[6] We used two methods to estimate $S_L(\infty)$: One is computing $S(t)$ at large t such as 500, 1000, 10000 and seeing that $S(t)$ remains constant within the standard error at these long times. The other is expanding the initial product state in terms of the eigenstates of H and giving each eigenstate a random phase (thus approximating infinite time) and computing the entanglement entropy from the state with random phases. We found these two methods give the same value within the error bar (fractional difference was less than 1.5%).

[7] The word "spreading" is already biased.

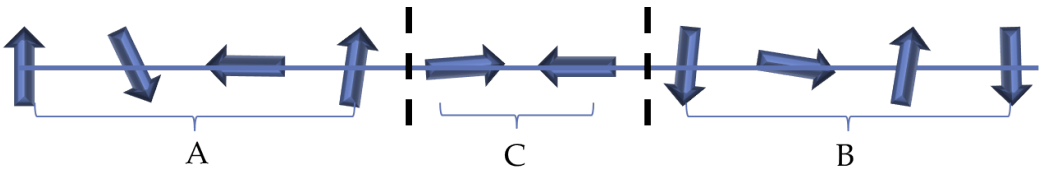

Figure 3.4: We consider a tripartite spin chain, ACB. A and B have the same length. We trace out the middle part C and compute entanglement between A and B using logarithmic negativity as a function of time. The initial condition is the same as we consider the bipartite entanglement entropy - random product states.

of entanglement entropy is proportional to the surface area of the cut [13]. These theorems support the idea of local spreading of entanglement entropy in a real space. Therefore, it would be nice if we have a direct measurement (at least theoretically) of local "wavefront-like" picture of entanglement entropy.

We consider a tripartite system, ABC as in Figure 3.4. Starting from the same initial condition, random product states, we first trace out the middle chain C and compute the entanglement entropy between the remaining parts A and B at time t. Since each spin is independent in an initial random product state, entanglement is zero everywhere in the beginning. If entanglement spreads over the space among each spin with finite rate, it would take finite time for A and B to become entangled and such entangling time (onset time when A and B begins to be entangled) would be a monotonic increasing function of the length of C. If entanglement entropy is truly a global quantity and does not allow any concept of local spreading, entanglement entropy between A and B would become nonzero instantaneously regardless of the length of C. Intuitively, the former should be true and we want to have a calculation that supports our intuition.

Negativity as a Computable Measure of Entanglement Entropy of a Mixed State

One problem with the above scenario is not that our physical intuition is wrong but the fact that we do not have a good *computable* measure of quantum entanglement entropy of a mixed state. The entire system ABC is a pure state but once we trace out C, the remaining state is in general mixed, not pure. What makes the quantum entanglement in a mixed state difficult is that the usual method (tracing out a part of the system and compute von Neumann entropy of the rest) cannot distinguish the quantum entanglement from *classical correlation*. If a state ρ can be represented by the following form (A and B are disjoint regions in the state space),

$$\rho = \sum_i c_i \rho_{i,A} \otimes \rho_{i,B} \tag{3.13}$$

then the two regions A and B are classically correlated. This implies that direct generalization of Schmidt decomposition will lead to classical correlation, not quantum entanglement. Therefore, von Neumann mutual information S between A and B,

$$S = \frac{1}{2}\left(S_A + S_B - S_{AB}\right) \ , \tag{3.14}$$

where S_A (S_B) is the von Neumann entropy of $\rho_A = Tr_B\rho$ ($\rho_B = Tr_A\rho$) and S_{AB} is the von Neumann entropy of the entire system, cannot separate the quantum entanglement from classical correlation.

Trivially, most states are mixed states, not pure states. A number of measures have been invented to quantify quantum entanglement of a mixed state, which can be found in Refs. [97, 12] and references therein. Each measure has its own physical meaning but most of them are involved with minimization over quantum states, which make them practically infeasible to compute. Therefore, we employ an incomplete

but computable measure of quantum entanglement of a mixed state, the *negativity* [25, 124]. The negativity is defined by the sum of negative eigenvalues of *partial transposition* of probability operator. Suppose we write the probability operator in the following form:

$$\rho = \sum_{\{i,k\},\{j,\ell\}} \rho_{ij,k\ell} |i\rangle\langle k| \otimes |j\rangle\langle \ell| \ , \tag{3.15}$$

where $|i\rangle\langle k|$ specifies region A and $|j\rangle\langle \ell|$ specifies region B. Then, partial transposition of A is

$$\rho^{T_A} = \sum_{\{i,k\},\{j,\ell\}} \rho_{ij,k\ell} |k\rangle\langle i| \otimes |j\rangle\langle \ell| \ . \tag{3.16}$$

Note that ρ^{T_A} is still hermitian and has unit trace $Tr\rho^{T_A} = 1$. However, ρ^{T_A} *may* have negative eigenvalues μ and thus its trace norm can be greater than one:

$$|\rho^{T_A}|_T = Tr\sqrt{\rho^{T_A}(\rho^{T_A})^\dagger} = 1 + 2\sum |\mu| = 1 + 2\mathcal{N}(\rho) \ , \tag{3.17}$$

where $\mathcal{N}(\rho)$ (the negativity) is the sum of absolute values of negative eigenvalues. Therefore, the negativity quantifies how much ρ^{T_A} fails to be positive semi-definite. It is proven that the existence of negativity is only a *sufficient* condition of quantum entanglement. There exist quantum entangled states without negativity. Thus, the negativity is an incomplete measure of quantum entanglement. However, it has a huge advantage over other more accurate measures of quantum entanglement: We can easily compute the negativity. This is the main reason why it is widely accepted measure to quantify quantum entanglement of a mixed state. To make the negativity similar to entanglement entropy, one can define the logarithmic negativity S_N:

$$S_N = \log |\rho^{T_A}|_T \ . \tag{3.18}$$

Note that when a state has no negativity, all eigenvalues of ρ^{T_A} is nonnegative and thus S_N is zero. In case of a pure state, S_N corresponds to Rényi entropy of index 1/2 [124][8]. This can be easily seen by the fact that for a given Schmidt spectrum λ_a of a given pure state,

$$|\rho^{T_A}|_T = 1 + 2\mathcal{N}(\rho) = \left(\sum_a \lambda_a\right)^2 . \tag{3.19}$$

We see that the Rényi entropy of index 1/2 is $2\log(\sum_a \lambda_a)$, which is precisely the logarithmic negativity.

Using Logarithmic negativity, we will provide an evidence of local real space picture of entanglement spreading. Starting from a random entangled product state, at time t we first trace out the middle chain C in Figure 3.4 and compute the logarithmic negativity of the remaining probability operator. Figure 3.5 is the logarithmic negativity as a function time and length of middle chain C while keeping the entire length of the system to be 16. As expected, the logarithmic negativity starts to build up at later time as the subsystems A and B become more separated (longer C). Note that the final saturation value of logarithmic negativity decreases as we increase the length of C, since the total length of the system L is fixed. Figure 3.6 is the plot of the onset time (time when the logarithmic negativity becomes nonzero [9]) vs. length of C. It clearly shows that the onset time gets delayed as the length of C becomes larger.

Since the negativity is a sufficient condition of entanglement entropy, these results may not be significant in a quantitative level. However, they provide a partial evidence of local "wave-front" like spreading of entanglement entropy.

[8]Rényi entropy of index q of a state ρ is defined by $S_q(\rho) = \frac{1}{1-q}\log(Tr\rho^q)$. It converges to von Neumann entropy in the limit of $q \to 1^+$.

[9]numerically we choose 10^{-5}

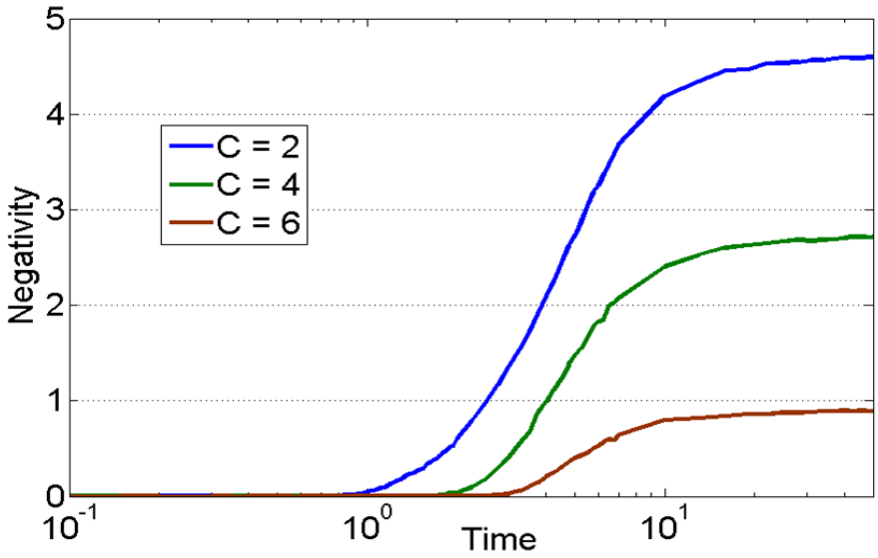

Figure 3.5: Logarithmic negativity as a function of time. While keeping the total length of the system $L = 16$, regions A and B begins to get entangled at a later time as we increase the length C.

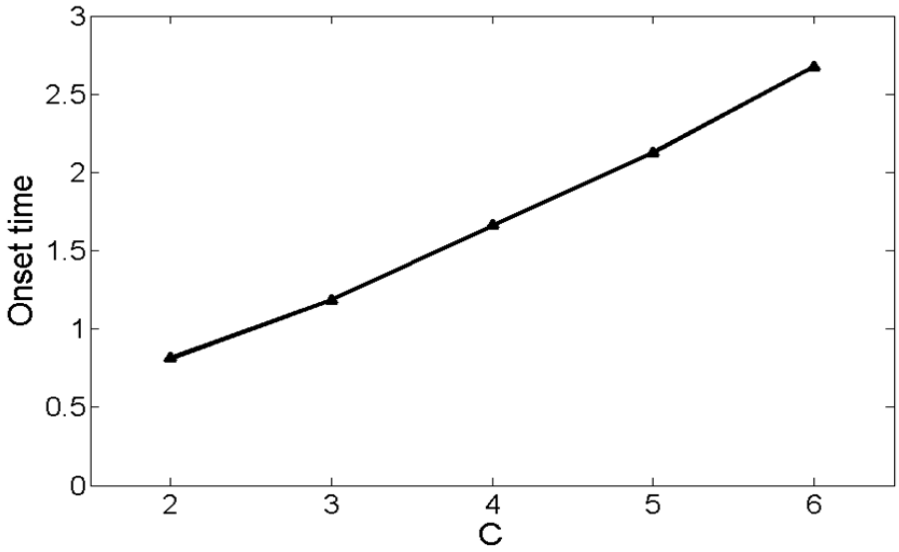

Figure 3.6: Onset time of logarithmic negativity as a function of the length of C (separation length between A and B). The onset time is delayed when separation becomes larger.

3.3.3 Roles of Energy Conservation in Entanglement Spreading

Figure 3.2 shows that entanglement spreading slows down in later stage before it approaches the saturation value and the saturation value is slightly smaller than the Page limit, $\frac{L}{2} - \frac{1}{2\ln 2}$. We attribute these to energy conservation, which is the only conservation law except for the global discrete symmetries. Stationary entanglement entropy means that initially out-of-equilibrium state completely equilibrated. This equilibration must be involved with reallocation of energy density, which is governed by slow diffusive energy current (see next section). Therefore, at later stage, we expect reduced spreading rate of entanglement entropy due to energy transport. The Page limit is the average entanglement entropy sampled from infinite temperature ensemble. On the other hand, our initial condition, random product state, may not sample all eigenstates with equal weight. Since the infinite temperature ensemble has the maximum entropy, any deviation from that ensemble will necessarily decrease the entanglement entropy and consequently we may have saturation value of entanglement smaller than Page limit. One way to check this hypothesis is to intentionally break the energy conservation of the system by making the Hamiltonian time-dependent.

Using the Hamiltonian H, let's first construct the Floquet unitary operator that unitarily evolves a quantum state. We decompose the Hamiltonian H into two parts: one consists of only σ^z operator (H_z) and the other one contains only σ^x operator (H_x).

$$H_z = \sum_i h\sigma_i^z + \sigma_i^z\sigma_{i+1}^z \tag{3.20}$$

$$H_x = \sum_i g\sigma_i^x \ . \tag{3.21}$$

Then, we drive the system with H_z for a period τ and apply H_x for τ and then repeat. This periodically driven Floquet system can be characterized by a unitary operator $U_F(\tau)$:

$$U_F(\tau) = \exp(-iH_x\tau)\exp(-iH_z\tau) \tag{3.22}$$

. Note that a conventional Floquet unitary operator should have time step 2τ ($U_F(2\tau)$) since our driving has a period of 2τ. However, we want to make a direct comparison with the ordinary propagator, $U(t) = \exp(-iHt)$, at each time point; any time t for a system evolving with $U(t)$ and a multiple of τ for a system evolving with $U_F(\tau)$. Therefore, we scale the period by half on purpose [10]. We choose τ to be 0.8.

The Floquet theorem states that we can characterize each eigenvalues of the Floquet operator by a real number λ, where the eigenvalue is $e^{i\lambda}$. This λ can be determined up to modulo 2π and the statistics of λ is expected to follow a Circular Ensemble (CE) statistics, which is similar to GOE statistics with modulo 2π [11] [34]. Furthermore, at long time limit, the Floquet operator "thermalizes" a system at infinite temperature ensemble [34, 98]. From this property, we expect that a state, initially prepared in a random product state, driven by the Floquet operator will have the saturation value of entanglement entropy equal to the Page limit. Also, the Floquet system does not conserve energy. $U_F(\tau)$ does not even have a "ground state" since everything is determined by phases [12]. Therefore, equilibration is possible without slow energy transport, which implies that the slowing down of entanglement spreading in the Hamiltonian system could be absent in the Floquet system.

Preparing two random product states, we evolve one state with $U_F(\tau)$ and the other state with $U(t)$ and then compare their entanglement entropy $S(t)$'s. For a

[10] Another way of looking at $U_F(\tau)$ is the first order Trotter decomposition of the propagator: $U(t) = \exp(-i(H_x + H_z)t) = \exp(-iH_xt)\exp(-iH_zt) + \mathcal{O}(t^2)$. Note that $\tau \to 0$ limit makes $U_F(N\tau) = (U_F(\tau))^N$ identical to $U(t)$, where $t = N\tau$.

[11] Similar to level repulsion in a RMT statistics, there is *phase* repulsion in CE statistics.

[12] There is no area law of entanglement in eigenstates of $U_F(\tau)$.

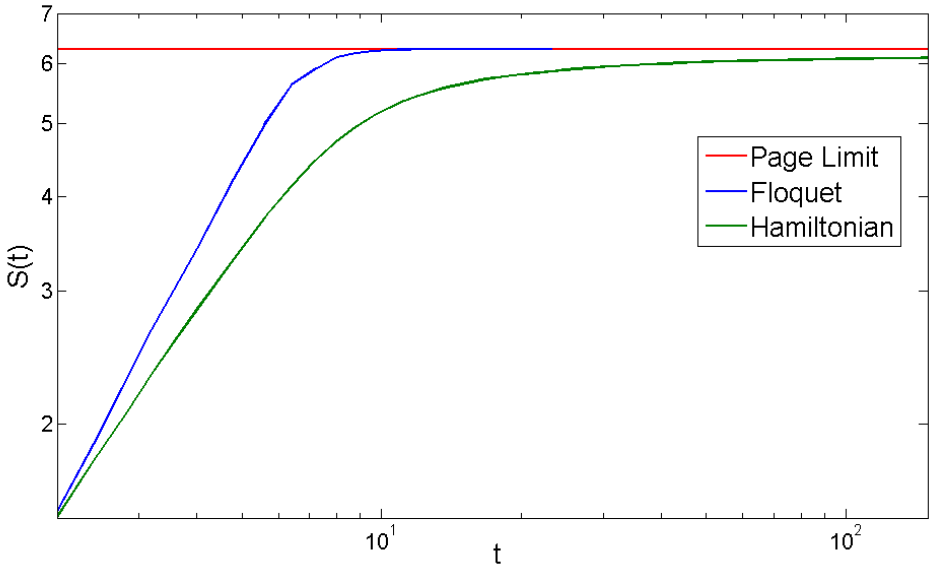

Figure 3.7: Comparison of Entanglement spreading of Floquet unitary operator (precisely defined in the main text) and that of Hamiltonian unitary operator. Both started from the same initial condition, random product state. Floquet system does not have strong signal of slow down of spreading near the saturation value. Also, the final saturation value is closer to Page limit, $L/2 - 1/(2\ln 2)$. The system size L is 14. We averaged over 50 realization of random states.

Floquet system, we only measure at a multiple of τ. Figure 3.7 is the plot of entanglement spreading under these two unitary operators. We clearly see that the Floquet system does not show significant slow down approaching the saturation of entanglement entropy compared to the Hamiltonian system and the final value of entanglement entropy is indeed same as the Page limit. This demonstrates that the energy conservation is responsible for two features of entanglement entropy at later time.

3.4 Diffusive Energy Transport

Now let's consider the diffusive dynamics of this system. As an example, we study the diffusive spreading of an initially localized energy inhomogeneity. First we prepare the system in the maximal thermodynamic entropy mixed state (equilibrium at

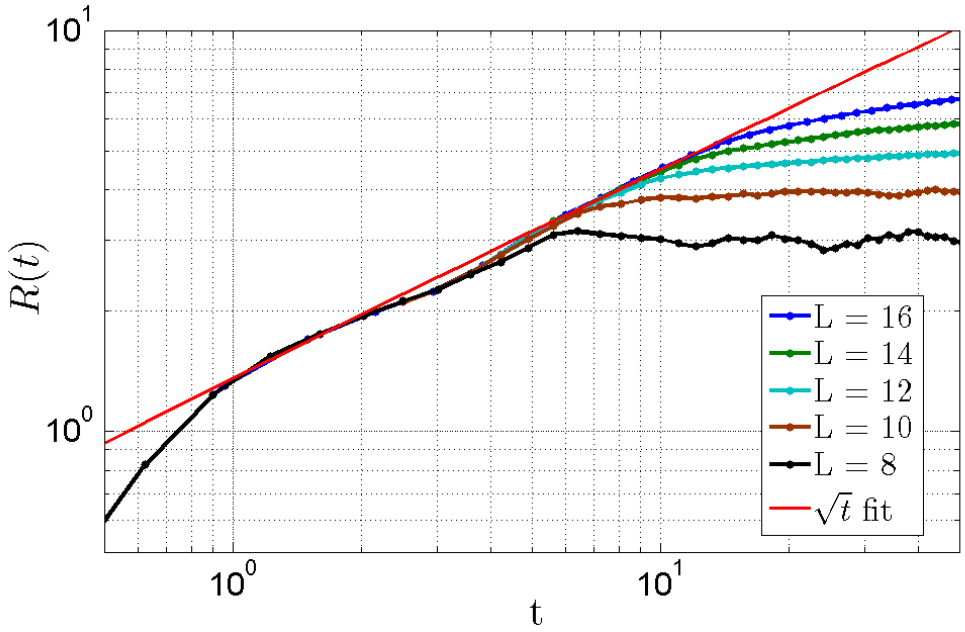

Figure 3.8: The average energy spreading, $R(t)$ (defined in the main text) vs. time. Before saturation, its behavior does not depend on the system size. As we increase the system size, diffusive $\sqrt{t}$ behavior becomes more apparent.

infinite temperature) and put a small energy perturbation on the center bond. Then we observe how this extra local energy spreads over the system under unitary time evolution. Specifically, the initial probability operator (density matrix) is

$$\rho(0) = \frac{1}{2^L}\left(I + \epsilon\sigma^z_{L/2}\sigma^z_{L/2+1}\right) \ , \tag{3.23}$$

where I is the identity operator and ϵ is a small number. Note that I commutes with H, so we only need to time evolve the perturbation. Then, we compute the local energy, $\langle H_r\rangle(t)$, at each site and bond r at time t. The position index r is an integer (1 to L) for each site and a half-integer (3/2 to L - 1/2) for each bond. Explicitly,

$$H_r = \begin{cases} g\sigma^x_r + h\sigma^z_r & \text{sites } 2 \le r \le L-1 \\ g\sigma^x_r + (h-J)\sigma^z_r & r = 1 \text{ or } L \\ J\sigma^z_{r-1/2}\sigma^z_{r+1/2} & \text{bonds } 3/2 \le r \le L-1/2 \ . \end{cases} \tag{3.24}$$

This is just a decomposition of the hamiltonian $H = \sum_r H_r$. Trivially, $\langle H_r \rangle = \epsilon \delta_{r,\frac{L+1}{2}}$ at time $t = 0$. To quantify the energy spreading at time t, we compute an average "distance" $R(t)$ that the energy has moved away from the center bond:

$$R(t) = \frac{2}{\langle H \rangle} \sum_r \left| r - \frac{L+1}{2} \right| \langle H_r \rangle(t) \ , \tag{3.25}$$

where $\langle H \rangle = \epsilon$ is the conserved total energy. Figure 3.8 is the plot of $R(t)$ for L = 8, 10, 12, 14, and 16. If the extra energy at long time is distributed equally to all sites and bonds, $R(\infty) \to \frac{L}{2}\frac{2L-2}{2L-1} \simeq \frac{L}{2}$ and thus close to the maximum value of entanglement spreading (the factor of 2 in Eq. 3.25 is to make the long time value of $R(t)$ comparable to that of $S(t)$). We find that the saturation value, $R(\infty)$ [13], grows linearly with the system size but is always slightly smaller than $L/2$ due to the final local energy distribution not being homogeneous near the ends of the chain.

If this dynamics is diffusive, the energy spread is $R(t) \approx \frac{4}{\sqrt{\pi}}\sqrt{Dt} \sim \sqrt{t}$ (one-dimensional random walk) for sufficiently large t ($t \geq 1$ in our case) before finite-size saturation begins. D is the energy diffusivity, which only depends on the interaction parameters, not the system size. Figure 3.8 clearly shows that $R(t)$ is independent of system size at early stages, and it grows as $\sim \sqrt{t}$ before saturation begins. For L = 8, the frequency scale of the many-body level-spacing is of order 0.1 and thus $R(t)$ begins oscillating around $t \sim 10$. Although the system sizes that we can diagonalize are not large enough to show a wide range of time scales, they do show that the speed of entanglement spreading becomes faster than the rate of diffusive energy spreading by direct comparison of $S(t)$ and $R(t)$. Figure 3.9 is the plot of $S(t)$ and $R(t)$ for L = 16. In the very beginning ($t \leq 1$), $R(t)$ grows faster than $S(t)$ due to microscopic details of the dynamics, but soon the linearly-growing $S(t)$ overtakes $R(t)$

[13] We estimated $R(\infty)$ as the average of a few values of well-spaced $R(t)$ near and beyond the time scale set by the inverse many-body energy-level spacing. For example, the inverse many-body level spacing for L = 14 is ≈ 533. Then, $R(\infty)$ is estimated by averaging $R(450)$, $R(600)$, $R(750)$, $R(900)$, and $R(1050)$. Fractional fluctuation within that time range was as small as 0.12% (this fractional fluctuation becomes smaller as we increase the system size).

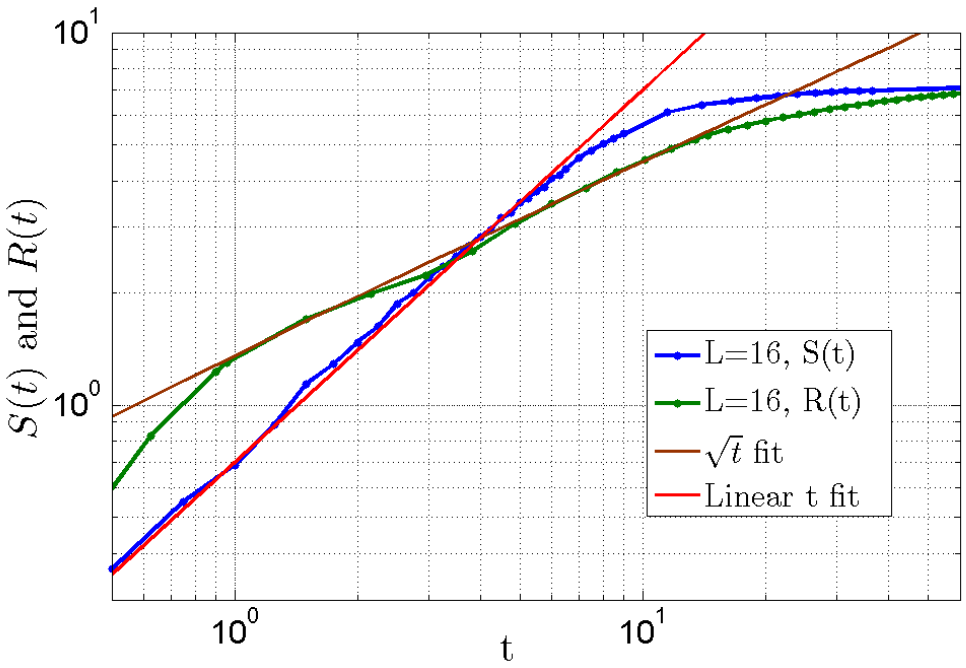

Figure 3.9: Direct comparison of $S(t)$ and $R(t)$ for $L = 16$. It is clear that the entanglement spreads faster than energy diffuses in the scaling regime before saturation.

and approaches its saturation while $R(t)$ is growing only as $\sim \sqrt{t}$. Therefore, this is a direct demonstration of the contrast between ballistic entanglement spreading and diffusive energy transport.

3.5 Conclusion

In conclusion, we have demonstrated that quantum entanglement spreads ballistically in a nonintegrable diffusive system. Since there are no ballistically traveling quasiparticles, the mechanism of entanglement spreading is different from what happens in integrable systems, where these quasiparticles can carry both energy and information. At high enough temperature, almost all states are relevant to the dynamics, and the dynamics is constrained by only few conservation laws (in our case, only the total energy). In this regime, the concept of quasiparticles is not well-defined for the system we have studied. Even so, if we do heuristically describe the dynamics of our

diffusive model in terms of quasiparticles, these quasiparticles scatter strongly and frequently and thus have a short mean free path. This limits the energy transport to be diffusive. But apparently the quantum information needed to spread entanglement is passed along in each collision, presumably to all outgoing quasiparticles from each collision. Thus this information spreads in a cascade or shower of collisions and the edges of this shower spread ballistically.

We conjecture that for highly-excited nonintegrable systems such as we study here, there are no *local* observables whose correlations spread more rapidly than diffusively, even though the entanglement spreads ballistically. Note that this is a strong conjecture that goes well beyond what we can test numerically.

We have used the analogy from Ref. [91] between the spreading of entanglement and the spreading of an epidemic. But it is an unusual sort of nonlocal epidemic, where the symptoms of the "disease" can not be detected by any local observables. In Refs. [73, 72] they make an analogy instead to a tsunami; again this appears to be a very gentle nonlocal tsunami, whose effects can only be detected by nonlocal observables. An interesting question that we leave for future work is: What is the simplest and most local operator that can detect this ballistically spreading entanglement? We detected it using the state of the full system, but if the entanglement has only traveled a distance ℓ in each direction from the central bond as partially demonstrated by using negativity measure of entanglement in real space, it should be detectable by some operators that only involve the spins within that distance.

Chapter 4

Thermalization and Construction of Slowly Relaxing Operators in a Nonintegrable Quantum System

From everyday experience, we know that an out-of-equilibrium system will eventually equilibrate with the environments. Then, what if we include everything, even the environments, and ask questions about equilibration? Does the whole system eventually equilibrates to thermal equilibrium? If so, then what would be the time scale of such phenomenon? In this chapter, we give partial answers to above questions using the exact diagonalization method and a new algorithm to search for slowly relaxing operators.

The results of section 2 in this chapter are the results of collaboration with Tatsuhiko N. Ikeda and David A. Huse (in preparation).The results of section 3 and 4 in this chapter are obtained through collaborations with Mari Carmen Bañuls, J. Ignacio Cirac, Matthew B. Hastings, and David A. Huse (in preparation).

We set the Planck constant $\hbar$ and the Boltzmann constant k_B to unity.

4.1 Introduction

Every child knows that a cup of hot coffee and a glass of cold beer will eventually reach the same temperature if they are put outside. This phenomenon is thermalization. The conventional explanation for the mechanism of thermalization uses an infinitely large heat bath with which an out of equilibrium system can exchange energy (and particles if allowed) to achieve thermal equilibrium. However, this mechanism is not applicable to thermalization of an *isolated* system. Classical mechanics can thermalize an isolated system by chaotic dynamics, which makes the system ergodic in the long time limit. For a quantum system, on the other hand, it is not yet completely settled (at least theoretically) whether a unitary quantum dynamics can bring an isolated nonequilibrium state to an ergodic phase [88, 6, 75] (known as Berry's conjecture).

To obtain a "quick" answer, we borrow results from experimental work. Various experiments with ultracold atoms, which we believe one of the most isolated quantum many-body systems on Earth, suggest that the answer is "yes", reporting that momentum distribution of ultracold atoms indeed in a good agreement with equilibrium statistical mechanics (see reviews [8, 44] and references therein). Therefore, we first admit that a generic isolated quantum system does thermalize and move on to the next question, *how*.

Quantum dynamics is unitary. A unitary dynamics keeps all information of the initial condition, and thus the entire system is apparently different from thermal state at all times. Consequently, quantum mechanics does not allow thermalization of a whole system unless the initial state is thermal. This does not contradict with our experience of thermalization as long as detailed information of initial condition is only accessible by global "observables" (hermitian operators), which no experimental apparatus can measure at a later time. Therefore, being thermalized means thermalization of *few-body* observables, which can be measured in experiment. Note that locality need not be restricted to real space: the momentum distribution is not local in

real space but local in momentum space and it can be written as a linear combination of one body operators in real space.

Many theoretical works have addressed the question of quantum thermalization (e.g. Refs. [125, 48, 102, 73, 72] and references therein), and one of the leading explanations for the thermalization of few-body observables in an isolated quantum system is the eigenstate thermalization hypothesis (ETH) [35, 119, 104]. ETH states that an eigenstate of a nonintegrable (quantum chaotic) Hamiltonian is thermal when only aspects of few-body observables are concerned, *i.e.* it gives the same expectation value as the Gibbs ensemble of the same fixed energy density (temperature). Many consequences of ETH have been numerically tested in many works [104, 108, 7, 58, 118] and appeared to be valid for almost all cases (see also Ref. [106] for the comparison of ETH with von Neumann's quantum ergodic theorem). Here we perform another stringent accuracy test of ETH. Numerically diagonalizing our model Hamiltonian (Eq. 1.3) we find the outlier states, which deviate the most from the predictions of ETH, and then check whether deviation decreases as the system size increases. We numerically show that even these outlier states obey ETH as the system approaches thermodynamic limit. Therefore, we provide numerical evidence that ETH is true for *all* states, not just almost all.

Given that ETH explains how quantum thermalization is possible, our next question is *how quickly* an out-of-equilibrium state thermalizes. Conventional theories of diffusive transport tell us that thermalization requires transport of local conserved quantities, energy and particles. Within a linear response theory, the time scale τ of transport is determined by the product of diffusivity D and the square of the longest wavelength of inhomogeneous profile of the conserved quantity, k^2; $\tau = 1/(Dk^2)$. However, the quantum theory only has a lower bound of thermalization time scale given by the Lieb-Robinson bound [70] and therefore possibilities of exponentially long time to thermalize are not excluded.

We will construct a local operator that takes the longest to relax to the equilibrium value. Using an efficient algorithm, we exhaustively consider all possible local operators of certain range M and find the slowest relaxing operator. We show that relaxation time scale of such operators is indeed longer than the diffusive transport. This is a new phenomenon that quantum mechanics with a diffusive Hamiltonian allows local operators to equilibrate slower than simple diffusion allows.

One remark is in order. There are two notable exceptions to canonical thermalization (thermalizing to the Gibbs state); integrable system and many-body localized system (MBL). An integrable system has an extensive number of local conservation laws. Therefore, the conventional Gibbs ensemble is not enough to fix the value of a few-body operator. It is conjectured that an expectation value of a few-body operator of an integrable system can be characterized by the Generalized Gibbs Ensemble (GGE) [105, 103, 92, 45, 77], while some recent literatures report insufficiencies of GGE in certain cases[46, 100, 80, 47]. Many-body localization happens when disorder is strong enough in an interacting system (see Refs. [1, 5, 84] and references therein). In an MBL phase, individual many-body eigenstate is localized and MBL truly disobeys ETH in every sense since all information is locked in localized many-body eigenstates. Although integrable systems and MBL systems are exciting and very active fields of research, we restrict ourselves to disorder-free, robustly nonintegrable Hamiltonian (Eq. 1.3) throughout this chapter.

4.2 Eigenstate Thermalization Hypothesis

Quantum dynamics is unitary. Since a unitary operator is mathematically just a basis transformation, the entire system contains all information about the initial condition, which is apparently different from thermal distribution if initially out of equilibrium. Instead, what thermalizes is *local, few-body* observables.

Formally, with a time-independent Hamiltonian H and an out of equilibrium initial state ρ, we write the expectation value of a few-body operator $\hat{O}$ at time t:

$$\langle \hat{O}(t) \rangle = Tr\left(e^{-iHt}\rho e^{iHt}\hat{O}\right) = \sum_{n,m} \rho_{n,m} O_{m,n} e^{-i(E_n - E_m)t} \ , \tag{4.1}$$

where $\rho_{n,m}$ and $O_{m,n}$ are matrix elements of the initial state ρ and the operator $\hat{O}$ in energy eigenbasis and E_n is the n'th eigenenergy of the Hamiltonian H. Assuming no degeneracies[1], off-diagonal terms will dephase in the long time limit and Eq. 4.1 will approach a stationary value in thermodynamic limit [71]. Note that Poincaré recurrence, in principle, happens for any finite system. The stationary value $\langle \hat{O} \rangle_{eq}$ should be the sum of diagonal elements and thus, time independent:

$$\langle \hat{O} \rangle_{eq} = \sum_{n} \rho_{n,n} O_{n,n} \ . \tag{4.2}$$

When this becomes valid, the system has *equilibrated* and not necessarily thermalized. Thermalization is a stronger statement and means that the equilibrium value is equal to thermal ensemble average at fixed conservation law. Assuming the energy is the only conserved quantity, which is determined by the inverse temperature β, thermalization is the following:

$$\langle \hat{O} \rangle_{eq} = \langle \hat{O} \rangle_{th} = \frac{1}{Z_\beta} Tr\left(e^{-\beta H}\hat{O}\right) = \frac{1}{N_E} \sum_{|E - E_n| \leq \Delta E} O_{n,n} \tag{4.3}$$

$$Tr(H\rho) = \frac{1}{Z_\beta} Tr\left(e^{-\beta H} H\right) \ . \tag{4.4}$$

In first line, we used the equality between canonical average and microcanonical average at thermodynamic limit (ΔE is a microcanonical window near the average energy E). The second line is how we define the inverse temperature β and Z_β is the

[1]Due to the level repulsion, this assumption is natural.

partition function. Eq. 4.3 implies that *all* initial conditions with the same energy density should thermalize the operator $\hat{O}$ to the *same* value. If this statement is true, we may consider an extreme situation: the initial state is an energy eigenstate ($\rho = |n\rangle\langle n|$). The fact that we can find a unique β_n that corresponds to the energy density of the eigenstate $|n\rangle$ implies that *the expectation value of a few-body operator of an energy eigenstate is thermal*. This highly nontrivial statement is the Eigenstate Thermalization Hypothesis (ETH) [35, 119, 104] [2].

Here we perform one stringent accuracy test of ETH. Numerically diagonalizing a finite size nonintegrable Hamiltonian H we used for entanglement spreading, we search for the outlier state, which numerically agrees the least with ETH. Then, we do a finite-size scaling of these outlier states as a function of system size. If ETH is true for all (not almost all) states in thermodynamic limit, even these outlier states (perhaps from a measure zero set in the space of eigenstates) should follow ETH.

The Hamiltonian is Eq. 1.3:

$$H = \sum_i \left(g\sigma_i^x + h\sigma_i^z + J\sigma_i^z\sigma_{i+1}^z \right) \ . \tag{4.5}$$

As before, the parameter choice is $(g, h, J) = ((\sqrt{5}+5)/8, (\sqrt{5}+1)/4, 1)$. This time we use the periodic boundary condition so that every site is equivalent and momentum is a good quantum number. The Hamiltonian can be written in a block diagonal form of each momentum sector, where the size of each block is of order $(2^L)/L$. This enables us to diagonalize slightly larger system size than open boundary condition; $L = 19$. We consider both even and odd length chains. Note that level repulsion of RMT statistics only holds within each momentum sector but ETH should be valid regardless of momentum [108].

[2] Sometimes this is referred as strong ETH in contrast to weak ETH, where average over a narrow energy window is allowed

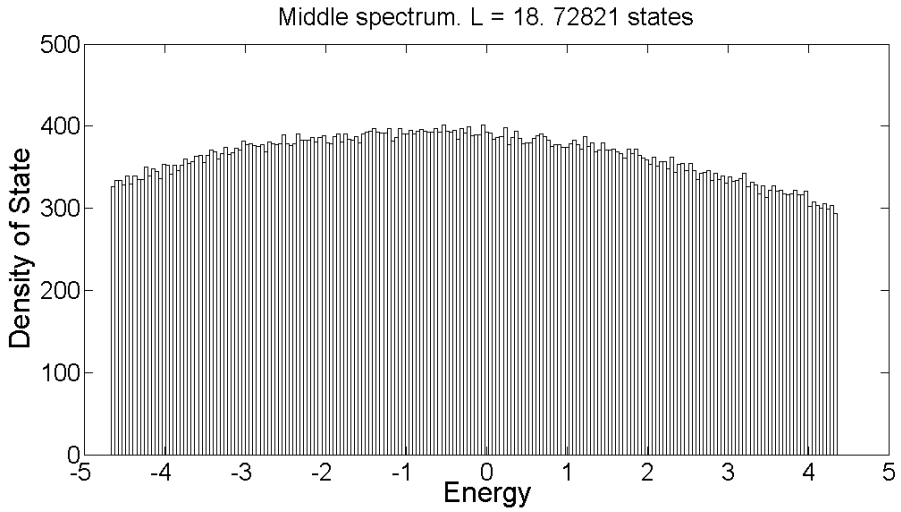

Figure 4.1: Histogram of density of state. The ratio of maximum to minimum is $\sim$ 1.20

4.2.1 ETH parameter

We want to quantify the accuracy of ETH. We consider the following parameter:

$$r_n = \langle n+1|\hat{O}|n+1\rangle - \langle n|\hat{O}|n\rangle \ , \tag{4.6}$$

where $\hat{O}$ is a local few-body operator and $|n\rangle$ is n's energy eigenstate. We assume no degeneracies and sort the eigenstate in an ascending order of energy ($E_{n+1} > E_n$). If ETH is true in a strong sense, each eigenstate $|n\rangle$ is thermal and expectation value of every local operator should be equal to the thermal expectation value. For each eigenstate, we can define an inverse temperature β_n by the following implicit equation:

$$E_n = \frac{tr(H\exp(-\beta_n H))}{tr(\exp(-\beta_n H))} \tag{4.7}$$

In thermodynamic limit, we know that $E_{n+1} - E_n \to 0$ and consequently $\beta_{n+1} - \beta_n$ (exception exists near ground state for a gapped system). Therefore, if ETH is true, r_n should vanish in thermodynamic limit. However, since everything is discrete in numerical study, a little caution is necessary. More precisely, suppose we have a

sequence of inverse temperatures $\{\ldots, \beta_n, \beta_{n+1}, \ldots\}$ ($\beta_n > \beta_{n+1}$), which corresponds to the sequence of eigenstates. Let's define $\delta\beta_n = \beta_n - \beta_{n+1} \ll 1$. Then, ETH says (up to first order in $\delta\beta_n$)

$$r_n = \frac{tr\left(\hat{O}\exp(-(\beta_n - \delta\beta_n)H)\right)}{tr\left(\exp(-(\beta_n - \delta\beta_n)H)\right)} - \frac{tr\left(\hat{O}\exp(-\beta_n H)\right)}{tr\left(\exp(-\beta_n H)\right)} \tag{4.8}$$

$$= \delta\beta_n \left[\frac{tr\left(\hat{O}(H - E_n)\exp(-\beta_n H)\right)}{tr(\exp(-\beta_n H))}\right] \tag{4.9}$$

$$\simeq -\delta\beta_n \frac{\partial\langle\hat{O}\rangle_\beta}{\partial\beta}\bigg|_{\beta=\beta_n}. \tag{4.10}$$

The last line is in the thermodynamic limit and $\langle\hat{O}\rangle_\beta = tr(\hat{O}\exp(-\beta H))/tr(\exp(-\beta H))$. From this equation, we can see that what makes r_n vanishing is $\delta\beta_n$, which is the spacing between two adjacent temperatures. Roughly, this quantity is inversely proportional to the density of state and thus approaches zero only in thermodynamic limit. Since the density of state and $\partial\langle\hat{O}\rangle_\beta/\partial\beta$ do vary over the range we study, direct comparison among bare values of r_n could be dangerous, especially those near the edge of the spectrum where the variation in density of state is the largest. Therefore, we first look at how the density of state varies in the middle half of the spectrum (we keep only the middle half of the entire states sorted by energy). If the density of state is Gaussian, as shown by Refs. [54, 53], then the fractional difference between the density of state at the edge of the spectrum we keep and the density of state in the middle is just 20%. Figure 4.1 is the histogram of density of state in the middle half of the spectrum for $L = 18$ and it shows that the fractional difference between the largest and the smallest is indeed about 20%. Since the largest value of r_n is larger than the typical value of r_n by an order of magnitude (see Figure 4.4), we may neglect the effects of density of states, which should be at most of an order of 20%. Furthermore, as we can see from Figure 4.2, the first derivative of expectation value of a few-body operator with respect to energy is roughly constant.

Thus, we may neglect the other contribution, $\partial\langle\hat{O}\rangle_\beta/\partial\beta$ as well. Consequently, we will compare face values of r_n in the middle half of the energy spectrum and find out which state is responsible for the extreme value of r_n.

4.2.2 Results

For few-body operators, we consider all single-site operators, σ^x and σ^z (expectation value of σ^y is zero by time-reversal symmetry), and two-sites operators, $\sigma^x\sigma^x$ and $\sigma^y\sigma^y$ (expectation value of $\sigma^z\sigma^z$ is fixed by two single-site operators from Hamiltonian). All of the results of these operators are qualitatively the same. Since the Hamiltonian is time-reversal invariant, momentum k and $-k$ have exactly the same spectrum, thus degenerate except $k = 0$ and π. We consider only nonnegative k's: for even L, we take k from 0 to π and for odd L, we take k from 0 to $(L-1)\pi/L$. Therefore, even chains have $(L+2)/2$ momentum sectors considered while odd chains have $(L+1)/2$ momentum sectors taken into account. This difference may affect the finite-size scaling of outliers (strong parity effect) but has no impact on other properties.

Figure 4.2 is the plot of $\langle n|\hat{O}|n\rangle$ as a function of energy density E_n/L. It is clear that as we increase the system size (approaching thermodynamic limit), the fluctuation becomes smaller and thus they agree better with ETH. Note that the fluctuations are not particularly wider near the edge compared to the center of the spectrum. This supports that our choice of ETH parameter, Eq. 4.6, is appropriate over the range we consider.

Figure 4.3 is the plot of normalized distribution of $|r_n|$. As we increase the system size, the distribution becomes more narrow and sharply peaked at zero. In thermodynamic limit, ETH predicts that $P(r)$ becomes a delta function, $\delta(r)$. The distribution can be well-fitted by Gaussian distribution and the fluctuation $\sigma = \sqrt{\langle r^2\rangle - (\langle r\rangle)^2}$ decreases exponentially with the system size L, which qualitatively agrees well with the results reported in Ref. [7].

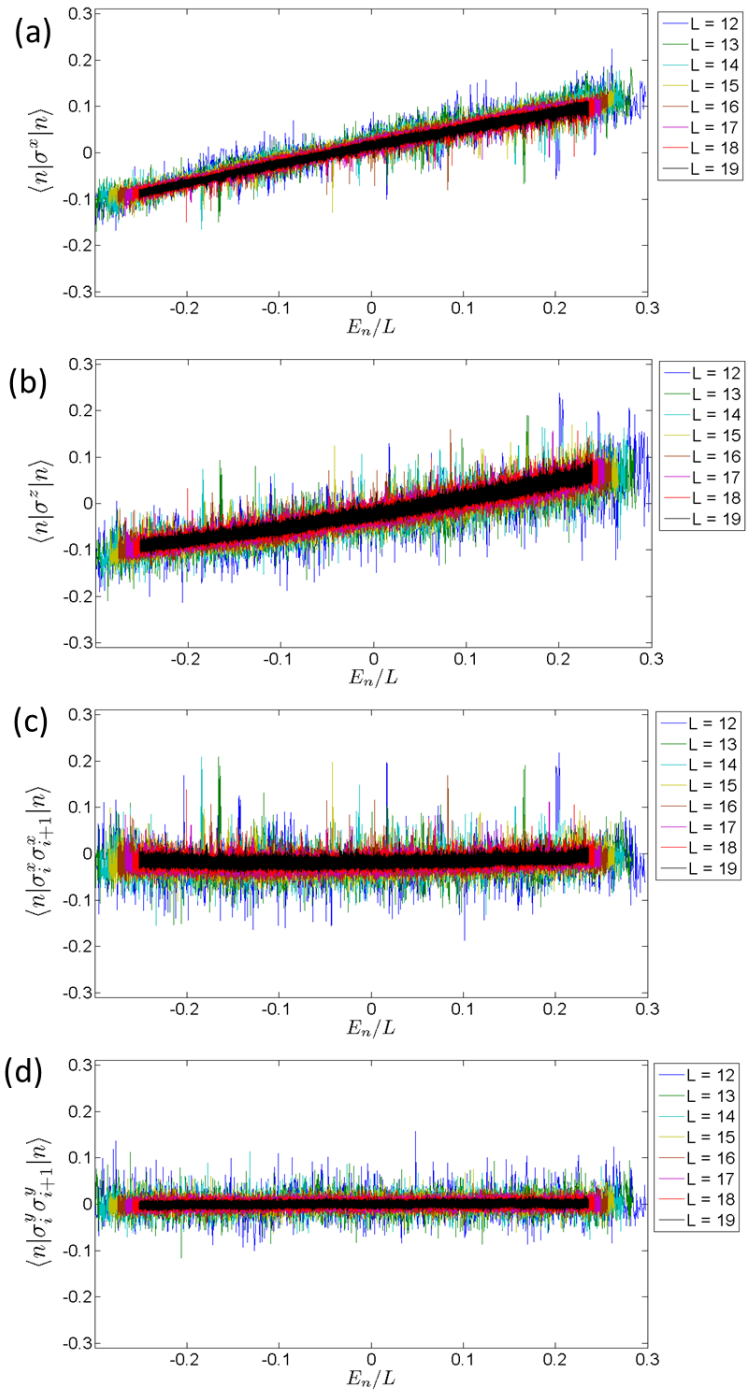

Figure 4.2: Expectation values of few-body operators vs. energy density: (a) σ_i^x (b) σ_i^z (c) $\sigma_i^x\sigma_{i+1}^x$ (d) $\sigma_i^y\sigma_{i+1}^y$. Due to translation invariance, the position i can be any site. The range of system size is $L = 12$ to 19. As we increase the system size, the fluctuation becomes small as ETH suggests.

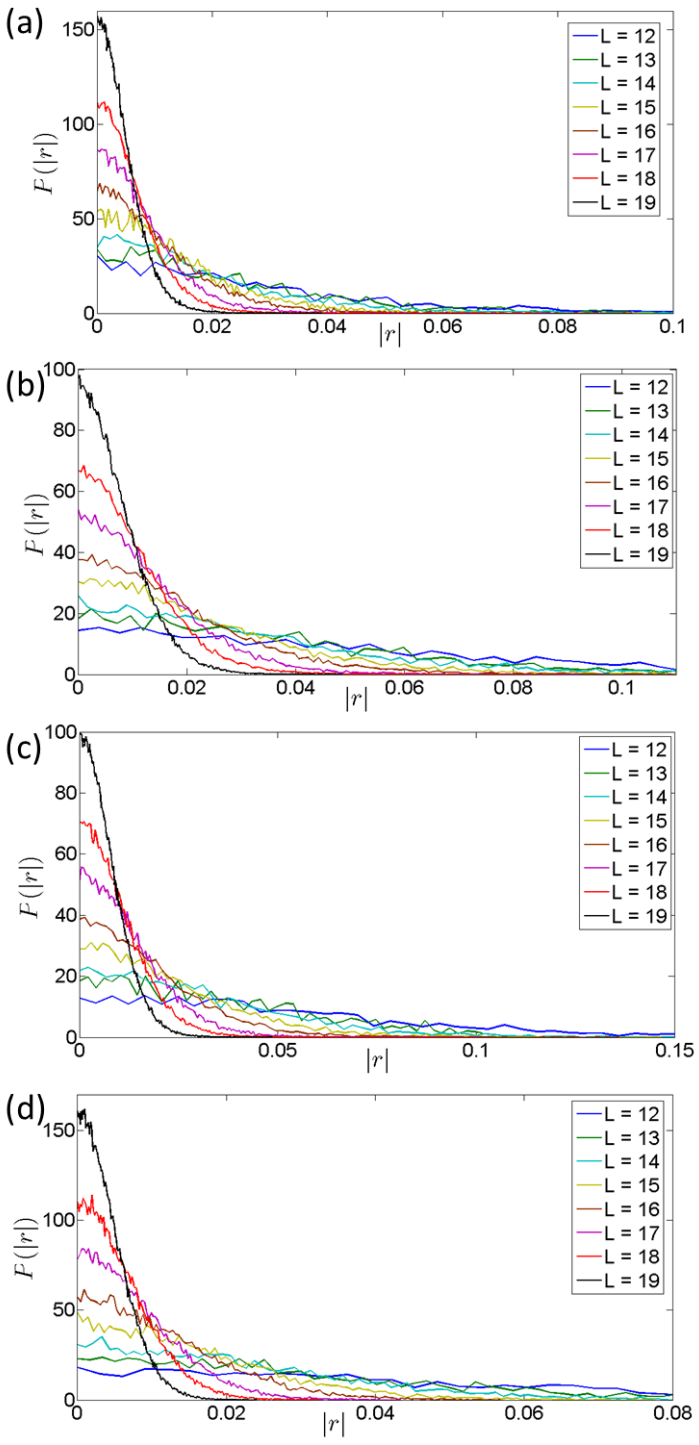

Figure 4.3: Normalized distribution of expectation values of few-body operators: (a) σ_i^x (b) σ_i^z (c) $\sigma_i^x\sigma_{i+1}^x$ (d) $\sigma_i^y\sigma_{i+1}^y$. Due to translation invariance, the position i can be any site. The range of system size is $L = 12$ to 19. As we increase the system size, the distribution becomes more sharply peaked near zero and its widths decreases exponentially with the system size.

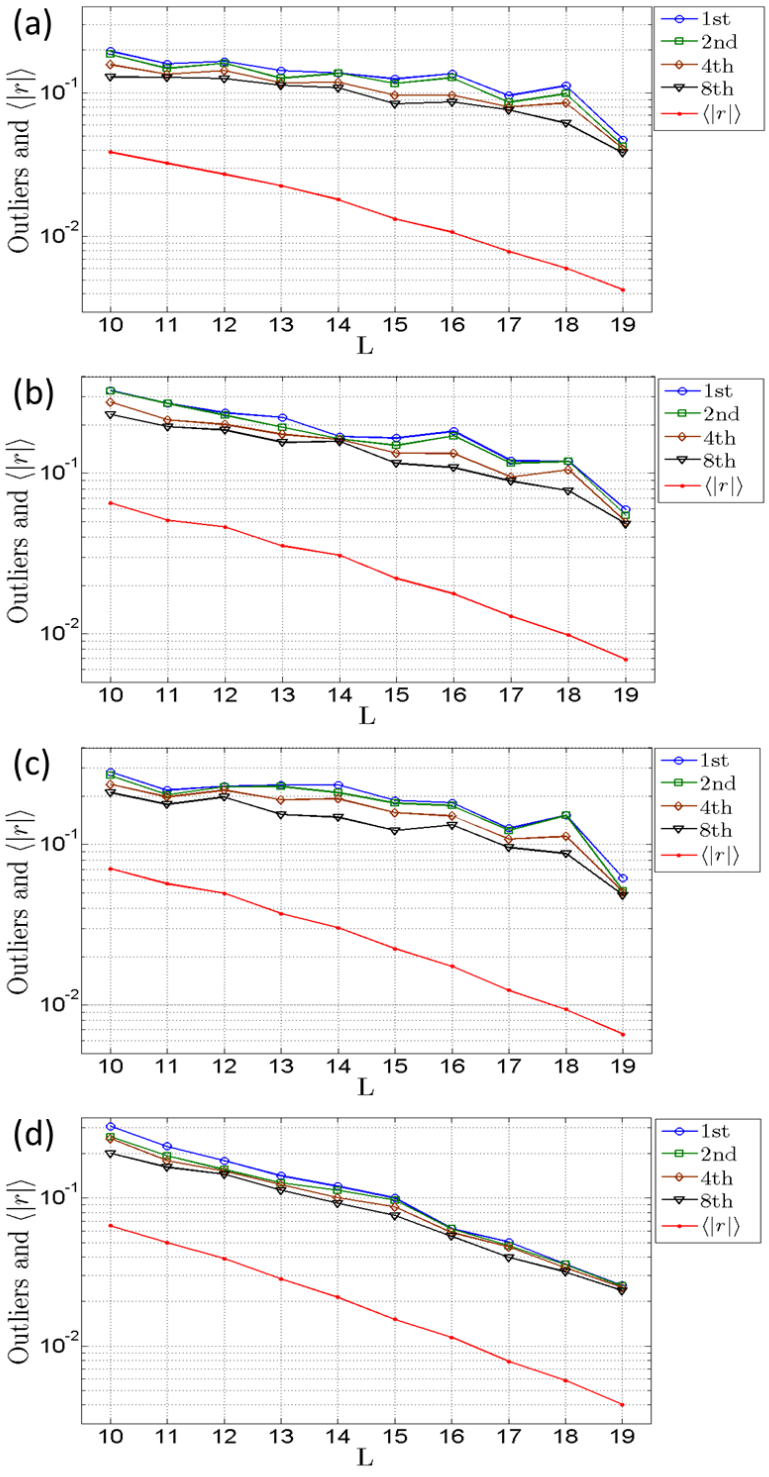

Figure 4.4: 1st, 2nd, 4th, 8th largest values of $|r|$ and the mean of all values of $|r_n|$: (a) σ_i^x (b) σ_i^z (c) $\sigma_i^x\sigma_{i+1}^x$ (d) $\sigma_i^y\sigma_{i+1}^y$. Even the largest outlier values decrease as approaching thermodynamic limit.

As long as the distribution $P(r)$ becomes sharply peaked near $r = 0$, the conventional microcanonical formulation of equilibrium statistical mechanics is valid, since the averaging over a microcanonical ensemble of a few-body observable is involved with exponentially many states in a narrow energy window at thermodynamic limit. There could be a measure-zero set of $r_n's$ which does not peaked at zero but these states does not contribute to the ensemble average. Therefore, Figure 4.3 provides numerical evidence that equilibrium statistical mechanics is still applicable to an isolated quantum system. This feature is also confirmed by several previous works [104, 108, 7]. This means *almost all* out-of-equilibrium initial state will eventually equilibrate and thermalize in terms of the expectation value of a few-body observable. This is enough for every practical purpose, since it is impossible to prepare an initial state with nontrivial weight on many-body eigenstates in such a measure zero set (the ground state, which is not thermal, should not be considered). However, the Eigenstate Thermalization Hypothesis is stronger: *every single* eigenstate is thermal [3]. The strong ETH does not allow the existence of measure zero set disobeying the hypothesis.

We introduce one way to numerically test the strong ETH; the finite size scaling of outliers. We define the outliers by the states that give large values of $|r_n|$ of Eq. 4.6. Since each r_n involves with two states, a large $|r_n|$ means either one state is an outlier and the other one is "normal" or both states are outliers of opposite signs. This also means that if two outliers are consecutive in energy spectrum, corresponding $|r_n|$ can be small. But in that case $|r_{n+1}|$ should be large again so we can spot the outlier state easily [4]. In any case, when ETH is correct in strong sense, even the largest value of $|r_n|$ should decrease to zero in thermodynamic limit. Figure 4.4 are the plots of 1st, 2nd, 4th, and 8th largest values of $|r_n|$ and the mean value of $|r_n|$.

[3] Some people say that ETH is overkill.

[4] there could be a consecutive sequence of outliers but such probabilities are so small that we do not see in our numerical data.

It is clear that the mean value $\langle|r|\rangle$ (averaged over the middle half of the spectrum) decreases exponentially with the system size. The exponential decrease of $\langle|r|\rangle$ shows that our quantum model is in a good agreement with microcanonical formulation of equilibrium statistical mechanics, although leaving the possibilities of existence of measure zero sets whose contribution to the mean is negligible. The central feature of Figure 4.4 is that even the largest value of $|r|$ decreases with the system size. Extrapolating this tendency, we provide a supporting evidence of the strong ETH, that every eigenstate far away from edge is thermal as far as the expectation value of a few-body operator is concerned.

Consequently, we conclude that our model does thermalize under its unitary quantum dynamics. Next section, we turn to the second question: can we construct a local operator which takes exponentially long to relax to equilibrium value?.

4.3 Slowest Relaxing Local Operators - Construction

In the previous section, we have learned that our nonintegrable Ising Hamiltonian Eq. 1.3 indeed follows the eigenstate thermalization hypothesis and thus an out-of-equilibrium initial state will eventually thermalize any few-body observables. However, ETH does not tell us about the thermalization time scale. Some operator can relax to its thermal value quickly while others may take very long. Now our task is to find a local operator that relaxes the slowest. Here, locality is very important since the individual population of eigenstates is conserved (does not relax) but an eigenstate of a generic Hamiltonian is generally non-local. In this section, we will systematically find a local operator that relaxes as slow as possible.

4.3.1 Objective

Quantum dynamics comes from the commutator with the Hamiltonian. Any operator which commutes with Hamiltonian is conserved and does not relax to thermal value if not initially. Therefore, it is a reasonable guess that a slowly relaxing operator would have a small magnitude of the commutator with Hamiltonian, whose meaning is defined shortly.

In order to quantify "how large" the commutator with Hamiltonian is, we need to understand operator norms. [5] There are three widely accepted ways to quantify an operator $\hat{A}$; "the" operator norm $||\hat{A}||$, the trace norm $|\hat{A}|_T$, and the Frobenius norm $|\hat{A}|_F$.

$$||\hat{A}|| = \text{Largest singular value of } \hat{A} \tag{4.11}$$

$$|\hat{A}|_T = Tr(\sqrt{\hat{A}\hat{A}^\dagger}) \tag{4.12}$$

$$|\hat{A}|_F = \sqrt{Tr(\hat{A}\hat{A}^\dagger)} \tag{4.13}$$

Each norm has its own merit. For a state ρ and an operator $\hat{A}$, the expectation value is $tr(A\rho)$. Suppose we cannot compute $Tr(\hat{A}\rho)$ directly but can compute $Tr(\hat{A}\rho')$ for some other state ρ'. Then, the question is how close these values are. Generally, the following holds:

$$|Tr(\hat{A}\rho) - Tr(\hat{A}\rho')| = |Tr(\hat{A}(\rho - \rho'))| \leq ||\hat{A}|||\rho - \rho'|_T = |\hat{A}|_T||\rho - \rho'|| \tag{4.14}$$

$$|Tr(\hat{A}\rho) - Tr(\hat{A}\rho')| = |Tr(\hat{A}(\rho - \rho'))| \leq |\hat{A}|_F|\rho - \rho'|_F \ . \tag{4.15}$$

Therefore, mathematicians say that the operator norm and the trace norm are dual norms and the Frobenius norm is self dual. Usually, the operator norm is used to bound an operator and the trace norm is used to bound a state. For example, let's

[5] Special thanks to Matthew Hastings for kindly explaining the meanings of operator norms.

consider a spin-1/2 chain of length L with σ_1^z on site 1 and identities elsewhere. The operator norm of this quantity is one, which is sensible as an operator, while the trace norm gives 2^L, which is sensible as a state. The Frobenius norm has, on the other hand, no particular physical meaning since it gives $2^{L/2}$. However, the Frobenius norm is the easiest to compute among them since the others require the knowledge of eigenvalues. Therefore, we will mostly rely on the Frobenius norm to search for slowest relaxing operators.

As a locality of an operator, we consider an operator of range M, $\hat{A}^M$. Here the "range" means the largest distance between two non-identity operators including the operators itself. For instance, an operator $\hat{O}$ acting on a spin chain, $\hat{O} = \sigma_1^x \otimes \sigma_2^0 \otimes \sigma_3^z \otimes \sigma_4^y$ (σ^0 is an identity), has range 4. $\hat{A}^M$ consists of local operators of range at most M. Note that our Hamiltonian belongs to the set of $\{\hat{A}^M | M = 2\}$. Then, we may ask two aspects of "slowness" of $\hat{A}^M$ (1) how slow $\hat{A}^M$ itself relaxes to thermal value? (2) how slow the expectation value of $\hat{A}^M$ approaches to thermal value for a given particular initial state?

(1) Suppose we prepare the initial state ρ as

$$\rho = \frac{1}{Z} I + \hat{A}^M \ . \tag{4.16}$$

We can always make the operator $\hat{A}^M$ traceless by trivial operation. Then, we compute the expectation value of $\hat{A}^M$ at time t:

$$\langle \hat{A}^M(t) \rangle = Tr \left(\hat{A}^M e^{-iHt} \hat{A}^M e^{iHt} \right) \ . \tag{4.17}$$

If this operator is simply an energy modulation of longest wavelength, the diffusion predicts that this quantity would decay exponentially, where the decay rate is determined by the diffusivity and the wave number. Simple diffusion states that the the mode associated with the longest wave number is the slowest mode. One question is

whether quantum mechanics of a nonintegrable Hamiltonian can beat this simple diffusion picture by having an operator that relaxes slower than diffusion of the longest wave number. We will later provide explicit numerical evidence that it is indeed possible to generate a local operator whose relaxation time scale is longer than the diffusive mode.

The way we construct such an operator is to minimize the Frobenius norm of a commutator with Hamiltonian: given M, we find $\hat{A}^M$ which gives the smallest value of $Tr([\hat{A}^M, H][\hat{A}^M, H]^\dagger)$. The physical meaning of such $\hat{A}^M$ is that it has the smallest relaxing "acceleration" at $t = 0$. This follows from the observation:

$$\frac{d}{dt}\langle \hat{A}^M(t)\rangle\big|_{t=0} = iTr([\hat{A}^M, H]\hat{A}^M) = 0 \tag{4.18}$$

$$\frac{d^2}{dt^2}\langle \hat{A}^M(t)\rangle\big|_{t=0} = Tr([\hat{A}^M, H][\hat{A}^M, H]^\dagger)\ . \tag{4.19}$$

Although this search only finds a slowly relaxing operator at $t = 0$, we will later see that this already beats the slowest diffusion mode.

(2) Now we study relaxation of expectation value of $\hat{A}^M$ for a specified initial state. We first consider the operator norm of a commutator, which is the most relevant norm in this case. Let us write $||[\hat{A}^M, H]|| \leq \chi(M)$ for some function $\chi(x)$. Then,

$$\frac{d}{dt}\hat{A}^M(t) = -i[\hat{A}^M(t), H] \tag{4.20}$$

$$\left|\left|\frac{d}{dt}\hat{A}^M(t)\right|\right| = \left|\left|e^{-iHt}\left(\frac{d}{dt}\hat{A}^M(t)\right)e^{iHt}\right|\right| = ||[\hat{A}^M(t=0), H]|| \leq \chi(M) \tag{4.21}$$

$$||\hat{A}^M(t) - \hat{A}^M(0)|| = \left|\left|\int_0^t \left(\frac{d}{d\tau}\hat{A}^M(\tau)\right)d\tau\right|\right| \leq \int_0^t \left|\left|\frac{d}{d\tau}\hat{A}^M(\tau)\right|\right|d\tau \leq \chi(M)t\ , \tag{4.22}$$

where we take Heisenberg picture in operator and used the fact that e^{iHt} is a norm-preserving unitary operator. This inequality bounds the distance of an operator evolving under Hamiltonian dynamics from its initial configuration. Now for an initial

state ρ, which is different from Eq. 4.16, we define $\gamma(M)$:

$$|\langle \hat{A}^M \rangle_0 - \langle \hat{A}^M \rangle_\beta| = \gamma(M), \tag{4.23}$$

where $\langle \hat{O} \rangle_0 = Tr(\hat{O}\rho)$ and $\langle \hat{O} \rangle_\beta$ is thermal average of β fixed by energy density of the initial state ρ. We want to compute the distance between expectation value of $\hat{A}^M$ at time t and thermal expectation value of $\hat{A}^M$. For time $t \leq \gamma(M)/\chi(M)$, using the triangular inequality, we have show the following:

$$\begin{aligned} |\langle \hat{A}^M \rangle_t - \langle \hat{A}^M \rangle_\beta| &= |\langle \hat{A}^M \rangle_t - \langle \hat{A}^M \rangle_0 + \langle \hat{A}^M \rangle_0 - \langle \hat{A}^M \rangle_\beta| \\ &\geq ||\langle \hat{A}^M \rangle_0 - \langle \hat{A}^M \rangle_\beta| - |\langle \hat{A}^M \rangle_t - \langle \hat{A}^M \rangle_0|| \geq \gamma(M) - t\chi(M) \end{aligned} \tag{4.24}$$

where $\langle \hat{O} \rangle_t = Tr(\hat{O}e^{-iHt}\rho e^{iHt})$. In the last inequality, we used the duality relation of the operator norm (Eq. 4.14) and the fact that $|\rho|_T = 1$. Therefore, if the operator norm of the commutator, $\chi(M)$ decreases exponentially with M ($\chi(M) \sim e^{-\alpha M}$) and $\gamma(M)$ does not decrease as fast as exponential, we have the thermalization time scale τ_M of $\hat{A}^M$ for the initial state ρ is

$$\tau_M \sim \frac{\gamma(M)}{\chi(M)} \sim e^{\alpha M}. \tag{4.25}$$

Consequently, this state takes exponentially long to thermalize the local operator $\hat{A}^M$. Later, we will show that this scenario is indeed possible.

4.3.2 Method

We construct an operator A^M whose range is limited by M-body.

$$\hat{A}^M = \sum_{i=1}^{L} \hat{A}_i^M \ , \tag{4.26}$$

where $\hat{A}_i^M$ contains n-body operators ($n \leq M$) acting nontrivially on site from i up to $i+M-1$. For a given M, we want to find an operator that minimizes the following:

$$\frac{tr([\hat{A}^M, H][\hat{A}^M, H]^\dagger)}{tr(\hat{A}^M \hat{A}^{M\dagger})} \tag{4.27}$$

Since $\hat{A}^M$ is an hermitian, $[\hat{A}^M, H]^\dagger = -[\hat{A}^M, H]$. Using translation invariance, we can write

$$tr(-[\hat{A}^M, H][\hat{A}^M, H]) = -\sum_{i,j=1}^{L} tr([\hat{A}_i^M, H][\hat{A}_j^M, H]) = -L\sum_{j=1}^{L} tr([\hat{A}_1^M, H][\hat{A}_j^M, H]) \ . \tag{4.28}$$

For a given block operator $\hat{A}_\ell^M$, only terms in H ranging from $\ell - 1$ to $\ell + M$ gives nonzero contribution in the commutator. We call this H_ℓ^M. Specifically,

$$H_\ell^M = \sigma_{\ell-1}^z \sigma_\ell^z + \sum_{k=\ell}^{\ell+M-1} \left(g\sigma_k^x + h\sigma_k^z + \sigma_k^z \sigma_{k+1}^z \right) \ . \tag{4.29}$$

In addition, when $|i-j| > M$, the two commutators in the trace do not overlap thus gives zero. In the end,

$$tr(-[\hat{A}^M, H][\hat{A}^M, H]) = -Ltr([\hat{A}_1^M, H_1^M]^2) - 2L\sum_{j=2}^{M+1} tr([\hat{A}_1^M, H_1^M][\hat{A}_j^M, H_j^M]) \ . \tag{4.30}$$

The factor of 2 comes from the translation invariance and the periodic boundary condition. The first term comes from the exact overlap of two commutators and the second term comes from the partial overlap of commutators that give nonzero contribution.

All non-identity operators of range at most M can be expressed in terms of the following operator basis.

$$\hat{A}_1^M = \sum_{i=1}^{2^{2M}-1} c_i \hat{O}_{1,i} \ , \tag{4.31}$$

where $\hat{O}_{1,i}$ is a string of operators;

$$\hat{O}_{1,i} = \prod_{j=1}^{M} \otimes \sigma_j^{\alpha_{i,j}} \ . \tag{4.32}$$

There is a string of $L - M$ identities next to the operator. The first subscript 1 represent the string operator begins at site 1. $\alpha_{i,j}$ determines an operator acting on site j, given the order of basis i. i can be interpreted as a number in the base 4. We assign 0 to identity, 1 to σ^x, 2 to σ^y, and 3 to σ^z. For example, if $i = 30$ and $M = 5$, then $\alpha_{i,j}$ is 00132. Therefore, $\hat{O}_{1,30}$ is

$$\hat{O}_{1,30} = \sigma_1^0 \otimes \sigma_2^0 \otimes \sigma_3^x \otimes \sigma_4^z \otimes \sigma_5^y \ . \tag{4.33}$$

To make the operator Hermitian, all coefficients c_i should be real.

Then, the commutator becomes

$$\begin{aligned} & Tr(-[\hat{A}^M, H][\hat{A}^M, H]) \\ & = -L2^{L-(M+2)} \sum_{i,j} c_i c_j Tr([\hat{O}_{1,i}, H_1^M][\hat{O}_{1,j}, H_1^M]) \\ & - 2L \sum_{i,j} c_i c_j \sum_{s=2}^{M+1} 2^{L-(M+s+1)} Tr([\hat{O}_{1,i}, H_1^M][\hat{O}_{s,j}, H_s^M]) \ . \end{aligned} \tag{4.34}$$

Here we explicitly put factors coming from the trace of a string of identities. It is natural to define a matrix $B_{i,j}$ as

$$\begin{aligned} B_{i,j} = & -2^{L-(M+2)} Tr([\hat{O}_{1,i}, H_1^M][\hat{O}_{1,j}, H_1^M]) \\ & - \sum_{s=2}^{M+1} 2^{L-(M+s+1)} Tr([\hat{O}_{1,i}, H_1^M][\hat{O}_{s,j}, H_s^M]) \\ & - \sum_{s=-M+1}^{0} 2^{L-(|s|+M+3)} Tr([\hat{O}_{s,i}, H_s^M][\hat{O}_{1,j}, H_1^M]) \end{aligned} \tag{4.35}$$

Here we make it look more symmetric. Then, calling $\mathbf{c} = (c_1, c_2, \ldots, c_{4^M-1})$, we have

$$Tr(-[\hat{A}^M, H][\hat{A}^M, H]) = L\mathbf{c}B\mathbf{c}^T \ . \tag{4.36}$$

The normalization part can also be written as

$$Tr(\hat{A}^M \hat{A}^M) = L2^{L-M} Tr((\hat{A}_1^M)^2) + 2L \sum_{s=2}^{M} 2^{L-(M+s-1)} Tr(\hat{A}_1^M \hat{A}_j^M) = L\mathbf{c}D\mathbf{c}^T \ ; \tag{4.37}$$

$$D_{i \leq j} = \sum_{s=1}^{M} 2^{L-(M+s-1)} Tr(\hat{O}_{1,i} \hat{O}_{s,j}) \tag{4.38}$$

Clearly, $D = D^T$.

Matrices B and D both include a common factor of 2^L. Therefore, this factor cancels out and we need not consider it when we compute the matrices and we essentially study an infinite system with translation invariance.

Now, we need minimize λ in the following problem:

$$\frac{\mathbf{c}B\mathbf{c}^T}{\mathbf{c}D\mathbf{c}^T} = \lambda \ . \tag{4.39}$$

Differentiating with respect to c_i,

$$\frac{(\mathbf{c}D\mathbf{c}^T)(B+B^T)\mathbf{c}^T-(\mathbf{c}B\mathbf{c}^T)(D+D^T)\mathbf{c}^T}{(\mathbf{c}D\mathbf{c}^T)^2}=0 \tag{4.40}$$

$$\Rightarrow B\mathbf{c}^T=\left(\frac{\mathbf{c}B\mathbf{c}^T}{\mathbf{c}D\mathbf{c}^T}\right)D\mathbf{c}^T=\lambda D\mathbf{c}^T\ , \tag{4.41}$$

which is a generalized eigenvalue problem. Our task is finding the smallest value of λ as a function M, which can be efficiently found using the Lanczos algorithm. However, this is still an exponential problem (in fact worse than diagonalizing the Hamiltonian) so the range of M is very limited. Naive brute force method can only access M up to 7 in a reasonable time [6]. See Appendix C for an efficient algorithm that enables us to find λ up to 11 [7].

In above, we only considered the translation invariant case. Computation in translationally non-invariant system (such as open edges) is straightforward: simply replace the matrix D with identity and adjust the boundary condition in the matrix B.

One remark is in order. Any local conserved quantity of range M should be detected in this approach. Therefore, if our system has an accidental local constant of motion, we should be able to know what it is. It turns out that up to $M = 11$, we have not found any local conserved quantity other than the Hamiltonian itself. When we take $h = 0$ in the model, the Hamiltonian becomes integrable and we can reconstruct all known local constants of motion up to range M.

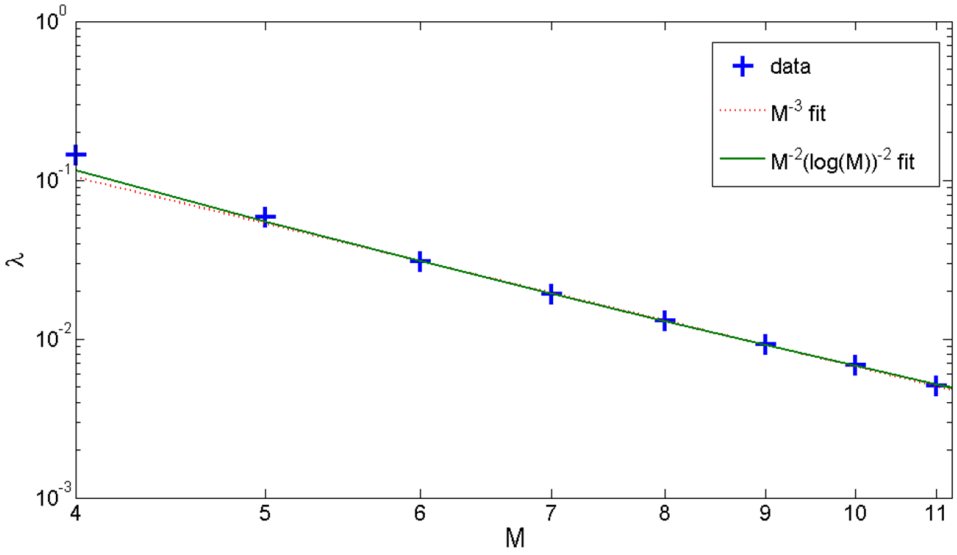

Figure 4.5: The minimum value of the Frobenius norm of the commutator, Eq. 4.27 in a translation invariant system.

4.4 Slowest Relaxing Local Operators - Results

4.4.1 Smallest Value of Commutator in the Frobenius Norm

Figure 4.5 is the minimum value of the commutator with Hamiltonian in Frobenius norm, Eq. 4.27 in a translation invariant system. Whether it decreases as a power-law or a logarithmic correction to M^{-2} is not clear to determine from the range we could access. Nevertheless, it is clear that the magnitude of commutator decreases reasonably fast, at least surely faster than M^{-2}, which we would derive from diffusive mode of energy modulation as we explain below.

Although translation invariance is convenient for many theoretical works and some numerical implementations such as infinite-Matrix Product State (iMPS), it is not the most convenient to visualize the shape of operators in real space. Therefore, we break the translation invariance (and also periodic boundary condition) and leave edge(s) open. This means removing the summation in Eq. 4.26. We consider two cases: (1)

[6] 280 hours using one 3.2GHz cpu with 64 GB of RAM
[7] 40 hours using the same resource

place our operator $\hat{A}^M$ at the edge of the chain and leave only one edge open and (2) place $\hat{A}^M$ in the middle of the chain so it could spread in both directions.

Before we look at the results, we first consider what scaling a diffusive mode in open boundary condition can give. The simplest diffusive operator we can construct is the modulation of energy density [8]:

$$\rho(t=0) = \frac{1}{Z}I + \sum_r e^{ikr} h_r = \frac{1}{Z}I + H(k) \tag{4.42}$$

$$h_r = g\sigma_r^x + h\sigma_r^z + \frac{1}{2}(\sigma_{r-1}^z\sigma_r^z + \sigma_r^z\sigma_{r+1}^z) \ , \tag{4.43}$$

where k is the wave vector of the modulation. $H(k)$ is the Fourier transform of Hamiltonian.

When the maximum range of operator is M, $k = 2\pi/(4M)$ is the smallest wave vector (thus longest wavelength) the system can have. This will correspond to the smallest diffusive mode. This initial condition will generate an energy current and this energy current will relax the energy inhomogeneity diffusively.

From the continuity equation, we can derive the energy current,

$$j_{r+1/2} = g(\sigma_r^y\sigma_{r+1}^z - \sigma_r^z\sigma_{r+1}^y) \tag{4.44}$$

and we can write the commutator explicitly:

$$[\rho(t=0), H] = [H(k), H] = i\,(2\sin(k/2))\,j(k) \simeq ikj(k) \ , \tag{4.45}$$

where $j(k)$ is the Fourier transform of current operator and we assumed k is small. Since this is the slowest diffusive mode for given k, if the diffusion is the only way to make the slowly relaxing operator, this mode should be our optimal result (Eq.4.27).

[8] In translation invariant system, only $k = 0$ is allowed.

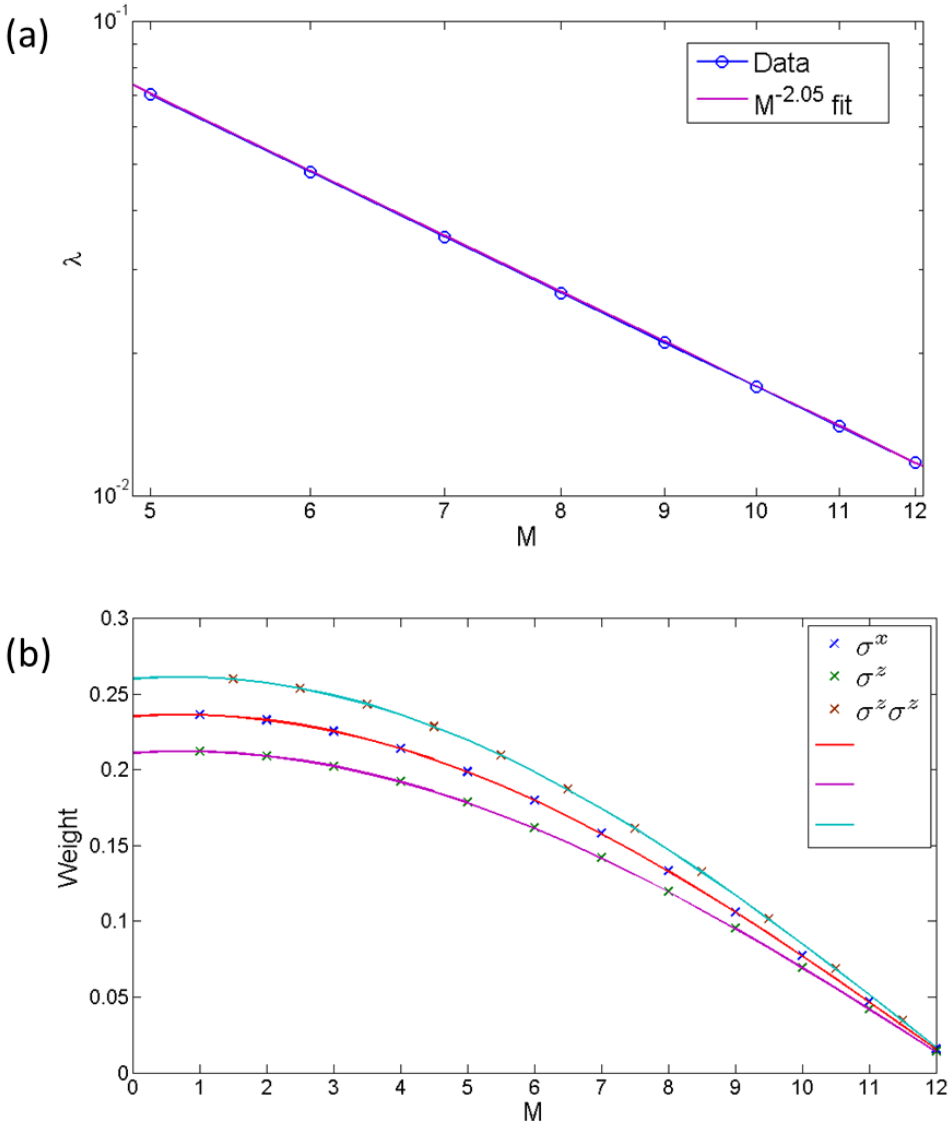

Figure 4.6: (a)The minimum value of the Frobenius norm of the commutator, Eq. 4.27 in a system with open boundary condition with only terms in the Hamiltonian are allowed. The scaling is very close to the prediction of simple diffusion, M^{-2}. We place the operator at one edge of the chain. (b) Weight of individual terms constituting $\hat{A}^{M=12}$. As expected, the operator has a nice modulation with wave length $4M$ and their relative magnitude is consistent with that of parameters in Hamiltonian (g, h, J).

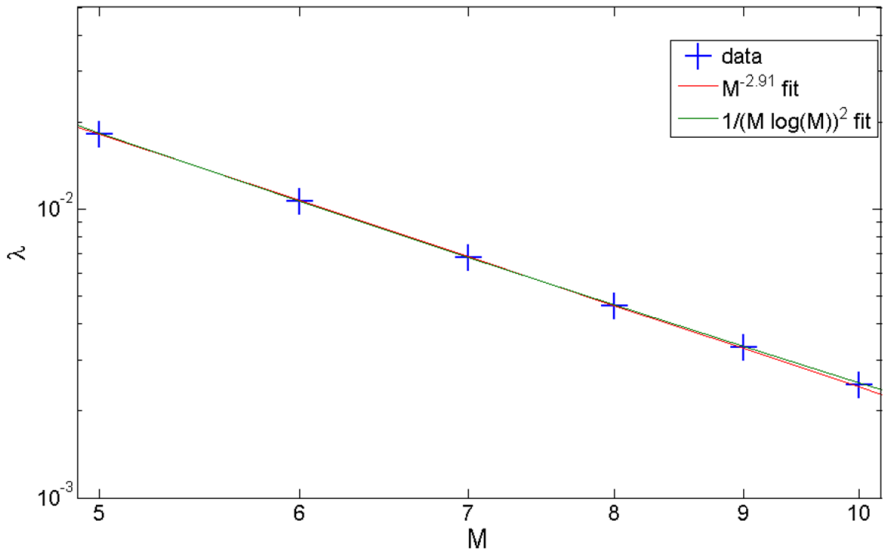

Figure 4.7: The minimum value of the Frobenius norm of the commutator, Eq. 4.27in a system with the open boundary condition. We place the operator $\hat{A}^M$ at one edge.

Then, we will get the commutator

$$Tr(-([H(k), H])^2) = -k^2 Tr((j(k))^2) \sim \frac{1}{M^2} \ . \tag{4.46}$$

Thus, the simplest diffusion will give the M^{-2} scaling. Note that this operator can be constructed using *only* σ^x, σ^z, and $\sigma^z \otimes \sigma^z$ operators. Figure 4.6 (a) is the minimum of Eq. 4.27 when only above three operators are used and the operator is placed at the edge of the chain. The scaling is very close to the expectation of simple diffusion. From figure 4.6 (b), we can see the weights of individual operators (magnitude of coefficient in expansion Eq. 4.31) give a modulating pattern in accordance with wave length $4M$. Also, the relative magnitude of three kinds of operator is precisely the same as the relative magnitude of parameters in Hamiltonian.

Now we turn to the fully optimal case with open boundary condition, where all operators up to range M are allowed and see how smaller they can make the commutator with Hamiltonian.

Figure 4.7 is the minimum values of Eq. 4.27 when the operator begins from one edge of the system so it can only spread to one direction. Although we cannot, again, conclusively determine whether its decay is a power-law fashion or a logarithmic correction to M^{-2}, we can clearly see that this gives much faster decease than simple energy modulation, Figure 4.6.

Therefore, we have numerically constructed operators that relaxes slower (at least at early times) than simple diffusive mode. As mentioned earlier, however, minimizing the Frobenius norm of the commutator with the Hamiltonian has a concrete physical meaning only at $t = 0$. What enables us to make a stronger statement is the magnitude of the operator norm of the commutator. Since it is numerically very challenging to optimize the operator norm, we will take an alternative route. We use the optimal operator $\hat{A}^M$ found with the Frobenius norm (Eq. 4.27), and compute its operator norm.

4.4.2 The Operator Norm and the Distance from Thermal State

This time let us place our operator in the middle of the chain with open boundary condition[9] Figure 4.8 is the plot of the operator norm and the Frobenius norm of the commutator of $\hat{A}^M$ and Hamiltonian. Note that here we take the square root of Eq. 4.27 for a fair comparison. For the range we could obtain exact operators, it appears that the operator norm decreases exponentially with M unlike the Frobenius norm ($\chi(M) \sim e^{-\alpha M}$). Therefore, once we find an initial condition satisfying that $\gamma(M) = |\langle \hat{A}^M \rangle_0 - \langle \hat{A}^M \rangle_\beta|$ does not decrease exponentially (or decrease slower than simple exponential), we have found a sequence of operators whose relaxation time

[9]It turns out that this gives the worst scaling in the Frobenius norm. Therefore, the other two cases should have better results than this condition.

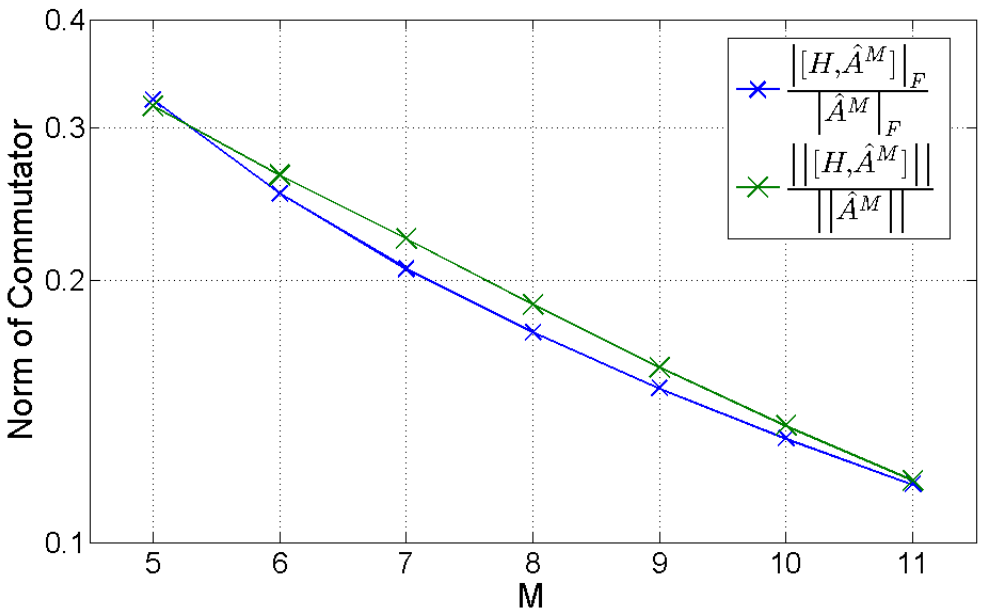

Figure 4.8: The operator norm and the Frobenius norm of the commutator, $[\hat{A}^M, H]$. $\hat{A}^M$ is found by minimizing the Frobenius norm of the commutator with H. The operator norm decreases exponentially with M.

scales increase exponentially with the range of operators unlike diffusion, which is quadratic in M.

Ref. [3] have studied the relaxation of fully polarized initial states using the same Hamiltonian with different parameter choices (they chose $(g, h, J) = (1.05, -0.5, -1)$). Up to the time scale they were able to reliably simulate (they used iMPS with transverse folding method), they found different results for three different polarizations; fast thermalization for the fully polarized state along y-direction, weak thermalization (thermalized after time average) for the fully polarized state along $-z$-direction [10], and nonthermalization (no signature of thermalization up to the time scale they can simulate) for the fully polarized state along x-direction. Therefore, we also consider the same initial conditions and see the distance between the thermal expectation value and initial expectation value of $\hat{A}^M$. Figure 4.9 is the plot of the distance for three fully polarized states. We can clearly see that the distance decreases exponentially

[10]Their definition of Hamiltonian is differ by a global sign from ours. We translate everything in our sign convention.

fast for y-polarized state while that of $-z$-polarized state has much more moderate decay. The most striking result is the x-polarized state for its distance from thermal state does not decrease with M but seems to saturate to finite value. Therefore, this is a numerical evidence that x-polarized state may have exponentially slow relaxing operators.

We have a visible tendency - exponential decrease of the operator norm and saturation of the distance from thermal state. It is encouraging that two independent methods (iMPS and our method) converge to the same answer: a fully polarized state along x-axis have an operator that takes fairly long to thermalize. However, one caveat in interpretation of the data is in order. The ratio of distance between initial expectation value and thermal expectation value to operator norm of the commutator is in fact smaller than one for the range we can compute. Thus, we expect to have exponentially increasing time scale as a function of M, but do not exactly have such time scale yet.

So far, we have focused on construction of slowly relaxing operators. In the following subsection, we will see their relaxation in real time to confirm our results.

4.4.3 Real Time Relaxation

In this section, we explicitly construct an operator and see how it relaxes in real time under exact quantum dynamics.

Using the optimal $\hat{A}^M$ that we constructed in the open boundary condition where only one edge is open (results of Figure 4.7), we construct an operator $\hat{\mathcal{A}}^M$ of length $2M$.

$$\hat{\mathcal{A}}^M = \hat{A}^M \otimes I^M - I^M \otimes (\hat{R}^M \hat{A}^M (\hat{R}^M)^{-1}), \tag{4.47}$$

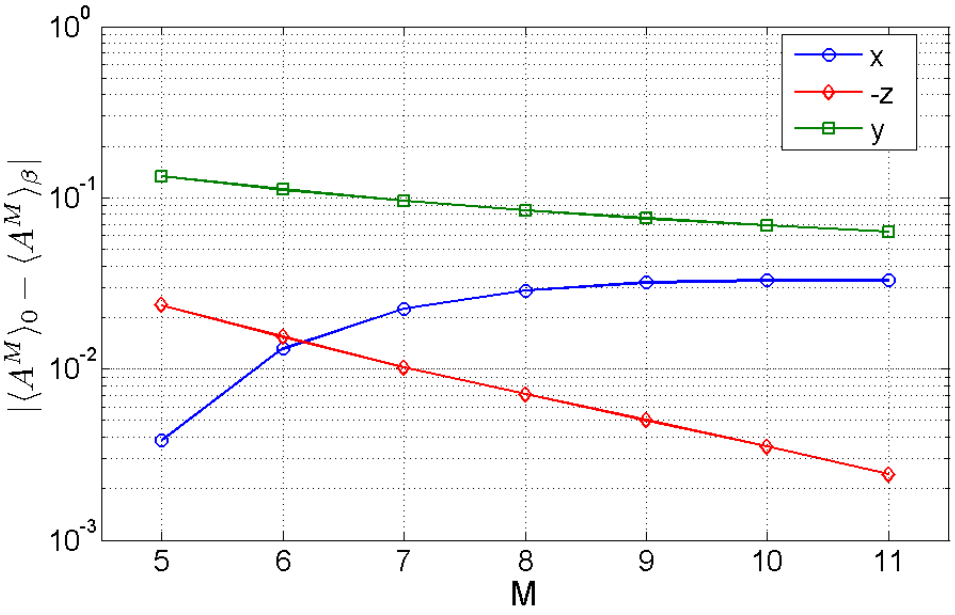

Figure 4.9: Distance between the thermal expectation value and the initial expectation value of $\hat{A}^M$. We consider fully polarized states. The distance appears to saturate with M for the x-polarized state while the distance decreases with M for other two polarizations.

where I^M is the identity operator acting on consecutive M spins and $\hat{R}^M$ is the reflection operator that reverses the order of an operator of range M. The new operator $\hat{\mathcal{A}}^M$ has an odd parity under inversion and is orthogonal to the Hamiltonian and thus its thermal expectation value at any temperature is zero. This implies that for a finite system, this operator will relax to very small number and begin oscillating around zero. For example, if $\hat{A}^M$ is made of only operators in Hamiltonian (σ^x, σ^z, and $\sigma^z\sigma^z$), $\hat{\mathcal{A}}^M$ is just a cosine energy modulation with wave length $4M$ as we have seen in Figure 4.6. Such a diffusive mode will relax exponentially with rate proportional to $1/M^2$. We want to see how slower the full optimal $\hat{A}^M$ constructed by using all possible operators up to range M relaxes to zero compared to the energy modulation.

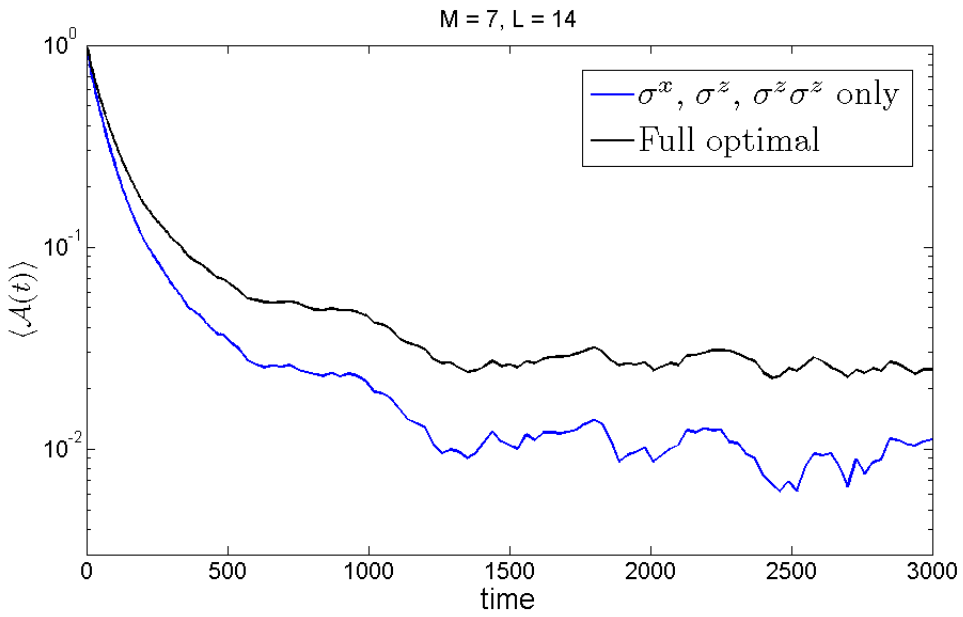

Figure 4.10: Comparison of real time relaxation of $\hat{\mathcal{A}}^{\mathcal{M}}$ made by two methods: only used operators in Hamiltonian (blue curve) and used all operators up to range M (black curve). Full optimal case is always slower than energy modulation even though it is optimized for $t = 0$.

As usual, we set up the initial condition as following ($L = 2M$):

$$\rho = \frac{1}{2^L} I^L + \hat{\mathcal{A}}^M \ . \tag{4.48}$$

Then, see expectation value of $\hat{\mathcal{A}}^M$ at time t:

$$\langle \hat{\mathcal{A}}^M(t) \rangle = tr\left(\hat{\mathcal{A}}^M e^{-iHt} \hat{\mathcal{A}}^M e^{iHt} \right) \ . \tag{4.49}$$

Figure 4.10 is the real time relaxation of two operators, one constructed by using only terms in Hamiltonian and the full optimal operator of range $M = 7$ (thus $L = 14$) [11]. We have normalized $\hat{\mathcal{A}}^M$ to have the Frobenius norm one, $tr(\hat{\mathcal{A}}^M \hat{\mathcal{A}}^{\dagger M}) = 1$. It is clear that the full optimal operator has always higher expectation value than the energy modulation has. This shows that an operator that is optimized to have the slowest

[11] Since this computation requires the full diagonalization of the Hatmiltonian of length L, the maximum range we can study is limited by $M = 8$.

relaxation at $t = 0$ actually remains slower than energy diffusion for all times. This is an explicit demonstration of slow relaxation of the operator we have constructed.

4.5 Outlook

In this chapter, we have seen that our nonintegrable quantum Ising model satisfies the eigenstate thermalization hypothesis at least for four few-body observables we have checked. Since ETH is a sufficient condition for thermalization of an isolated quantum system, we may safely conclude that our model does equilibrate and thermalize.

Still, there are many open questions about ETH. First of all, we have only considered one site and two sites operators. There are numerous few-body operators that are nonlocal in space, e.g. expectation value of momentum distribution. We have not tested such operators and have not excluded possibilities that there could exist few-body operators in which the values of outliers do not decrease. Second, it is not clear whether these outlier states do form a "measure zero set" or constitute a set of finite, although small, measure. Another related issue is how these outlier states are robust against small changes in parameters in Hamiltonian. Third, there could be other nonintegrable models that would violate the strong ETH. It is also not settled whether there is a quantum analog of Kolmogorov-Arnold-Moser (KAM) theorem, which states that ergodicity requires a finite amount of integrability breaking perturbation: we know that over the parameter space, ETH breaks down at integrable point and ETH appears to be valid far away from it. But it is not clear until when ETH holds as we approach the integrable point if starting from a point in parameter space far away from integrability [103, 88]. We leave these interesting questions to future investigation.

Given our model relaxes to thermal equilibrium, we have constructed a sequence of local operators indexed by its maximum range M, which evolves the slowest under

unitary quantum dynamics. In contrast to a naive expectation that an energy modulation with the longest wavelength would be the slowest mode by energy diffusion, we have shown that there exist operators that relax slower than trivial diffusion. This seemingly striking result certainly needs further investigation. First of all, we do not know the nature of these operators constructed from the algorithm. We know that these do not resemble an energy modulation and these contain every single allowed operator in the basis. Also, we know that the overlap between $\hat{A}^M$ and $\hat{A}^{M+1}$ is actually very small. Once we have a better understanding of what these operators are, we may be able to construct $\hat{A}^M$ for much larger M and see cleaner scaling to determine whether the decay of the Frobenius norm of the commutator is actually a power-law with some exponent greater than 2 or just a logarithmic correction.

There are only two known slow (or static) modes; transport of conserved quantities or projection onto eigenstates (static). Since these operators are different from energy modulation, it should be either projection onto an eigenstate or something new. Whichever it turns out to be, it would be interesting in its own way.

Finally, our new algorithm allows to find any existing local conservation laws. Therefore, we can apply this method to find local constant of motion in an integrable system or even a many-body localized system.

Appendix A

Scaling Form of Transport Coefficients of Ultracold Atoms

In chapter 2, we found a certain scaling form of transport coefficient in the lowest nontrivial order in momentum expansion. In this appendix, we prove that the same scaling form remains true in all orders of expansion.

A.1 κ' and S'_s

First let's consider κ' and S'_s when $\nabla p = 0$.

Observe that $\nabla p = 0$ and mechanical equilibrium condition imply

$$\frac{\nabla n_\uparrow}{n_\uparrow} = \frac{\nabla n_\downarrow}{n_\downarrow} = \frac{\nabla n}{n} = -\frac{\nabla T}{T} \ . \tag{A.1}$$

Therefore, Eq. (2.13) simplifies to

$$\psi_i = \lambda \sum_{\ell=0}^{L} C_{\ell i} q_i^{2\ell} \frac{\mathbf{q}_i \cdot \nabla T}{T} \ , \tag{A.2}$$

where we abbreviated $C_{\ell ii} + C_{\ell ij} \equiv C_{\ell i}$. Following the procedure explained in the main text, we can obtain the following set of linearly independent equations ($m = 1, 2, \cdots, L$).

$$n_\uparrow \lambda^3 \left[\beta_0 C_{0\uparrow} + \beta_1 C_{1\uparrow} + \cdots \beta_L C_{L\uparrow}\right] + n_\downarrow \lambda^3 \left[\beta_0 C_{0\downarrow} + \beta_1 C_{1\downarrow} + \cdots \beta_L C_{L\downarrow}\right] = 0 \tag{A.3}$$

$$\alpha_{00} \left(C_{0\uparrow} - C_{0\downarrow}\right) + \alpha_{01} \left(C_{1\uparrow} - C_{1\downarrow}\right) + \cdots + \alpha_{0L} \left(C_{L\uparrow} - C_{L\downarrow}\right) = A_0 \tag{A.4}$$

$$n_\downarrow \lambda^3 \left[\alpha_{m0} \left(C_{0\uparrow} - C_{0\downarrow}\right) + \left(\alpha_{m1\uparrow} C_{1\uparrow} + \alpha_{m1\downarrow} C_{1\downarrow}\right) + \cdots + \left(\alpha_{mL\uparrow} C_{L\uparrow} + \alpha_{mL\downarrow} C_{L\downarrow}\right)\right] = A_m \tag{A.5}$$

$$n_\uparrow \lambda^3 \left[-\alpha_{m0} \left(C_{0\uparrow} - C_{0\downarrow}\right) + \left(\alpha_{m1\downarrow} C_{1\uparrow} + \alpha_{m1\uparrow} C_{1\downarrow}\right) + \cdots + \left(\alpha_{mL\downarrow} C_{L\uparrow} + \alpha_{mL\uparrow} C_{L\downarrow}\right)\right] = A_m \ . \tag{A.6}$$

Here, $\{\alpha_{00}, \alpha_{0n}, \alpha_{m0}, \alpha_{mn\sigma}\}$ ($m, n = 1, 2, \ldots, L$ and $\sigma = \uparrow, \downarrow$) are dimensionless numbers which may depend on $(\lambda/a)^2$ through the exponential integral and incomplete Gamma functions and implicitly depend on the order of approximation L but do not explicitly depend on temperature and densities. $\{A_\ell, \beta_\ell\}$ are determined by Gaussian integrals as following:

$$A_\ell = \int \frac{d^3\mathbf{q}}{(2\pi)^3} \left(\frac{q^2}{4\pi} - \frac{5}{2}\right) q^{2\ell} q_z^2 e^{-q^2/4\pi} = \frac{1}{3} 2^{3+2\ell} \pi^{\frac{1}{2}+\ell} \ell \Gamma\left[\frac{5}{2} + \ell\right] \tag{A.7}$$

$$\beta_\ell = \int \frac{d^3\mathbf{q}}{(2\pi)^3} q^{2\ell} q_z^2 e^{-q^2/4\pi} = \frac{1}{3} 2^{3+2\ell} \pi^{\frac{1}{2}+\ell} \Gamma\left[\frac{5}{2} + \ell\right] \ , \tag{A.8}$$

where $\Gamma[x]$ is the Gamma function and A_ℓ and β_ℓ are purely numerical numbers independent of physical parameters. Note that the first equation, Eq. (A.3) fixes the frame to be $\mathbf{j}_\uparrow + \mathbf{j}_\downarrow = \mathbf{0}$. From dimensional analysis and the symmetry under $\uparrow \leftrightarrow \downarrow$, we may write an ansatz solution of the above equations in the following form

$(m = 1, 2, \ldots, L)$:

$$C_{0\uparrow} = -\frac{1}{\lambda^3}\left(\frac{a_0}{n_\uparrow} + \frac{b_0}{n_\downarrow} + \frac{c_0}{n}\right) \tag{A.9}$$

$$C_{0\downarrow} = -\frac{1}{\lambda^3}\left(\frac{b_0}{n_\uparrow} + \frac{a_0}{n_\downarrow} + \frac{c_0}{n}\right) \tag{A.10}$$

$$C_{m\uparrow} = -\frac{1}{\lambda^3}\left(\frac{a_m}{n_\uparrow} + \frac{b_m}{n_\downarrow}\right) \tag{A.11}$$

$$C_{m\downarrow} = -\frac{1}{\lambda^3}\left(\frac{b_m}{n_\uparrow} + \frac{a_m}{n_\downarrow}\right) \ , \tag{A.12}$$

where $\{a_\ell, b_\ell, c_0\}$ $(\ell = 0, 1, 2, \ldots, L)$ are $2L+3$ unknown dimensionless numbers which may depend only on $(\lambda/a)^2$. Since the above set of equations should hold for any values of $n_\uparrow$ and $n_\downarrow$, once we insert the ansatz to the above equations, we obtain $2L + 3$ linear equations in terms of $\{a_\ell, b_\ell, c_0\}$. Since we are still using the same set of coefficients $\{\alpha_{00}, \alpha_{0n}, \alpha_{m0}, \alpha_{mn\sigma}\}$ and $\{\beta_\ell\}$, it is easy to see that once the original set of equations is linearly independent (which is a necessary condition to have an approximate solution of the Boltzmann equation), the set of descendent equations is also linearly independent. Therefore, once we determine all $\{a_\ell, b_\ell, c_0\}$, the above ansatz is the (L'th order) approximate solution of the Boltzmann equation.

When $\nabla p = 0$, we know that $\mathbf{j}_{spin} = -S_s'\nabla T$. It is straightforward to show that

$$S_s' = -\frac{\hbar}{m}\frac{n_\uparrow}{T}\left(\sum_{\ell=0}^{L}\beta_\ell C_{\ell\uparrow}\right) \tag{A.13}$$

$$= \frac{\hbar}{m}\frac{1}{T}\frac{1}{\lambda^3}\left(\sum_{\ell=0}^{L}\beta_\ell a_\ell + \frac{n_\uparrow}{n_\downarrow}\sum_{\ell=0}^{L}\beta_\ell b_\ell + \frac{n_\uparrow}{n}\beta_0 c_0\right) \ . \tag{A.14}$$

Since $\{a_\ell, b_\ell, c_0\}$ satisfies Eq. (A.3), we have two identities:

$$\sum_{\ell=0}^{L}\beta_\ell a_\ell = -\frac{1}{2}\beta_0 c_0 \tag{A.15}$$

$$\sum_{\ell=0}^{L}\beta_\ell b_\ell = 0 \ . \tag{A.16}$$

Inserting these identities to Eq. (A.14), we finally obtain the full polarization and temperature dependence of the Seebeck coefficient ($\beta_0 = 2\pi$).

$$S'_s = \frac{\hbar}{m}\frac{n_\uparrow - n_\downarrow}{n\lambda^3}\frac{\pi}{T}c_0 \ . \tag{A.17}$$

This proves that the scaling of Eq. (2.19) is indeed true at all orders of approximation. Furthermore, we see that the dimensionless scaled function $h_L(x)$ (L is the order of approximation) is

$$h_L((\lambda/a)^2) = \pi c_0 \ . \tag{A.18}$$

It should be noted that c_0 implicitly depends on the order of approximation.

For the thermal conductivity κ', we are only interested in the first term, κ'_1, which directly comes from the energy current $\mathbf{j}_\epsilon$.

$$\kappa'_1 = -\frac{1}{4\pi}\frac{\hbar}{m}\sum_{\ell=0}^{L} B_\ell(n_\uparrow C_{\ell\uparrow} + n_\downarrow C_{\ell\downarrow}) \ , \tag{A.19}$$

where $B_\ell = 4\pi(5/2+\ell)\beta_\ell$. Plugging in ansatz solution and using Eq. (A.3), we obtain κ'_1.

$$\kappa'_1 = \frac{\hbar}{m}\frac{1}{\lambda^3}\sum_{\ell=1}^{L}\left(\frac{n_\uparrow^2 b_\ell + 2n_\uparrow n_\downarrow a_\ell + n_\downarrow^2 b_\ell}{n_\uparrow n_\downarrow}\right)\ell\beta_\ell \tag{A.20}$$

Again, we emphasize that a_ℓ and b_ℓ are function of $(\lambda/a)^2$ and implicitly depend on the order of approximation. This proves that the algebraic form of the polarization dependence of the thermal conductivity obtained in the main text remains to all orders of approximation.

A.2 D_s and P_s'

Now we study D_s and P_s' when $\nabla T = 0$ (thus $\nabla n = 0$). As we did in the previous subsection, we want to express $\nabla n_\uparrow$ and $\nabla n_\downarrow$ in terms of $n\nabla p$.

$$\frac{\nabla n_i}{n_i} = \epsilon^i \frac{n\nabla p}{2n_i} \ , \tag{A.21}$$

where $\epsilon^\uparrow = 1$ and $\epsilon^\downarrow = -1$. Then, the ansatz, Eq. (2.13), takes the following form $(i \neq j)$:

$$\psi_i = -\epsilon^i \lambda \frac{n}{2} \sum_{\ell=0}^{L} \left(\frac{C_{\ell ii}}{n_i} - \frac{C_{\ell ij}}{n_j} \right) q_i^{2\ell} \mathbf{q}_i \cdot \nabla p \tag{A.22}$$

Once we define

$$\tilde{C}_{\ell i} \equiv -\frac{n}{2} \left(\frac{C_{\ell ii}}{n_i} - \frac{C_{\ell ij}}{n_j} \right) \ , \tag{A.23}$$

we reduce the system similar to the previous case. The $2(L+1)$ linearly independent equations are $(m = 1, 2, \cdots L)$

$$n_\uparrow \lambda^3 \left[\beta_0 \tilde{C}_{0\uparrow} + \beta_1 \tilde{C}_{1\uparrow} + \ldots \beta_L \tilde{C}_{L\uparrow} \right] - n_\downarrow \lambda^3 \left[\beta_0 \tilde{C}_{0\downarrow} + \beta_1 \tilde{C}_{1\downarrow} + \ldots \beta_L \tilde{C}_{L\downarrow} \right] = 0 \tag{A.24}$$

$$\alpha_{00} \left(\tilde{C}_{0\uparrow} + \tilde{C}_{0\downarrow} \right) + \alpha_{01} \left(\tilde{C}_{1\uparrow} + \tilde{C}_{1\downarrow} \right) + \cdots + \alpha_{0L} \left(\tilde{C}_{L\uparrow} + \tilde{C}_{L\downarrow} \right) = \tilde{A}_0 \tag{A.25}$$

$$\frac{n_\uparrow n_\downarrow \lambda^3}{n} \left[\alpha_{m0} \left(\tilde{C}_{0\uparrow} + \tilde{C}_{0\downarrow} \right) + \left(\alpha_{m1\uparrow} \tilde{C}_{1\uparrow} - \alpha_{m1\downarrow} \tilde{C}_{1\downarrow} \right) + \cdots + \left(\alpha_{mL\uparrow} \tilde{C}_{L\uparrow} - \alpha_{mL\downarrow} \tilde{C}_{L\downarrow} \right) \right] = \tilde{A}_m \tag{A.26}$$

$$\frac{n_\uparrow n_\downarrow \lambda^3}{n} \left[-\alpha_{m0} \left(\tilde{C}_{0\uparrow} + \tilde{C}_{0\downarrow} \right) + \left(\alpha_{m1\downarrow} \tilde{C}_{1\uparrow} - \alpha_{m1\uparrow} \tilde{C}_{1\downarrow} \right) + \cdots + \left(\alpha_{mL\downarrow} \tilde{C}_{L\uparrow} - \alpha_{mL\uparrow} \tilde{C}_{L\downarrow} \right) \right] = -\tilde{A}_m \ . \tag{A.27}$$

$\alpha' s$ and β_ℓ are same as in the previous subsection and $\tilde{A}_\ell = \beta_\ell$.

Although coefficients of Eqs. (A.26) and (A.27) are linearly dependent, once we combine them, we obtain another L linearly independent equations.

$$\sum_{n=1}^{L}(\alpha_{mn\uparrow} - \alpha_{mn\downarrow})(\tilde{C}_{n\uparrow} - \tilde{C}_{n\downarrow}) = 0 \ . \tag{A.28}$$

Together with Eq. (A.28), we have $2(L+1)$ linearly independent equations that uniquely determine all $\tilde{C}_{\ell i}$.

First observe that the solution of Eq. (A.28) is trivial; $\tilde{C}_{m\uparrow} = \tilde{C}_{m\downarrow}$. Then, we use the following ansatz [1]:

$$\tilde{C}_{0\uparrow} = -\frac{1}{\lambda^3}\left(\frac{\tilde{a}_0}{n_\uparrow} + \frac{\tilde{b}_0}{n_\downarrow}\right) \tag{A.29}$$

$$\tilde{C}_{0\uparrow} = -\frac{1}{\lambda^3}\left(\frac{\tilde{b}_0}{n_\uparrow} + \frac{\tilde{a}_0}{n_\downarrow}\right) \tag{A.30}$$

$$\tilde{C}_{m\uparrow} = -\frac{1}{\lambda^3}\frac{n\tilde{c}_m}{n_\uparrow n_\downarrow} = \tilde{C}_{m\downarrow} \ . \tag{A.31}$$

$\{\tilde{a}_0, \tilde{b}_0, \tilde{c}_m\}$ are dimensionless numbers that may only depend on $(\lambda/a)^2$. Substituting the above into original linear equations, we obtain the same linearly independent equations in terms of $\{\tilde{a}_0, \tilde{b}_0, \tilde{c}_m\}$. Therefore, once we determine them, we have the approximate solution of the Boltzmann equation.

Following the same procedure when we obtained S'_s and κ'_1, we can show that

$$D_s = \frac{\hbar}{m}\frac{2\pi}{\lambda^3}(\tilde{a}_0 - \tilde{b}_0) \tag{A.32}$$

$$P'_{s1} = \frac{\hbar}{m}\frac{T}{n\lambda^3}\sum_{\ell=1}^{L}\left(\frac{n_\uparrow^2 - n_\downarrow^2}{n_\uparrow n_\downarrow}\right)\tilde{c}_\ell \ell \beta_\ell \ , \tag{A.33}$$

[1] Motivation of this choice came from the observation that the right hand side of the linear equation does not depend on densities. Therefore, a quantity in the big parenthesis in the left hand side must be proportional to $n/(n_\uparrow n_\downarrow)$.

where P'_{s1} is the first term in the Peltier coefficient. Once we scale the scattering length with λ, the polarization and temperature dependence of D_s and P'_{s1} at an arbitrary L remains the same as for $L = 1$. This proves that the scaling structure of the transport coefficients remains the same to all orders of approximation.

Appendix B

Hamiltonian Parameter Choice

The model we consider is the one dimensional Ising chain with transverse and longitudinal field with open boundary condition.

$$H = \sum_{i=1}^{L} (g\sigma_i^x + h\sigma_i^z) + \sum_{i=1}^{L-1} J\sigma_i^z\sigma_{i+1}^z \ . \tag{B.1}$$

Strictly speaking, this model is nonintegrable as long as all parameters, g, h, and J, are nonzero. However, since the accessible size of exact diagonalization method is limited, some choices of parameters can be superior than other choices to do finite size scaling. One characteristic feature of a nonintegrable system is that its eigenvalues show level repulsion [79]. One convenient quantity to look at its level statistics is the ratio distribution of adjacent eigenvalues [89, 2]. First, order the eigenvalues in ascending order, then compute the distribution of $r_i = (\lambda_{i+2} - \lambda_{i+1})/(\lambda_{i+1} - \lambda_i)$, where λ_i is the i'th eigenvalue. For a nonintegrable system, this distribution should follow the Wigner-like surmise while an integrable system should exhibit Poissonian distribution [2]. Figure B.1 is the ratio distributions for two different set of parameters, $(g, h, J) = (0.6, 1.0, 1.0)$ and $(g, h, J) = ((\sqrt{5}+5)/8, (\sqrt{5}+1)/4, 1.0)$, within even sector of $L = 16$. Although both of them are far from Poissonian and look similar to Wigner's surmise, $(g, h, J) = ((\sqrt{5}+5)/8, (\sqrt{5}+1)/4, 1.0)$ case shows stronger level re-

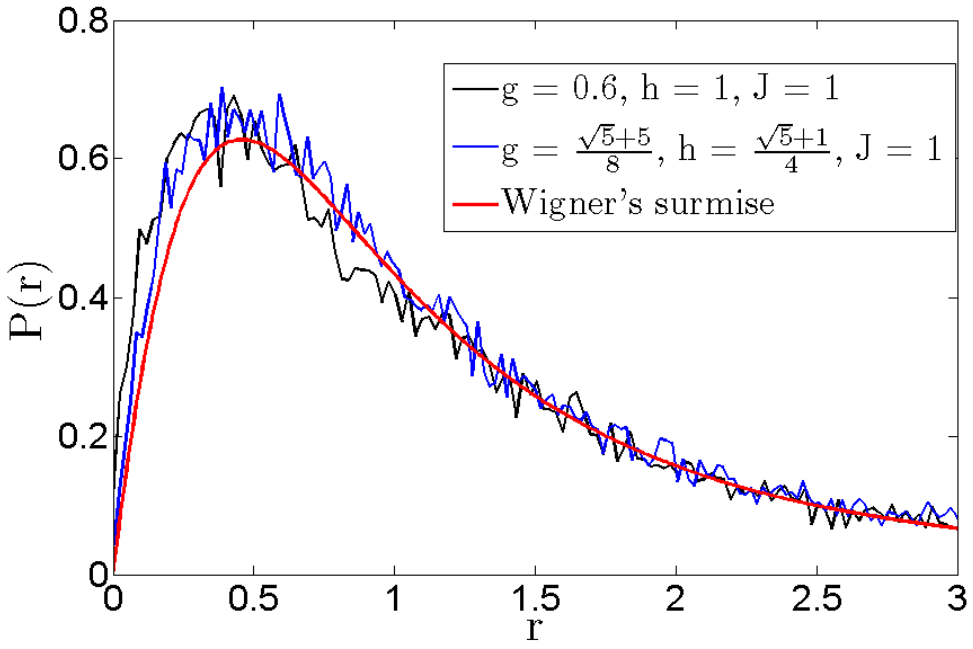

Figure B.1: Ratio distribution of level spacing for two sets of parameter choices. r is the ratio of level spacings between two adjacent energy gaps. For $L = 16$, there are 32896 eigenvalues in even parity eigenstates, from which we obtain 32894 ratios. This ratio distribution is computed from the histogram of the lowest 32000 ratios with 250 equally spaced bins. $(g, h, J) = ((\sqrt{5}+5)/8, (\sqrt{5}+1)/4, 1.0)$ case shows better level repulsion near $r = 0$.

pulsion and agrees with the Wigner's surmise better. To minimize finite size effect, the latter choice of parameter should be more appropriate. Another aspect to consider is the structure of eigenvalues. For a generic nonintegrable model, we expect the distribution of eigenvalues to be featureless with Gaussian density of state [54, 53]. Figure B.2 is the histogram of 32896 even state eigenvalues for the same two sets of parameters with $L = 16$. Clearly, $(g, h, J) = (0.6, 1.0, 1.0)$ case shows the reminiscent feature of $g = 0$, quasi-periodic eigenvalues with small perturbation coming from nonzero g, which could make the finite size scaling very difficult under the limited accessible system size. Therefore, $(g, h, J) = ((\sqrt{5}+5)/8, (\sqrt{5}+1)/4, 1.0)$ is a better choice of parameters. Note that checking only one of the criteria used here might not be sufficient to accept the parameters, as Figure B.1 shows that $(g, h, J) = (0.6, 1.0, 1.0)$

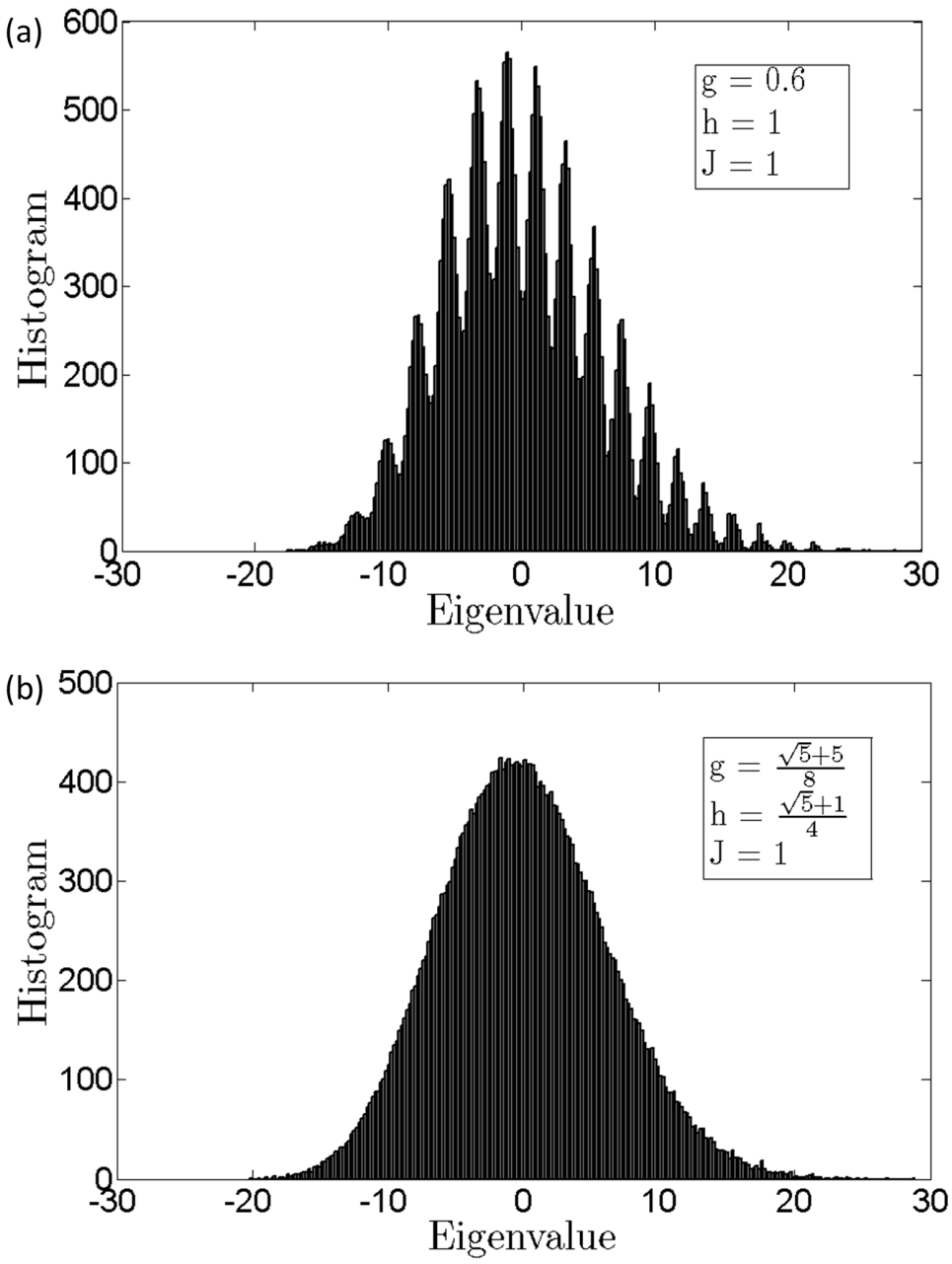

Figure B.2: Histogram of 32896 even state eigenvalues for two sets of parameters. $(g, h, J) = (0.6, 1.0, 1.0)$ case has quasi-periodic structure whereas the other case is featureless Gaussian. In order to study generic properties of nonintegrable systems with limited accessible system size, we should use parameters with which the distribution of eigenvalues does not have distinct structure.

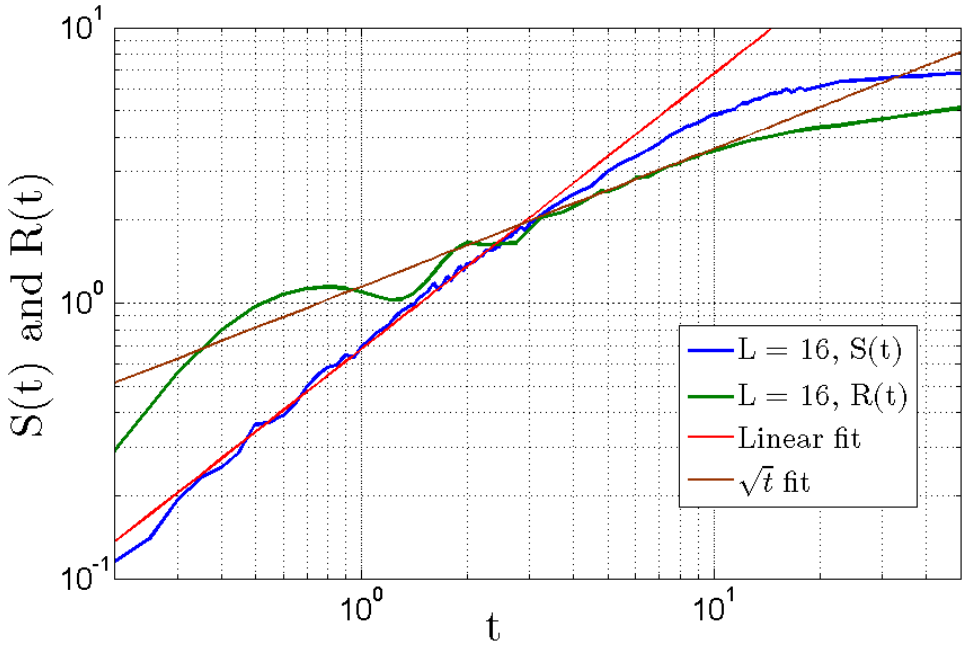

Figure B.3: Direct comparison of the entanglement spreading $S(t)$ and the energy diffusion $R(t)$ for $L = 16$ and $(g, h, J) = (-1.45, \pi/2, 1.0)$. Entanglement spreading is faster than energy diffusion but direct comparison is more difficult than Figure 3.9 in the main text.

option may not appear too bad and the density of states of the integrable case ($h = 0$) seems to be very similar to that of $(g, h, J) = ((\sqrt{5}+5)/8, (\sqrt{5}+1)/4, 1.0)$.

As long as the magnitude of g and h are comparable, most, if not all, choices of parameters satisfy the above two criteria. Here we present the result obtained from another choice; $(g, h, J) = (-1.45, \pi/2, 1.0)$. Figure B.3 is the central plot of the main text using this set of parameters. It shows the same qualitative features; ballistically spreading entanglement, initial wiggle of energy diffusion, diffusive transport of energy, and the same final saturation value of entanglement. However, compared to the choice given in the main text, this option yields earlier deviation from ballistic spreading of entanglement and especially extended initial transient in energy diffusion. What mostly limits the choice of parameters is the irregular initial behavior of energy diffusion while spreading of entanglement has appeared relatively insensitive to the choice of parameters. Figure B.4 shows that the initial non-diffusive behavior

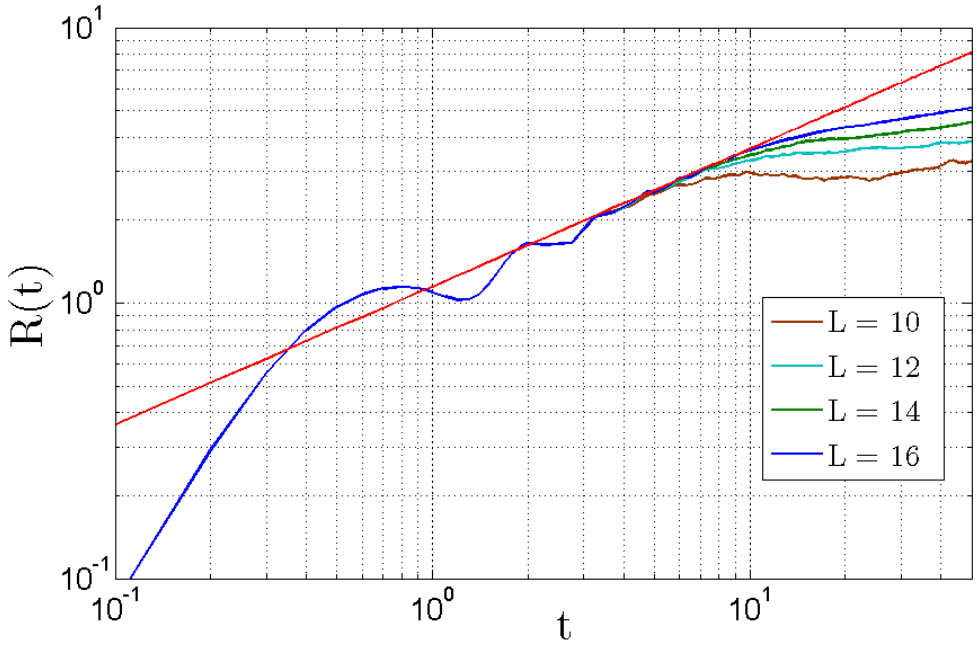

Figure B.4: Energy diffusion measure $R(t)$ (defined in the main text) for $(g, h, J) = (-1.45, \pi/2, 1.0)$. The initial transient does not scale with the system size and thus it is irrelevant in thermodynamic limit. Before finite size effect begins to matter, it shows diffusive behavior which extends as the system size increases. The red line is a $\sqrt{t}$ guide line.

does not scale with the system size and thus does not affect any asymptotic properties. Although it is still apparent that the entanglement spreading is faster than the energy diffusion, the directly comparable range is smaller than that in the main text. This is the main reason of the parameter choice in the main text.

We emphasize that the reason for the careful choice of parameters is mainly due to the restricted accessible system size of exact diagonalization method. We can still see the ballistic spreading of entanglement and diffusive behavior of energy transport even with the parameter choice of $(g, h, J) = (0.6, 1.0, 1.0)$. This set of parameters just gives small scaling range and very strong initial transient in energy diffusion that makes direct comparison difficult.

Appendix C

Efficient algorithm to find slowest relaxing operators

In chapter 4, we find slowest relaxing operators by searching for local operators that give the smallest value of the commutator with Hamiltonian in Frobenius norm. This searching process is an exponential problem, since there are total $4^M - 1$ basis operators for a given M. Even if we take into account that the slowest operator can be written with only real operators in σ^z basis (even number of σ^y operators), we still need to consider 2^{2M-1} commutators. Then, we have to find the smallest eigenvalue of the matrix equation. Clearly, this is a much worse problem than diagonalizing spin-1/2 Hamiltonian, which has 2^L scaling. Therefore, this may seem impossible to go beyond $M = 8$. However, once we fully manipulate the sparseness of the matrix and structure of commutators among Pauli operators, we can in fact proceed up to $M = 11$ using reasonable resources [1]. Beyond $M = 12$, finding the smallest eigenvalue (using Lanczos algorithm) limits the feasibility of computation.

Since we cannot improve the speed of finding the smallest eigenvalue from the Lanczos methods, speed up should be gained from construction of the B matrix, Eq.

[1] Using a 3.2 GHz cpu with 64 GB of RAM, it takes about 40 hours

4.35. There are three key observations to make the algorithm efficient: (1) In the set of basis operators, most commutators among them vanish so the matrix B is sparse. (2) Trace of a product of two Pauli operators are zero unless the operators are the same. (3) Matrix multiplication is much faster than running "for" loops. The speed up is dramatic especially when the matrices are sparse.

Another observation is that Hamiltonian can also be written in terms of basis operators:

$$H = \sum_{\ell}{}' h_\ell \hat{O}_\ell \ , \tag{C.1}$$

where $\acute{\Sigma}$ contains only the indexes of basis operator in Hamiltonian. Then, writing

$$\hat{A}^M = \sum_{i=1}^{4M-1} c_i \hat{O}_i, \tag{C.2}$$

we want to compute the following:

$$Tr(-[\hat{A}^M, H][\hat{A}^M, H]) = -\sum_{i,j}\sum_{\ell,k}{}' c_i c_j h_\ell h_k Tr([\hat{O}_i, \hat{O}_\ell][\hat{O}_j, \hat{O}_k]) \tag{C.3}$$

$$= -\sum_{i,j} c_i c_j B_{i,j} \ . \tag{C.4}$$

Notice that a product of two Pauli operators is just another Pauli operator with coefficient, $\pm i$. For each pair of strings of Pauli operators, we define a matrix $\beta_{i,j}$ and $\gamma_{i,j}$ and a function $f(i,j)$:

$$[\hat{O}_i, \hat{O}_j] = \beta_{i,j}\hat{O}_i\hat{O}_j = \beta_{i,j}\gamma_{i,j}\hat{O}_{f(i,j)} \ . \tag{C.5}$$

Determining $\beta_{i,j}$, $\gamma_{i,j}$, and $f(i,j)$ for given i and j is straightforward. In fact, most of $\beta_{i,j}$ are zero so we rarely need to compute $\gamma_{i,j}$ and $f(i,j)$. Then, Eq. C.3 becomes,

$$tr(-[\hat{A}^M, H][\hat{A}^M, H]) = -\sum_{i,j} c_i c_j \sum_{\ell,k}{}' \beta_{i,\ell}\gamma_{i,\ell}h_\ell \beta_{j,k}\gamma_{j,k}h_k tr(\hat{O}_{f(i,\ell)}\hat{O}_{f(j,k)}) \tag{C.6}$$

$$= -\sum_{i,j} c_i c_j \sum_{\ell,k}{}' \tilde{\beta_{i,\ell}}\tilde{\beta_{j,k}}\delta_{f(i,\ell),f(j,k)} \tag{C.7}$$

$$= -\sum_{i,j} c_i c_j B_{i,j} \ , \tag{C.8}$$

where $\tilde{\beta_{i,j}}$ is

$$\tilde{\beta}_{i,j} = \beta_{i,j}\gamma_{i,j}h_j \ . \tag{C.9}$$

Also we used the observation (2).

For translation invariant system, we need to consider overlapping contribution [2]. Using the observation (2), we immediately know that the overlapping term is nonzero only if the indexes $f(i,\ell)$ and $f(j,k)$ differ by a power of 4. Eventually, the B matrix becomes:

$$B_{i,j} = \sum_{s=0}^{M} \sum_{\ell,k}{}' \tilde{\beta}_{i,\ell}\tilde{\beta}_{j,k}\delta_{f(i,\ell)\times 4^s, f(j,k)} \ . \tag{C.10}$$

We can go further. Use the fact that $\delta_{i,j} = \delta_{i,\alpha}\delta_{\alpha,\beta}\delta_{\beta,j}$, we can write

$$B_{i,j} = \sum_{s=0}^{M} \sum_{\ell,k}{}' \sum_{\alpha,\gamma} \tilde{\beta}_{i,\ell}\delta_{f(i,\ell),\alpha}\delta_{4^s\alpha,\gamma}\delta_{\gamma,f(j,k)}\tilde{\beta}_{j,k} \ . \tag{C.11}$$

[2] For an open boundary condition, this step can be skipped.

Now we define $\eta_{\alpha,\gamma}(s)$ and $\theta_{i,\alpha}$ as

$$\eta_{\alpha,\gamma}(s) = \delta_{4^s\alpha,\gamma} \tag{C.12}$$

$$\Theta_{i,\alpha} = \sum_{\ell}{}' \tilde{\beta}_{i,\ell}\delta_{f(i,\ell),\alpha} \ . \tag{C.13}$$

Finally, the B matrix is

$$B_{i,j} = \sum_{s=0}^{M}\sum_{\alpha,\gamma}\Theta_{i,\alpha}\eta_{\alpha,\gamma}(s)\Theta_{\gamma,j} \ . \tag{C.14}$$

Therefore,

$$B = \sum_{s=0}^{M}\Theta\eta(s)\Theta^T \tag{C.15}$$

which is just a sum of product of three sparse matrices. Now the task is to find two matrices, Θ and $\eta(s)$. Running MatLab in a machine with 3.2GHz CPU and 64 GB of RAM, brute force calculation (running many "for" loops to construct B matrix) takes about 280 hours for $M = 7$ while the efficient algorithm takes about 24 seconds and uses RAM less than 1GB.

Bibliography

[1] P.W. Anderson. Absence of diffusion in certain random lattices. *Phys. Rev.*, 109:1492, 1958.

[2] Y. Y. Atas, E. Bogomolny, O. Giraud, and G. Roux. Distribution of the ratio of consecutive level spacings in random matrix ensembles. *Phys. Rev. Lett.*, 110:084101, 2013.

[3] M. C. Bañuls, J. I. Cirac, and M. B. Hastings. Strong andweak thermalization of infinite nonintegrable quantum systems. *Phys. Rev. Lett.*, 106:050405, 2011.

[4] J. H. Bardarson, F. Pollmann, and J. E. Moore. Unbounded growth of entanglement in models of many-body localization. *Phys. Rev. Lett.*, 109:017202, 2012.

[5] D. Basko, I. Aleiner, and B. Altshuler. Metal-insulator transition in a weakly interacting many-electron system with localized single-particle states. *Ann. Phys.*, 321:1126, 2006.

[6] M. Berry and M. Tabor. Level clustering in the regular spectrum. *Proc. R. Soc. A*, 356:375, 1977.

[7] W. Beugeling, R. Moessner, and M. Haque. Finite-size scaling of eigenstate thermalization. *Phys. Rev. E*, 89:042112, 2014.

[8] I. Bloch, J. Dalibard, and W Zwerger. Many-body physics with ultracold gases. *Rev. Mod. Phys.*, 80:885, 2008.

[9] O. Bohigas, M. J. Giannoni, and C. Schmit. Characterization of chaotic quantum spectra and universality of level fluctuation laws. *Phys. Rev. Lett.*, 52:1, 1984.

[10] L. W. Boltzmann. *Vorlesungen über Gastheorie* (Translated as *Lectures on Gas Theory.* Cambridge University Press, 1964). Barth, Leipzig, 1896.

[11] T. Bourdel, J. Cubizolles, L. Khaykovich, K. M. F. Magalhaẽs, S. J. J. M. F. Kokkelmans, G. V. Shlyapnikov, and C. Salomon. Measurement of the interaction energy near a Feshbach resonance in a ^{6}Li fermi gas. *Phys. Rev. Lett.*, 91:020402, 2003.

[12] F. G. S. L. Brandao, M. Christandl, and J. Yard. Faithful squashed entanglement. *Commun. Math. Phys.*, 306:805, 2011.

[13] S. Bravyi, M. B. Hastings, and F. Verstraete. Lieb-Robinson bounds and the generation of correlations and topological quantum order. *Phys. Rev. Lett.*, 97:050401, 2006.

[14] G. Breit and P.T. Zilsel. The scattering of slow neutrons by bound protons. II. *Phys. Rev.*, 71:232, 1947.

[15] G. M. Bruun. Spin diffusion in fermi gases. *New J. Phys.*, 13:035005, 2011.

[16] G. M. Bruun, A. D. Jackson, and E. E. Kolomeitsev. Multichannel scattering and Feshbach resonances: Effective theory, phenomenology, and many-body effects. *Phys. Rev. A*, 71:052713, 2005.

[17] G. M. Bruun, A. Recati, C. J. Pethick, H. Smith, and S. Stringari. Collisional properties of a polarized fermi gas with resonant interactions. *Phys. Rev. Lett.*, 100:240406, 2008.

[18] A. Bulgac, J. E. Drut, and P. Magierski. Spin 1/2 fermions in the unitary regime: A superfluid of a new type. *Phys. Rev. Lett.*, 96:090404, 2006.

[19] A. Bulgac and M. M. Forbes. Unitary fermi supersolid: The larkin-ovchinnikov phase. *Phys. Rev. Lett.*, 101:215301, 2008.

[20] A. Bulgac, M. M. Forbes, and A. Schwenk. Induced p-wave superfluidity in asymmetric fermi gases. *Phys. Rev. Lett.*, 97:020402, 2006.

[21] E. Burovski, N. Prokofev, B. Svistunov, , and M. Troyer. Critical temperature and thermodynamics of attractive fermions at unitarity. *Phys. Rev. Lett.*, 96:160402, 2006.

[22] C. K. Burrell and T. J. Osborne. Bounds on the speed of information propagation in disordered quantum spin chains. *Phys. Rev. Lett.*, 99:167201, 2007.

[23] H. T. C. Stoof C. H. Wong and R. A. Duine. Spin-Seebeck effect in a strongly interacting fermi gas. *Phys. Rev. A*, 85:063613, 2012.

[24] P. Calabrese and J. Cardy. Evolution of entanglement entropy in one-dimensional systems. *J. Stat. Mech.*, P04010, 2006.

[25] P. Calabrese, J. Cardy, and E. Tonni. Entanglement negativity in quantum field theory. *Phys. Rev. Lett.*, 109:130502, 2012.

[26] P. M. Chaikin and T. C. Lubensky. *Principles of Condensed Matter Physics*. Cambridge University Press, 1995.

[27] B. S. Chandrasekhar. A note on the maximum critical field of high-field superconductors. *App. Phys. Lett.*, 1:7, 1962.

[28] M. Žnidarič, T. Prosen, and P. Prelovšek. Many-body localization in the Heisenberg XXZ magnet in a random field. *Phys. Rev. B*, 77:064426, 2008.

[29] F. Chevy. Universal phase diagram of a strongly interacting fermi gas with unbalanced spin populations. *Phys. Rev. A*, 74:063628, 2006.

[30] S. Chiacchiera, T. Lepers, D. Davesne, and M. Urban. Collective modes of trapped fermi gases with in-medium interaction. *Phys. Rev. A*, 79:033613, 2009.

[31] S. Chiacchiera, T. Lepers, D. Davesne, and M. Urban. Role of fourth-order phase-space moments in collective modes of trapped fermi gases. *Phys. Rev. A*, 84:043634, 2011.

[32] A. M. Clogston. Upper limit for the critical field in hard superconductors. *Phys. Rev. Lett.*, 9:266, 1962.

[33] R. Combescot, A. Recati, C. Lobo, and F. Chevy. Normal state of highly polarized fermi gases: Simple many-body treatment. *Phys. Rev. Lett.*, 98:180402, 2007.

[34] Luca D'Alessio and Marcos Rigol. Long-time behavior of periodically driven isolated interacting quantum systems. *arXiv:1402.5141v1*, 2014.

[35] J. M. Deutsch. Quantum statistical mechanics in a closed system. *Phys. Rev. A*, 43:2046, 1991.

[36] K. Dieckmann, C. A. Stan, S. Gupta, Z. Hadzibabic, C. H. Schunck, and W. Ketterle. Decay of an ultracold fermionic lithium gas near a Feshbach resonance. *Phys. Rev. Lett.*, 89:203201, 2002.

[37] B. Dietz and F. Haake. Talyor and padé analysis of the level spacing distributions of random-matrix ensembles. *Z. Phys. B*, 80:153, 1990.

[38] R.A. Duine and H.T.C. Stoof. Atom-molecule coherence in bose gases. *Physics Reports*, 396:115, 2004.

[39] A. Einstein, B. Podolsky, and N. Rosen. Can quantum-mechanical description of physical reality be considered complete? *Phys. Rev.*, 47:777, 1935.

[40] Z. Szatmári F. Iglói and Y.-C. Lin. Entanglement entropy dynamics of disordered quantum spin chains. *Phys. Rev. B*, 85:094417, 2012.

[41] E. Fermi. Motion of neutrons in hydrogenous substances. *Ricerca Sci.*, 7:12, 1936.

[42] J. Flipse, F. L. Bakker, A. Slachter, F. K. Dejene, and B. J. van Wees. Direct observation of the spin-dependent Peltier effect. *Nature Nanotechnology*, 7:166, 2012.

[43] P. Calabrese G. De Chiara, S. Montangero and R. Fazio. Entanglement entropy dynamics of heisenberg chains. *J. Stat. Mech.*, P03001, 2006.

[44] S. Giorgini, L.P. Pitaevskii, and S. Stringari. Theory of ultracold atomic fermi gases. *Rev. Mod. Phys.*, 80:1215, 2008.

[45] C. Gogolin, M. P. Müller, and J. Eisert. Absence of thermalization in nonintegrable systems. *Phys. Rev. Lett.*, 106:040401, 2011.

[46] G. Goldstein and N. Andrei. Equilibration and generalized GGE in Tonks Girardeau regime. *arXiv:1309.3471v2*, 2013.

[47] G. Goldstein and N. Andrei. Failure of the GGE hypothesis for integrable models with bound states. *arXiv:1405.4224v1*, 2014.

[48] S. Goldstein, J.L. Lebowitz, R. Tumulka, and N. Zangh. Long-time behavior of macroscopic quantum system. *Eur. Phys. J. H*, 35:173, 2010.

[49] C. Grenier, C. Kollath, and A. Georges. Probing thermoelectric transport with cold atoms. *arXiv:1209.3942v4*.

[50] T. Hartman and J. Maldacena. Time evolution of entanglement entropy from black hole interiors. *arXiv:1303.1080v2*, 2013.

[51] R. Haussmann, W. Rantner, S. Cerrito, and W. Zwerger. Thermodynamics of the BCS-BEC crossover. *Phys. Rev. A*, 2007.

[52] D. A. Huse and V. Oganesyan. A phenomenology of certain many-body-localized systems. *arXiv:1305.4915v1*, 2013.

[53] J.P.Keating, N. Linden, and H.J.Wells. Random matrices and quantum spin chains. *arXiv:1403.1114*, 2014.

[54] J.P.Keating, N. Linden, and H.J.Wells. Spectra and eigenstates of spin chain hamiltonians. *arXiv:1403.1121*, 2014.

[55] L. P. Kadanoff and G. Baym. *Quantum Statistical Mechanics*. W. A. Benjamin, Inc. New York, 1962.

[56] K.B.Gubbels and H.T.C.Stoof. Imbalanced fermi gases at unitarity. *arXiv:1205.0568v3*, 2012.

[57] W. Ketterle and M. W. Zwierlein. Making, probing and understanding ultracold fermi gases. *arXiv:0801.2500*, 2008.

[58] S. Khlebnikov and M. Kruczenski. Thermalization of isolated quantum systems. *arXiv:1312.4612*, 2013.

[59] Hyungwon Kim and D. A. Huse. Heat and spin transport in a cold atomic fermi gas. *Phys. Rev. A*, 86:053607, 2012.

[60] Hyungwon Kim and D. A. Huse. Superdiffusive nonequilibrium motion of an impurity in a fermi sea. *Phys. Rev. A*, 85:043603, 2012.

[61] Hyungwon Kim and D. A. Huse. Ballistic spreading of entanglement in a diffusive nonintegrable system. *Phys. Rev. Lett.*, 111:127205, 2013.

[62] T. Kimura, Y. Otani, T. Sato, S. Takahashi, and S. Maekawa. Room-temperature reversible spin hall effect. *Phys. Rev. Lett.*, 98:156601, 2007.

[63] T. Kinoshita, Trevor Wenger, and D.S.Weiss. Observation of a one-dimensional Tonks-Girardeau gas. *Science*, 305:1125, 2004.

[64] T. Kinoshita, Trevor Wenger, and D.S.Weiss. A quantum Newton's cradle. *Nature*, 440:900, 2006.

[65] M. Kliesh, C. Gogolin, and J. Eisert. Lieb-Robinson bounds and the simulation of time evolution of local observables in lattice systems. *arXiv:1306:0716v1*, 2013.

[66] M. J. H. Ku, A. T. Sommer, L. W. Cheuk, and M. W. Zwierlein. Revealing the superfluid lambda transition in the universal thermodynamics of a unitary fermi gas. *Science*, 335:563, 2012.

[67] S. Langer, M. Heyl, I.P. McCulloch, and F. Heidrich-Meisner. Real-time energy dynamics in spin-1/2 Heisenberg chains. *Phys. Rev. B*, 84:205115, 2011.

[68] Y. Liao, A. S. C. Rittner, T. Paprotta, W. Li, G. B. Partridge, R. G. Hulet, S. K. Baur, and E. J. Mueller. Spin-imbalance in a one-dimensional fermi gas. *Nature*, 467:567, 2010.

[69] Y. A. Liao, M. Revelle, T. Paprotta, W. Li A. S. C. Rittner, G. B. Partridge, and R. G. Hulet. Metastability in spin-polarized fermi gases. *Phys. Rev. Lett.*, 107:145305, 2011.

[70] E. H. Lieb and D. W. Robinson. The finite group velocity of quantum spin systems. *Commun. Math. Phys.*, 28:251, 1972.

[71] N. Linden, S. Popescu, A.J. Short, and A. Winter. Quantum mechanical evolution towards thermal equilibrium. *Phys. Rev. E*, 79:061103, 2009.

[72] H. Liu and S. J. Suh. Entanglement growth during thermalization in holographic systems. *Phys. Rev. D*, 89:066012, 2014.

[73] H. Liu and S. J. Suh. Entanglement tsunami: Universal scaling in holographic thermalization. *Phys. Rev. Lett.*, 112:011601, 2014.

[74] C. Lobo, A. Recati, S. Giorgini, and S. Stringari. Normal state of a polarized fermi gas at unitarity. *Phys. Rev. Lett.*, 97:200403, 2006.

[75] W. Luo and P. Sarnak. Quantum variance for hecke eigenforms. *Ann. Scient. Ec. Norm. Sup.*, 37:769, 2007.

[76] J. M. Luttinger. Theory of thermal transport coefficients. *Phys. Rev.*, 135:A1505, 1964.

[77] F.H.L. Essler M. Fagotti, M. Collura and P. Calabrese. Relaxation after quantum quenches in the spin-1/2 Heisenberg XXZ chain. *Phys. Rev. B*, 89:125101, 2014.

[78] Z. Papić M. Serbyn and D. A. Abanin. Universal slow growth of entanglement in interacting strongly disordered systems. *Phys. Rev. Lett.*, 110:260601, 2013.

[79] M. L. Metha. *Random Matrix Theory*. Springer, New York, 1990.

[80] M. Mierzejewski, P. Prelovšek, and T. Prosen. Breakdown of the generalized Gibbs ensemble for current-generating quenches. *arXiv:1405.2557v1*, 2014.

[81] C. Mora and F. Chevy. The normal phase of an imbalanced fermi gas. *Phys. Rev. Lett.*, 104:230402, 2010.

[82] H. Mori. Statistical-mechanical theory of transport in fluids. *Phys. Rev.*, 112:1829, 1958.

[83] B. Nachtergaele and R. Sims. Lieb-Robinson bounds in quantum many-body physics. *Contemp. Math.*, 529:141, 2010.

[84] R. Nandkishore and D. A. Huse. Many body localization and thermalization in quantum statistical mechanics. *arXiv:1404.0686*, 2014.

[85] A. Nanduri, Hyungwon Kim, and D. A. Huse. Entanglement spreading in a many-body localized system. *arXiv:1404.5216*, 2014.

[86] S. Nascimbene, N. Navon, K. J. Jiang, F. Chevy, and C. Salomon. Exploring the thermodynamics of a universal fermi gas. *Nature*, 463:1057, 2010.

[87] N. Navon, S. Nascimbene, F. Chevy, and C. Salomon. The equation of state of a low-temperature fermi gas with tunable interactions. *Science*, 328:729, 2010.

[88] C. Neuenhahn and F. Marquardt. Thermalization of interacting fermions and delocalization in fock space. *Phys. Rev. E*, 85:060101, 2012.

[89] V. Oganesyan and D. A. Huse. Localization of interacting fermions at high temperature. *Phys. Rev. B*, 75:155111, 2007.

[90] K. M. O'Hara, S. L. Hemmer, S. R. Granade, M. E. Gehm, J. E. Thomas, V. Venturi, E. Tiesinga, and C. J. Williams. Measurement of the zero crossing in a Feshbach resonance of fermionic ^{6}Li. *Phys. Rev. A*, 66:041401, 2002.

[91] R. Omness. On locality, growth and transport of entanglement. *arXiv:1212.0331v1*, 2012.

[92] F. H. L. Essler P. Calabrese and M. Fagotti. Quantum quench in the transverse-field ising chain. *Phys. Rev. Lett.*, 106:227203, 2011.

[93] D. N. Page. Average entropy of a subsystem. *Phys. Rev. Lett.*, 71:1291, 1993.

[94] G. B. Partridge, W. Li, R. I. Kamar, Y. Liao, and R. G. Hulet. Pairing and phase separation in a polarized fermi gas. *Science*, 311:503, 2006.

[95] G. B. Partridge, W. Li, Y. A. Liao, R. G. Hulet, M. Haque, and H. T. C. Stoof. Deformation of a trapped fermi gas with unequal spin populations. *Phys. Rev. Lett.*, 97:190407, 2006.

[96] M. Pasienski, D. McKay, M. White, and B. DeMarco. A disordered insulator in an optical lattice. *Nature Physics*, 6:677, 2010.

[97] M. B. Plenio and S. Virmani. An introduction to entanglement measures. *Quant. Inf. Comput.*, 7:1, 2007.

[98] Pedro Ponte, A. Chandran, Z. Papić, and Dmitry A. Abanin. Periodically driven ergodic and many-body localized quantum systems. *arXiv:1403.6480v1*, 2014.

[99] C. E. Porter. *Statistical Theories of Spectra: Fluctuations*. Academic Press, New York, 1965.

[100] B. Pozsgay, M. Mestyán, M. A. Werner, M. Kormos, G. Zaránd, and G. Takács. Correlations after quantum quenches in the XXZ spin chain: Failure of the generalized Gibbs ensemble. *arXiv:1405.2843v1*, 2014.

[101] N. V. Prokof'ev and B. V. Svistunov. Fermi-polaron problem: Diagrammatic Monte Carlo method for divergent sign-alternating series. *Phys. Rev. B*, 77:020408, 2008.

[102] A. Reira, C. Gogolin, and J. Eisert. Thermalization in nature and on a quantum computer. *Phys. Rev. Lett.*, 108:080402, 2012.

[103] M. Rigol. Breakdown of thermalization in finite one-dimensional systems. *Phys. Rev. Lett.*, 103:100403, 2009.

[104] M. Rigol, V. Dunjko, and M. Olshanii. Thermalization and its mechanism for generic isolated quantum systems. *Nature*, 452:854, 2008.

[105] M. Rigol, V. Dunjko, V. Yurovsky, and M. Olshanii. Relaxation in a completely integrable many-body quantum system: An ab initio study of the dynamics of the highly excited states of 1d lattice hard-core bosons. *Phys. Rev. Lett.*, 98:050405, 2007.

[106] M. Rigol and M. Srednicki. Alternatives to eigenstate thermalization. *Phys. Rev. Lett*, 108:110601, 2012.

[107] S. Sachdev. *Quantum phase transitions*. Cambridge University Press, 2011.

[108] L. F. Santos and M. Rigol. Localization and the effects of symmetries in the thermalization properties of one-dimensional quantum systems. *Phys. Rev. E*, 82:031130, 2010.

[109] E. Schrödinger. Mathematical proceedings of the cambridge philosophical society. *Proc. Cambridge Philos. Soc.*, 32:446, 1936.

[110] D. E. Sheehy and L. Radzihovsky. BEC-BCS crossover, phase transitions and phase separation in polarized resonantly-paired superfluids. *Ann. Phys.*, 322:1790, 2007.

[111] Y. Shin. Determination of the equation of state of a polarzied fermi gas at unitarity. *Phys. Rev. A*, 77:041603, 2008.

[112] Y. Shin, C. H. Schunck, A. Schirotzek, and W. Ketterle. Phase diagram of a two-component fermi gas with resonant interactions. *Nature*, 451:689, 2008.

[113] Y. Shin, M. W. Zwierlein, C. H. Schunck, and and W. Ketterle A. Schirotzek. Observation of phase separation in a strongly interacting imbalanced fermi gas. *Phys. Rev. Lett.*, 97:030401, 2006.

[114] J. Sirker, R.G. Pereira, and I. Affleck. Diffusion and ballistic transport in one-dimensional quantum systems. *Phys. Rev. Lett.*, 103:216602, 2009.

[115] H. Smith and H.H. Jensen. *Transport Phenomena*. Clarendon Press, Oxford, 1989.

[116] A. Sommer, M. Ku, G. Roati, and M. W. Zwierlein. Universal spin transport in a strongly interacting fermi gas. *Nature*, 472:201, 2011.

[117] A. Sommer, M. Ku, and M. W. Zwierlein. Spin transport in polaronic and superfluid fermi gases. *New J. Phys.*, 13:055009, 2011.

[118] S. Sorg, L. Vidmar, L. Pollet, and F. Heidrich-Meisner. Relaxation and thermalization in the one-dimensional bose-hubbard model: A case study for the interaction quantum quench from the atomic limit. *arXiv:1405.5404v1*, 2014.

[119] M. Srednicki. Chaos and quantum thermalization. *Phys. Rev. E*, 50:888, 1994.

[120] N. Strohmaier, Y. Takasu, K. Günter, R. Jördens, M. Köhl, H. Moritz, and T. Esslinger. Interaction-controlled transport of an ultracold fermi gas. *Phys. Rev. Lett.*, 99:220601, 2007.

[121] K. R. Thurber, A. W. Hunt, T. Imai, and F. C. Chou. ^{17}O NMR study of q=0 spin excitations in a nearly ideal s=1/2 1d Heisenberg antiferromagnet, Sr_2CuO_3, up to 800 K. *Phys. Rev. Lett.*, 87:247202, 2001.

[122] A. Trenkwalder, C. Kohstall, M. Zaccanti, D. Naik, A. I. Sidorov, F. Schreck, and R. Grimm. Hydrodynamic expansion of a strongly interacting fermi-fermi mixture. *Phys. Rev. Lett.*, 106:115304, 2011.

[123] K. Uchida, S. Takahashi, K. Harii, J. Ieda, W. Koshibae, K. Ando, S. Maekawa, and E. Saitoh. Observation of the spin Seebeck effect. *Nature*, 455:778, 2008.

[124] G. Vidal and R. F. Werner. Computable measure of entanglement. *Phys. Rev. A*, 65:032314, 2002.

[125] J. von Neumann. Beweis des ergodensatzes und des h-theorems in der neuen mechanik. *Zeitschrift für Physik*, 57:30, 1929.

[126] R. Vosk and E. Altman. Many-body localization in one dimension as a dynamical renormalization group fixed point. *Phys. Rev. Lett.*, 110:067204, 2013.

[127] E. Wille, F. M. Spiegelhalder, G. Kerner, D. Naik1, A. Trenkwalder, G. Hendl, F. Schreck, R. Grimm, T. G. Tiecke, J. T. M. Walraven, S. J. J. M. F. Kokkelmans, E. Tiesinga, and P. S. Julienne. Exploring an ultracold fermi-fermi mixture: Interspecies Feshbach resonances and scattering properties of ^{6}Li and ^{40}K. *Phys. Rev. Lett.*, 100:053201, 2008.

[128] S. A. Wolf, D. D. Awschalom, R. A. Buhrman, J. M. Daughton, S. von Molnar, M. L. Roukes, A. Y. Chtchelkanova, and D. M. Treger. Spintronics: A spin-based electronics vision for the future. *Science*, 294:1488, 2001.

[129] M. W. Zwierlein, A. Schirotzek, C. H. Schunck, and W. Ketterle. Fermionic superfluidity with imbalanced spin populations. *Science*, 311:492, 2006.

[130] M. W. Zwierlein, C. A. Stan, C. H. Schunck, S. M. F. Raupach, A. J. Kerman, and W. Ketterle. Condensation of pairs of fermionic atoms near a Feshbach resonance. *Phys. Rev. Lett.*, 92:120403, 2004.